UNIVERSITÀ DELLA CALABRIA

UNIVERSITA' DELLA CALABRIA

Dipartimento di Fisica

Dottorato di Ricerca in

Scienze e Tecnologie Fisiche, Chimiche e dei Materiali
in convenzione con il Consiglio Nazionale delle Ricerche (CNR)

CICLO

XXXII

TITOLO TESI

Monitoring of mercury and organic pollutants in different environmental compartments through traditional and innovative approaches

Settore Scientifico Disciplinare

CHIM/12 Chimica dell'ambiente e dei beni culturali

Coordinatore: Prof.ssa Gabriella Cipparrone
Firma [redacted]

Supervisori: Dott
Fi
Dott.
Firma [redacted]

Firma oscurata in base alle linee guida del Garante della privacy

Dottoranda:
Dott.ssa Antonella Tassone
Firma [redacted]

Firma oscurata in base alle linee guida del Garante della privacy

Content

Abstract

Negli ultimi decenni il problema dell'inquinamento ambientale ha acquisito notevole importanza su scala globale sia per il continuo aumento dei livelli di inquinanti che per l'introduzione di nuovi contaminanti. Gli effetti tossici sulla salute umana e sugli ecosistemi rappresentano la più grande minaccia di questi inquinanti. Pertanto, negli ultimi anni la comunità scientifica si è impegnata nel monitoraggio questi inquinanti in tutti i settori ambientali, come aria, acqua, suolo e sistemi viventi con lo scopo di garantire un controllo rigoroso della loro presenza nell'ambiente e successivamente regolamentarli. Infatti, le diverse proprietà fisico-chimiche delle varie sostanze fanno sì che siano distribuiti nei vari comparti secondo un preciso ciclo biogeochimico. È per questo motivo che studi di monitoraggio adatti a ciascun comparto ambientale sono necessari. Nella maggior parte dei casi, i metodi analitici impiegati si basano su tecniche obsolete, che non trovano impiego per via dell'uso di sostante nocive o di un grande dispendio di tempo e risorse. In questo contesto, esiste una domanda crescente di metodi analitici innovativi, rapidi, eco-compatibili, a basso costo, semplici da impiegare. Il lavoro di ricerca presentato in questa tesi riguarda il monitoraggio del mercurio e di alcuni inquinanti organici emergenti, quali esteri organofosfati, benzotriazoli, benzotiazoli e benzosulfonammidi, mediante l'impiego di approcci analitici sia tradizionali che innovativi. Lo studio condotto durante il corso del dottorato ha riguardato l'indagine di diversi settori ambientali, come l'ambiente atmosferico di vari siti, interessati da fonti di inquinamento antropiche oltre che naturali. Inoltre, oggetto d'indagine sono stati anche l'ambiente acquatico del Mar Mediterraneo e il biota campionato in terreni agricoli di San Giovanni in Fiore (CS). Inoltre, lo studio del particolato atmosferico è stato condotto attraverso lo sviluppo di nuovi metodi analitici eco-compatibili per la determinazione di esteri organofosfati, benzotriazoli, benzotiazoli e benzosulfonammidi mediante estrazione mediata da microonde seguita da microestrazione in fase solida e quantificazione mediante gascromatografia-spettrometria di massa tandem.

Abstract

In the last decades, the issue of environmental pollution has acquired considerable importance at a global scale due to both the continuous increase in pollutant levels and the introduction of new contaminants. The toxic effects on human health and other ecosystems represent the greatest threat posed by these pollutants. Therefore, with the aim to ensure a strict control of their presence in the environment and subsequently regulate them, in recent years the scientific community has engaged in monitoring these pollutants in all environmental sectors, such as air, water, soil and living systems. Indeed, the different physico-chemical properties of the various substances ensure that they are distributed in the various compartments according to their own biogeochemical cycle. It is for this reason that monitoring studies suitable for each sector are necessary. In most cases, the analytical methods traditionally used are obsolete, relying on techniques that are no longer used. In this context, there is a growing demand for innovative analytical methods, which are fast, environmentally friendly, low cost, simple to use.

Among the major ambient pollutants, the research work presented in this thesis is addressed to the monitoring of mercury and some emerging organic pollutants, i.e. organophosphate esters, benzotriazoles, benzothiazoles, and benzenesulfonamides, exploiting both traditional and innovative approaches. The investigation concerned the atmospheric environment of various sites affected by anthropic as well as natural emission sources, the aquatic environment of the Mediterranean Sea and the biota specimen collected in croplands from San Giovanni in Fiore (CS). Furthermore, the airborne particulate matter was monitored as an environmental matrix with the aim to detect organic pollutants through the use of new eco-friendly analytical methods.

Acknowledgements

Firstly, I would like to express my deep gratitude to Dr. Roberto Bartolino and to Dr. Nicola Pirrone for the opportunity to pursue the Ph.D. studies as fundamental part of my education and training from both a scientific and personal point of view.
Furthermore, I would like to express my sincere thankfulness to my supervisors Dr. Francesca Sprovieri and Dr. Attilio Naccarato for their guidance, motivation and patience. They really helped me during each stage of the Ph.D. studies, also providing me the opportunity to widen my knowledge through the participation in various conferences and courses. I am also grateful for the opportunity to take part in the oceanographic campaign, which was an amazing experience that incredibly enriched me. I would also acknowledge all the researchers of the University of Calabria, who gave me the opportunity to collaborate with their research activities.

Then, I thank my fellow labmates, Sacha, Maria and Giovanni for the time spent working together, the stimulating discussions, and for all the fun we have had in the last three years. In addition, I would like to acknowledge all personnel of the CNR-IIA for their insightful comments and encouragement, but also for the familiar atmosphere where I worked everyday.

Last but not least, I would like to thank my lovely family: my parents, my brother, my boyfriend and my sister-in-law for the continuous support throughout studying, writing this thesis and my life in general.

List of figures

List of Tables

Preface

The term ambient pollution refers to any chemical, physical or biological agent that modifies the natural environment. Nowadays, modern society is intrinsically linked to the extensive use of these agents to either improve the quality of life or achieve more efficient and economically suitable industrial processes. Unfortunately, they have been produced and used in an unregulated way, resulting in the contamination of the surrounding environment. Therefore, a great concern about the connection between pollution and unhealthy impact on the environment and living species has increased over the last decades, inducing policymakers to create numerous monitoring programs at a national and international scale. At the same time, the scientific community has been focused on monitoring emerging and already known compounds, which have not been regulated yet, as well as on the determination of regulated compounds through innovative techniques. In this framework, technical advances in analytical chemistry in terms of the development of more sensitive and selective techniques have helped researchers worldwide determining chemical compounds present in the environment, that even at very low levels are potentially harmful to human health. Depending on their physicochemical properties, they can distribute among the various compartments, taking part in biogeochemical cycles, which makes them persistent. Among the major ambient pollutants, toxic metals, particulate matter, organic compounds, and gases like nitrogen oxides, carbon monoxide, and ozone, play a key role and pose a global threat for both human health and the environment.

The work carried out during the Ph.D. studies deals with the analytical monitoring of certain classes of contaminants in the various environmental compartments, integrating to the conventional approaches also innovative ones. For a better structuring, this thesis was divided into two sections. Section I includes studies based on mercury monitoring in different environmental matrices. In Section II, the work focuses on the development of new analytical methods for the analysis of emerging contaminants (ECs), which can frequently be detected in the particulate matter. As regards Section I, mercury (Hg) is among the toxic metals for both human health and ecosystems, being involved in complex biogeochemical cycles, and a persistent

contaminant in atmosphere, waters and biological systems. Therefore, in Chapter 1, an introduction to the threat of mercury pollution in its different forms is fully described. Chapter 2 summarizes the common methods employed for the measurement of this pollutant in atmosphere, water, and biological samples. Both active and passive sampling methods of Hg species were explored, thus the principles behind these approaches are displayed. In Chapter 3, three applications (case studies) of the aforementioned techniques are reported, i.e., the monitoring of Hg species in the marine environment of the Mediterranean Sea, the comparison of the performances of newly-developed passive devices with the conventional active sampling, and the monitoring of total Hg and other heavy metals in fertilized soils and in a generalist predatory living in them, namely *Harpalus (Pseudoophonus) rufipes*.

The first case study reports the results of measurements performed during an oceanographic cruise campaign organized within the MED-Oceanor program coordinated by the Italian National Research Council - Institute of Atmospheric Pollution Research (CNR-IIA) during summer 2017. The overall aim was to investigate the potential influence of volcanic emissions on the Hg distribution and pattern in the atmosphere as well as in the vertical profile along the route followed by the research vessel of the CNR, using traditional instrumental techniques to assess Hg concentrations. The second case study was performed in the framework of the project "Development of a Plan for Global Monitoring of Human Exposure to and Environmental Concentrations of Mercury" carried out by the United Nations Environmental Program (UNEP) in close collaboration with CNR-IIA and the World Health Organization (WHO). This project aimed to harmonize approaches for mercury monitoring and to strengthen the capacity for mercury analysis in humans and in the environment in support of the requirements of the Minamata Convention on Mercury. In this context, the active sampling, which the common Hg analyzers are based on, was compared with the performances of newly developed passive devices, improved during my Ph.D. studies and tested in the field through an intercomparison campaign lasting three months, from February to April 2019. These devices exploit the photocatalytic properties of Titania nanoparticles (TiO_2) and the affinity between gold and mercury to obtain a selective sorbent material to be implemented into a common axial sampler. The result is an efficient passive device, capable of binding Hg from the

atmosphere without the use of mechanical pumps or electricity and releasing it under thermal treatment for quantification. The third case study deals with the monitoring of total mercury and other heavy metals in crop fields, treated with fertilizers, in San Giovanni in Fiore (CS) and in an insect species living in them, in order to evaluate its potential use as a bioindicator through the calculation of a bioaccumulation factor. The Hg determination was carried out with a sample preparation protocol different from that suggested in the EPA method 1631, being based on acid digestion assisted by microwaves instead of the acid digestion at high temperature, which is known to be both time and reagent consuming, as well as less reproducible. This study was carried out in collaboration with the Department of Biology, Ecology and Earth Sciences of the University of Calabria, which was in charge of sampling the beetles and soils, as well as of studying the ecological impacts of the obtained results.

As regards Section II, emerging contaminants have become a highly relevant topic in the scientific community because of their increasing release into the environment, potential adverse effects on human health or ecosystem safety and the need for the development of suitable analytical methods for their determination. A few examples of ECs are represented by pharmaceuticals, disinfectants, plasticizers, and preservatives. As for Hg, ECs can also occur in various compartments, with the atmospheric particulate matter being one of the most important since it potentially allows the distribution even over long distances. In this context, particulate matter (PM) can act not only as a source of pollution itself but also as a carrier of these contaminants. Therefore, in Chapter 4, particulate matter as an environmental matrix is investigated. As an overview, in Chapter 5 the most common methods for the quantification of the organic pollutants bound to PM are described, with special care for those involved in my Ph.D. studies. Chapter 6 reports the development of new analytical strategies for the quantification of some classes of emerging organic contaminants, namely organophosphate esters (OPEs), benzotriazoles (BTRs), benzothiazoles (BTHs), and benzenesulfonamides (BSAs), bound to PM. These contaminants find wide applications as flame-retardants, plasticizers, corrosion inhibitors, anti-icing fluids, and other many uses, conferring them the definition as high production volume (HPV) chemicals. The key point of the proposed strategies

resides in the use of an eco-friendly solvent mixture for the microwave-assisted extraction of the analytes from particulate filters, followed by a solid-phase microextraction (SPME) step and a gas chromatography-tandem mass spectrometry. In addition, the reported optimal working conditions for each of these steps are the result of the multivariate analysis of the experimental design, which allowed for the investigation of all the variables affecting the methods simultaneously.

Section I

Chapter 1

Mercury as a global pollutant

1.1 Introduction

Mercury (Hg) is a heavy metal, which due to its high mobility and long residence time in the environment has been classified as a persistent, bioaccumulative toxin (PBT) [1], representing a threat of global concern for both human health and ecosystems [2]. Its peculiar physical and chemical properties make it a unique natural metal, which appears as a dense liquid that easily vaporizes at ambient temperature and pressure. Apart from its liquid state at ambient temperature, it shows some anomalies compared to other metals, such as its boiling point below 650°C [3].

Owing to its electronic configuration, it is a quite inert metal with a high ionization potential, which can be present in the elemental (Hg^0) or oxidized (Hg^+ and Hg^{2+}) state. Nevertheless, compounds containing Hg^+ are less frequent, since they mainly consist of dimers of Hg atoms covalently bounded (Hg_2^{2+}), which tend to disproportionate, resulting in Hg^{2+} and Hg^0 [4].

Peculiar chemistry characterizes mercury, since it easily reacts with metals, namely gold, silver, and copper, to form very stable alloys known as amalgams, and non-metals, such as oxygen, sulfur, and halogens to form salts [5]. These inorganic compounds appear in the form of white powder or crystals, except for cinnabar (mercuric sulfide HgS), the main mineral form of mercury in the environment [1], which is brick-red (Fig. 1.1). In the form of salts, mercuric compounds show higher solubility, thus increasing bioavailability and potential adverse effects [6].

Fig. 1.1 Cinnabar (HgS) mineral [7]

Mercury can also combine with carbon, resulting in organometallic or organomercury compounds, as dimethylmercury ($(CH_3)_2Hg$), the cation methylmercury (CH_3Hg^+), as well as other minor species (cation ethylmercury, $CH_3CH_2Hg^+$, and cation phenylmercury, $C_6H_5Hg^+$). These cationic species also exist in the form of salts, e.g., methylmercury chloride or phenylmercuric acetate.

The chemical form of mercury controls its bioavailability, transport, persistence, and impact on the human body; although all the mercury compounds potentially show adverse effects, organic mercury compounds are generally more toxic than inorganic, and a special concern is reserved to the methylmercury cation. Indeed, this species has been recognized as the most toxic for both human health and ecosystem safe, due to its lipophilic properties, which makes it capable to permeate through biological membranes, resulting in bioaccumulation and biomagnification along the trophic chain. For example, fish tissues typically show concentrations of methylmercury more than 10^6 times higher than ambient water, as reported by WHO [8] and EPA [9].

The occurrence and fate of all the mercury compounds in each environmental compartment have therefore prompted both scientists and policymakers to a deeper knowledge of the transformations involved in the global biogeochemical cycle, as well as the processes by which it travels.

1.2 Mercury biogeochemical cycle

Mercury in the environment is continuously cycled and re-cycled as a consequence of natural and anthropogenic activities (Fig. 1.2). Natural sources mainly include volcanoes, but also soil degassing and evasion from water surfaces, as well as

weathering processes of Earth crust and forest wildfires. Gaseous Elemental Mercury (GEM), that is Hg^0 vapor, is the primary form emitted into the atmosphere, where it can circulate for a long time, from 0.5 to 2 year [10]; hence, it is well mixed and subjected to transport even to remote areas. The geothermal activity of volcanoes, being active or passively degassing, is responsible for the release of large quantities of elemental mercury to the free troposphere and stratosphere.

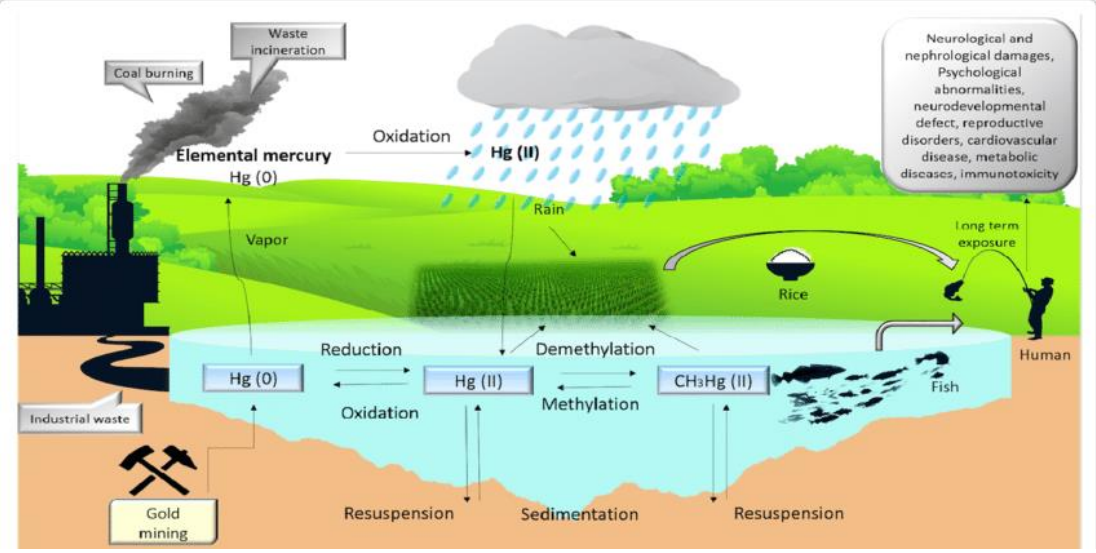

Fig. 1.2 Mercury biogeochemical cycle [11]

An estimation of Hg emission from volcanoes and other geothermal activities (e.g. calderas) are about 90 Mg yr^{-1} [2], which accounts for 2% of the total contribution from natural processes. In general, volcanoes, fumaroles, solfataras, contributions from widespread geological anomalies, mainly include mercury in the elemental form; nevertheless, inorganic mercury Hg^{2+} in the gas phase (Gaseous Oxidized Mercury, GOM) or bound to particulate matter (Particulate Bound Mercury, PBM) can be emitted [12].

Upon photochemical oxidation of the atmospheric GEM to Hg^{2+}, mercury is deposited following wet or dry deposition processes. Once in the soil, Hg^{2+} accumulates as long as a physical event, such as forest fires and biomass burning, leads to its re-mobilization and re-volatilization toward the atmosphere. Within the ocean, mercury can undergo different reactions, it can be readily transformed into insoluble mercury sulfide or bound to organic matter, it can be reduced again to Hg^0, or it can be

converted by bacteria into methylmercury. In the first case, the insoluble mercury sulfide, as well as many complexes formed with the organic matter, is again deposited into sediments; conversely, when inorganic mercury is photoreduced to Hg^0 [13], which is volatile, surface waters become supersaturated in the elemental form with respect to the atmosphere, thus promoting evasion processes toward the atmosphere. Alternatively, the presence in water of various microorganisms leads to the biomobilization of mercury through biotic and abiotic processes, which result in the methylation of Hg^{2+}, as well as the degradation of the methylmercury itself. Then, the methylmercury released by bacteria can adsorb to plankton, which is consumed by the next higher organisms up the food chain. Since organisms require a long time to eliminate methylmercury, bioaccumulation, and biomagnification up to the higher trophic levels occur. This relationship continues as bigger fish feed on progressively smaller fishes until they are finally eaten by humans or other animals. In this sense, mercury poses a threat to human health and ecosystems. Anthropic activities have affected the biogeochemical cycle of mercury through direct emission into air, as well as mercury release into natural ecosystems. Important anthropogenic sources of mercury include coal-fired power plants, waste incinerators, processing of mineral resources (like gold mining), and chlor-alkali production [2,14]. Human activities emit both elemental (GEM) and oxidized mercury (as GOM or PBM), which have different residence time: GEM has a longer lifetime throughout the troposphere than GOM and PBM, which deposit near emission sources (tens to hundreds of km).

Due to this persistence in the atmosphere and to the long-range transport, even smaller environmental sources (i.e. the combustion of coal, and municipal solid waste) result in a widespread increase of mercury concentrations, also in remote regions.

The global contribution to mercury emission from man-made sources was 2190 tons in 2000, [15] with the largest emissions (about 65%) occurring from the combustion of fossil fuels, main coal in industrial and residential boilers. Asian countries (China, India, Japan, etc.) represented the major contributors, with 1179 tons of Hg emitted, corresponding to the 54% of the total global emissions, owing to their well-developed industrial activities mainly based on combustion of fossil fuels (especially coal) and to incineration of waste material. In particular, China resulted first in the list of the 10 Asian countries with 600 tons of Hg emitted from anthropic activities. North America

and Europe instead contributed less than 25% of the total global emissions [15]. Data from the 2010 emissions inventory, reported in [1], show that the emission from anthropogenic sources is estimated as 1960 tons, corresponding to 30% of the total global emissions to the atmosphere. Natural sources constitute about 10% of this total, whereas the remaining 60% is due to re-emissions and re-mobilization sources. The greatest contribution to anthropogenic emissions still remains the coal-burning for energy (85%), while mining, smelting, and production, cement production, artisanal and small-scale gold mining represent smaller percentages. Additional ways for mercury to enter the environment come from the slow release by different consumer products, like dental fillings, thermometers, barometers, fluorescent lamps, mercuric oxide, and other batteries, as well as by pharmaceuticals, skin lightening cosmetics, antiseptic creams, and insecticidal [16,17]. With the aim to control emissions from anthropogenic sources, numerous international actions and conventions have been implemented in recent years, encouraging the expansion of long-term data monitoring, even in the areas where data are limited or do not exist. Some of these include the UNEP Mercury Program, the United Nations Economic Commission for Europe - Long-Range Transboundary Air Pollution (UNECE-LRTAP), and the Minamata Convention. On a regional scale, environmental measurement networks have included the European Monitoring and Evaluation Programme (EMEP), the Arctic Monitoring and Assessment Programme (AMAP), and the Canadian Atmospheric Mercury Measurement Network (CAMNet).

The overall goal of these global treaties is to safeguard human health and the environment from the releases of mercury and its compounds by minimizing anthropogenic sources. In this way, the burden of disease can be reduced, and protection can be ensured toward the future generations, and particularly vulnerable populations, such as pregnant women and children. This would also reduce costs from the impact of mercury on health. An important step in this direction was taken in 2013 with the adoption of the Minamata Convention on Mercury, which was signed by more than 120 nations and entered into force on 16 August 2017. According to the Article 22, "*…the Conference of the Parties shall, at its first meeting, initiate the establishment of arrangements for providing itself with comparable monitoring data on the presence and movement of mercury and mercury compounds in the environment*

as well as trends in levels of mercury and mercury compounds observed in biotic media and vulnerable populations" [18]. The primary objective of the convention is to protect human health and the environment from anthropogenic emission and releases of mercury and mercury compounds. Therefore, each possible anthropogenic source, as Hg mining, is to be phased out, air emissions are to be controlled and artisanal/small scale gold mining is to be regulated [1]. Through these treaties, a number of countries have actually achieved significant reductions in emissions and releases of Hg from consumers' products and industrial processes over time. Significant support has been given from the numerous scientific works and information about the production, use, emissions, releases, handling, and disposal of Hg. Indeed, as the Minamata Convention has moved into its implementation phase, there has been a need for a deeper knowledge of the Hg chemical transformation, processes, and source emissions, to be gained through long-term monitoring actions. In this scenario, in November 2010 the European Project GMOS - Global Mercury Observation System was promoted and coordinated by the Institute of Atmospheric Pollution of the National Research Council (CNR-IIA), with the aim to establish a global Hg monitoring network, involving also those areas where data have been still scarce or completely absent. Nowadays, the GMOS network involves more than twenty research institutions with air monitoring stations in Europe, North and South America, Asia and Africa. Through this network data and key information aimed at filling the gaps in the Hg knowledge were gained through measurements performed both in 40 ground-based stations, in the marine environment and air, through the coordination of oceanographic campaigns and aircraft measurements. Currently, the GMOS is part of the GEO strategic plan (2016–2025) aimed to develop a global observing system for Hg and Persistent Organic Pollutants (POPs), and particularly within the flagship on "tracking persistent pollutants" GOS^{4}M (Global Observation System for Mercury). One of the major outcomes of the GMOS has been an interoperable e-infrastructure developed following the Group on Earth Observations (GEO) data sharing and interoperability principles, which revealed fundamental to provide support to UNEP for the implementation of the Minamata Convention.

1.2.1 Mercury in the atmospheric environment

As previously mentioned, the most common form of mercury in the atmosphere is the elemental one, Hg^0, also referred to as Gaseous Elemental Mercury, GEM. This form has a long residence time into the atmosphere, varying from 6 to 18 months, is relatively insoluble in water and has a low deposition velocity (0.05-0.1 cm s^{-1}); thus, it is transported on a global scale, reaching also remote regions [19]. However, its persistence in the atmosphere strongly depends on the presence of oxidants and their concentrations. For example, in the Arctic, in springtime, during Atmospheric Mercury Depletion Events (AMDEs), GEM can easily be oxidized due to the high concentration of Br radicals and deposited as Hg^{2+} in a few days to hours [20,21]. Indeed, photo-oxidation reactions occurring in the atmosphere lead to the formation of GOM (Gaseous Oxidized Mercury) or can adhere to particulate matter, resulting in the formation of PBM (Particulate Bound Mercury).

The physical and chemical structure of these two forms cannot be exactly identified since they include numerous compounds of divalent mercury. Indeed, the term GOM refers to water-soluble oxidized mercury species with a vapor pressure sufficiently high to exist in the gas phase. It is also known as Reactive Gaseous Mercury (RGM), due to reactivity towards stannous chloride, which acts as a reducing agent and converts RGM into GEM without any pre-treatment procedure. The most likely candidate for RGM compounds is $HgCl_2$ [22], along with other divalent mercury species, such as $HgBr_2$, HgBrOH [21,23], HgO [21], or other compounds [24]. The sum of GEM and GOM is referred to as Total Gaseous Mercury (TGM), with RGM representing 1–3% of TGM in clean, background air [22].

Particulate Bound Mercury instead refers to mercury, as elemental and divalent, bound or adsorbed to airborne particulate matter, like dust, soot, and sea salt aerosol. Unlike GEM, both GOM and PBM have a short lifetime (1-7 days), since they have higher deposition velocities (1-5 cm s^{-1} and 0.1-1 cm s^{-1}, respectively) [2]. Thus, they undergo wet or dry deposition processes near the emission sources, e.g., incinerators, non-metal smelters, and power plants [22,25]. Their levels into the atmosphere are typically 2–3 orders of magnitude lower than GEM.

1.2.2 Mercury in the aquatic environment

Once in the atmosphere, mercury can reach the aquatic environment through different deposition processes, which promote its global cycling. Indeed, elemental mercury can be physically adsorbed (reversibly or irreversibly) on atmospheric particulate matter and deposited into oceans, or it can be scavenged by cloud and fog droplets. In addition, the higher solubility of RGM in water allows its dissolution in rainwater and subsequent wet deposition [26]. Thus, rainfall and snow can contain different forms of mercury. The main form is inorganic mercury, whereas methylmercury represents less than 1%.

As regards the marine and freshwater compartments, the dominant form of Hg is the inorganic mercury Hg^{2+}, which can exist in dissolved or particulate form. Indeed, it can be sorbed onto suspended particulate matter (SPM), which includes both organic matter and inorganic particles, as well as living species like phytoplankton and zooplankton [4]. A small amount of mercury (less than 30%) in the aquatic system is in the elemental form, Hg^0, which is volatile, and together with dimethylmercury ($(CH_3)_2Hg$) constitutes the Dissolved Gaseous Mercury (DGM) [27]. Once Hg^0 is entered into the aquatic environment, it could be subject to chemical and photochemical reactions; for example, following the oxidation to Hg^{2+}, it could undergo methylation through biological and abiotic mechanisms, with the former being more likely than the latter. Once formed, methylmercury can be photo-reduced to Hg^0, demethylated or can bioaccumulate and biomagnificate through the food web.

1.2.3 Air-Sea exchange

The atmosphere provides the main environmental pathway for redistribution of Hg around the globe; therefore, quantifying the transfer of Hg from the air to the Earth's surface via wet and dry deposition is critically important. As previously mentioned, a wide variety of reactions, involving oxidation and reduction, among the two common oxidation states in different environmental compartments affects Hg biogeochemical cycle.

Several studies are focused to understand the flux between atmosphere and oceans in the marine boundary layer (MBL), since photochemical processes in the MBL enhance oxidation of Hg^0, thus increasing Hg^{2+} and TPM concentrations via gas-particle

partitioning [28–30]. As Hg^{2+} dissolves or Hg^0 evaporates from the surface water, this exchange is established, with the direction depending on the saturation state of each compartment. Indeed, it is well known that oceans act both as a sink and as a source for mercury compounds, since different deposition mechanisms transfer Hg from air to oceans and conversely the Hg accumulated in water is re-emitted into the air through evasion processes.

Evasion flux, which seems to be predominant over deposition, mainly depends on three factors: the Hg concentration gradient at the interface air-water, the solar radiation, which is responsible for the photo-reduction of Hg^{2+}, and the temperature of both the surface water and air at the interface [2,29,31]. Different studies reported that the evasion of mercury from freshwater, especially, lake surfaces is generally higher than that observed over the sea. Typical values of mercury emission rates from ocean basins and lakes account for 2778 Mg y^{-1} of net evasion to the atmosphere [2]. The contribution of the Mediterranean Sea was reported to be 70 Mg y^{-1}, as a result of modeling estimates by Hedgecock et al. [32]. Moreover, seasonality exists in the evasion rates, with lower fluxes in winter, as suggested by the global model of Strode et al. [33].

1.2.4 Mercury in biota

Mercury methylation consists of the formation of organic mercury compounds resulting from the addition of one or more covalently bound carbon atoms to an oxidized mercuric species [34]. This process can be due to both biotic and abiotic mechanisms: substances, as methylcobalamin and humic matter, are responsible for the methylation in seawater whereas biologic methylation occurs in sediments mediated by sulfate-reducing bacteria.

The greater lipid solubility due to the presence of organic moieties results in the accumulation in biological tissues, with an assimilation rate faster than it is excreted, conferring it a long biological half-life (2 years or more). Thus, after biota at lower trophic levels uptakes mercury compounds from the water, it undergoes the accumulation of mercury, which then is transferred along the trophic chain.

As methylmercury is the only biomagnified form of mercury [35], species that accumulate high levels of inorganic mercury, like mussel, copepods, and shrimps,

which uptake the 90 % of their Hg content in the inorganic form contained in detritus [35], obscure trends of trophic level bio-transference. Nevertheless, virtually all mercury (70% to 100%) in the muscular tissues is in the methylated form [36,37] and therefore bioavailable for transference to upper trophic levels [38]. Consequently, the mercury burden of fish increases with trophic level to humans via the ingestion of methylmercury species accumulated in fishery products.

1.3 Toxicity and health effects

Although mercury has been recognized as one of the most hazardous environmental pollutants, it received more attention after the Minamata Bay tragedy, where over 2000 people, the majority of whom died, were affected by mercury poisoning due to the consumption of contaminated fish. The contamination originated when the Japanese company Chisso Corporation released industrial wastewater containing inorganic mercury in the Shiranui Sea between 1932 and 1968, which resulted in a very high concentration of Hg in water [39]. Another case of mercury poisoning epidemic, which affected more than 6000 individuals with 400 deaths, occurred in Iraq between 1972 and 1973, where bread resulted contaminated by organomercury fungicides on the agricultural crops for the grain seeds [19].

Considering that the main exposure pathway of Hg to humans is through seafood consumption [34], US-FDA has recommended the limited consumption of marine fish [40]. Actually, the mercury problem is not limited to the aquatic food chain: recently, rice has been proposed as the major source of methylmercury from food in various parts of the Chinese population [41]. Anyway, humans are generally exposed at non-toxic acute levels, except for well-documented cases of severe mercury poisoning such as Minamata Bay. The maximum intake of methylmercury, as recommended by the World Health Organization (WHO), is 1.6 μg kg^{-1} body weight per week whereas the United States Environmental Protection Agency developed a reference dose of 0.1 μg kg^{-1} body weight per day for adults [34].

Numerous studies have reported the adverse effects caused by mercury. These effects strongly depend on the chemical form of mercury. Indeed, when metallic mercury enters the human body, it can be retained for weeks or months, being mostly accumulated in kidneys, until it leaves the body through the urinary apparatus. For the

inorganic mercury, the path across the human body is the same as organic Hg. The major threat to human health is methylmercury, due to its capacity to be easily absorbed from the gastrointestinal tract and to pass the blood-brain barrier.

Considering the strong affinity of methylmercury for sulfhydryl groups present in blood proteins, once reached the circulatory system, Hg undergoes differential partitioning, with the methylmercury mostly accumulating in erythrocytes and inorganic mercury in the plasma fraction [42].

This is the likely cause of the increased mobility of methylmercury, which is transported and distributed throughout the entire body, whereas the inorganic forms concentrate primarily on the internal organs. Methylmercury can also pass through the placenta barrier causing severe effects on the neurological development of a fetus - retardation, ataxia, damage to hearing and speech, and loss of peripheral vision, which together characterize the so-called 'Minamata-syndrome' [43]. Even in adults, its primary effect is impaired neurological development, resulting in permanent damage to the brain and its associated functions, including cognitive thinking, memory, attention, language, and fine motor and visual-spatial skills. The main exposure pathway of Hg to humans is through the consumption of contaminated food, as marine fishery products (fish, shellfish, crustaceans), even if also the inhalation of mercury vapor, as well as the dermal exposure, can result in harmful effects. Symptoms include tremors, insomnia, memory loss, neuromuscular effects, headaches and cognitive and motor dysfunction. The inorganic salts of mercury are corrosive to the skin, eyes and gastrointestinal tract, and may induce problems to kidney ranging from proteinuria (increased protein in the urine) to kidney failure [16].

Chapter 2

Analytical methods for mercury monitoring in different matrices

2.1 Introduction

Nowadays, next to the conventional instruments used for Hg monitoring, a lot of innovative approaches are reported in the literature, which show numerous advantages and allow monitoring in remote areas. Many scientists are currently developing new methods for the quantification of mercury. These methods rely on the passive sampling of the analyte without power supply or mechanical pumps. Thus, in the following sections, all the techniques used in this thesis are summarized, including both traditional and innovative techniques, as regards the active and passive measurements in the atmosphere, respectively. Moreover, traditional automated techniques for determination of the total mercury in aqueous matrices, following the EPA method 1631, are reported. As regards the total mercury quantification in solid matrices, a sample preparation approach alternative to that suggested by the same EPA method 1631 (appendix B) is briefly explained.

2.2 Traditional techniques for active monitoring of Hg in air

All the instrumental techniques used for the sampling of mercury in the atmospheric environment have historically relied on the fact that noble metals can be used to amalgamate Hg [44]. Amalgamation with gold is the principal method used to sample Hg^0 for atmospheric measurements worldwide [45]. Thus, a gold surface, in the form of cartridges, traps, or membranes has been extensively used to preconcentrate Hg^0 during the sampling step. Once trapped, mercury has been quantified by thermal desorption of the amalgam at 550°C. In particular, one of the most common instruments that uses this principle for the sampling and analysis of mercury in air is the mercury analyzer 2537, commercialized by Tekran (Tekran Instrument Corp., Ontario, Canada) which provides continuous analysis of gaseous mercury in air at sub-nanogram per cubic meter (ng m^{-3}) level. This instrument is based on the Cold Vapor Atomic Fluorescence Spectrometry (CVAFS) for the quantification of the mercury

adsorbed on cartridges containing ultra-pure gold adsorbent media. Briefly, the instrument samples air though the solid gold cartridge, which selectively traps elemental mercury vapors, owing to the amalgam formation. The desorption step occurs by heating the gold matrix at 550°C, thus the adsorbed mercury is thermally released into an inert, ultra-high purity argon carrier gas. A dual cartridge design (A and B) allows alternating cycles of sampling and desorption, resulting in an automated measurement of gaseous mercury which is continuous, with no data gaps. Indeed, during the analysis cycle, cartridge A collects mercury from the sample stream while the mercury vapors previously trapped on cartridge B are desorbed into the argon carrier flow and are sent to the CVAFS detector for quantification. At the end of the analytical cycle, the roles of the gold cartridges are reversed. This double alternating action allows a continuous 5-minutes sampling of the inlet stream.

In the detector, mercury vapors reach a quartz cuvette illuminated by a low-pressure mercury-vapor lamp, which emits monochromatic UV radiation at 253.7 nm. This radiation excites any mercury atom present, which then re-radiates (that is fluoresces) at the same wavelength with a specific incident angle. A photomultiplier tube (PMT) views the cell through a monochromatic filter at right angles to the incident light, whereas direct light from the source is not seen. This allows CVAFS to be more sensitive than other analytical techniques, for example, Cold Vapor Atomic Absorption Spectrometry (CVAAS), and reaching a lower detection limit.

The fluorescence signal intensity (F), after the baseline correction, is directly proportional to the amount of mercury vapor in the cuvette (C_{Hg}):

$$F = I_s * C_{Hg}$$

where I_s represents the intensity of the radiation emitted by the lamp source.

In addition to being much more sensitive than atomic absorption, CVAFS is not subject to positive interferences, while some negative interference could result from quenching of the fluorescence signal in the presence of molecular species. To avoid this inconvenience, the interior of the detector is purged with ultrapure carrier gas so that oxygen, nitrogen oxides, as well as organic molecules that could affect the baseline and the peak narrowness, are removed.

Following this analysis cycle (Fig.2.1), the instrument provides for the 5 minutes integrated mercury concentration, expressed as ng m^{-3} at standard temperature and pressure, with detection limits of 0.1 ng m^{-3}.

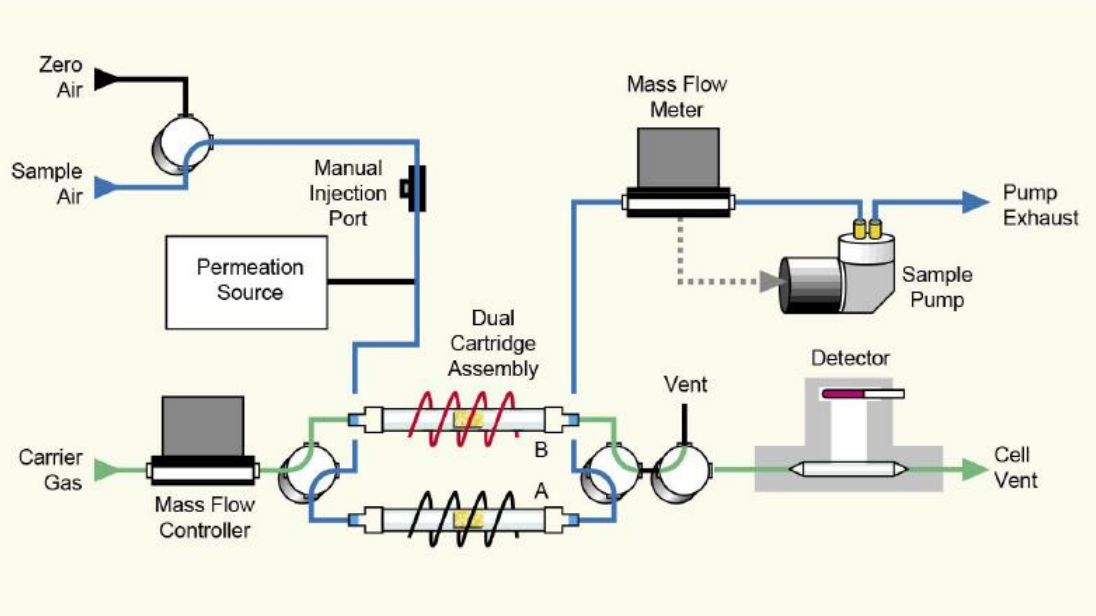

Fig. 2.1 Scheme of the analytical cycle of Tekran 2537 Hg Analyzer [46]

The accuracy of the measurements is obtained after the calibration with a known amount of Hg^0 vapor, which can be automatic, relying on the use of a permeation source located inside the instrument, or manual, for which Hg vapors, withdrawn from an external Hg source (namely Tekran 2505 Unit), are injected using an automatic gas-tight syringe. The external calibration unit Tekran 2505 represents a primary source of elemental mercury useful for calibration or quality control evaluation of ultra-trace mercury analytical systems. This unit is based on the well-known principle of Hg vapor pressure as a function of temperature: at a certain temperature value, a precise mass concentration of saturated mercury is present in the vapor phase and can be withdrawn for the calibration of any analytical systems [47].

Obviously, calibration represents a crucial step for the evaluation of the measurement results. Various SOPs within GMOS, described in D'amore et al. [48] and Sprovieri et al. [49], provided a list of criteria to be fulfilled to validate the speciation measurement.

The 2537 unit does not allow the measurement of the different Hg species in the atmosphere; the quantification of the speciated Hg is therefore achieved after its coupling with other modules, 1130 and 1135, which are located upstream to the 2537 unit, for the analysis of GOM and PBM fractions, respectively. Tekran 1130 analyzer is currently the only commercially available system for automated measurement of gaseous oxidized mercury (GOM), which relies on a preconcentration step before quantification due to the low GOM concentration in the atmosphere. Indeed, it exploits potassium chloride (KCl)-coated denuders for the selective collection of GOM in an air sample. Nevertheless, in recent years many studies reported the occurrence of artifacts, oxidation/reduction transformations, water vapor passivation and incomplete GOM retention as issues affecting measurements [45]. Moreover, additional bias results from the observation that the system does not quantify all the GOM forms equally, and interferences with water vapor and ozone occur [12,50]. Thus, current research aims at developing efficient calibration methods for GOM species [45] to certify Tekran measurements. The module 1130 (Fig. 2.2) is composed of a weatherproof, temperature-controlled enclosure, which houses the core of the instrument that is the annular denuder. This denuder is composed of two coaxial quartz tubes, with a KCl layer covering the inner surface of the outer tube and the outer surface of the inner one, for the selective adsorption of GOM. After sampling step, which usually occurs for 2 hours, the annular denuder is flooded with zero air and heated to 500°C, for 15 minutes, so that the collected GOM is reduced to elemental form. The released GEM easily travels through the sampling lines up to the Tekran 2537 analyzer, in order to be detected and quantified by CVAFS, according to the steps previously reported. The desorption period is not instantaneous but usually, three measurement cycles, 5-minutes each, are necessary to completely remove the adsorbed mercury. Typically, most of the loading is released during the first cycle; however, the actual GOM concentration is represented by the sum of all the three measurements. The desorption step also regenerates the denuder coating, which is ready for another cycle, after cooling.

In addition, the sorbent surface in the denuder can be periodically recoated with a sub-saturated KCl solution.

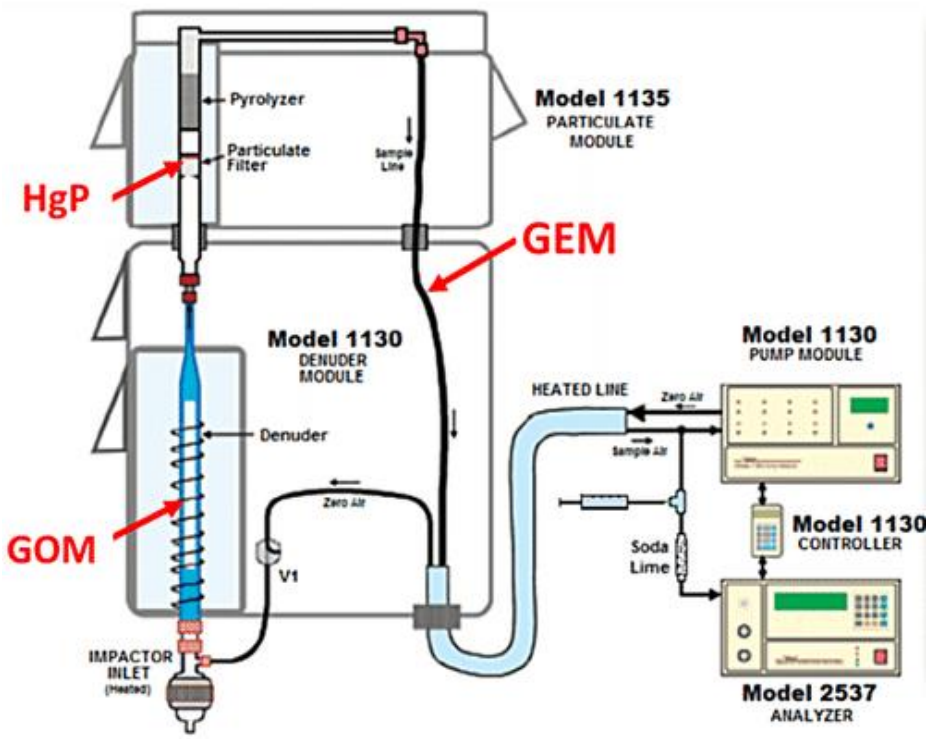

Fig. 2.2 Schematic diagram of 1130-1135 speciation units [46]

For example, SOPs established in the framework of the GMOS network requires denuder recoating after 15 days [51].

The Tekran unit 1130 can be interfaced with another module, Tekran 1135 unit (Fig. 2.2), which allows the sampling of particulate bound mercury (PBM), which is then determined by CVAFS, through the Tekran 2537 analyzer. All the considerations about the difficulties in obtaining reliable measurements of GOM also apply to PBM sampling, as confirmed by the occurrence of artifacts during sampling widely discussed in the literature [45]. Biased measurements are also due to the uncertainties about the PBM exact composition: less is known about the chemical forms of mercury that are adsorbed on airborne particulate matter. The analytical strategy currently used for the determination of PBM into an air sample stream, therefore, relies on the collection of this fraction on a particulate filter, which is then subjected to analysis. Even in this case, the only automated method that is commercially available is the

Tekran module 1135, which uses a regenerable particulate filter (RPF) to capture the finer fraction of particulate, which is less than 2.5 um diameter. This step is achieved by passing the air stream through an impactor before entering the denuder in order to eliminate coarse particles (> 2.5 um). The resulting air stream flows through the RPF, which traps the required fraction, while GEM passes through. Then, RPF is heated to 800°C in order to desorb the captured particulate, which reaches the pyrolyzer. The pyrolyzer consists of a quartz tube (approximately 50 cm length and 0.95 cm diameter) filled with densely-packed quartz chips, which are maintained at 800°C, in order to ensure a complete decomposition of PBM to elemental Hg [52]. Thus, PBM is quantified as GEM using CVAFS in the downstream 2537 analyzer, after being cooled in a long quartz tail. As for GOM, the desorption step is not immediate; the concentration of PBM, therefore, results from the sum of the concentration of the three particulate heat cycles, subtracted of the blank value of the particulate filter. As previously mentioned, the 1135 particulate unit is also implemented to 2537 analyzer along with the 1130 for GOM determination, allowing a complete speciation analysis of mercury in the air. In this configuration, the three units are synchronized: during the sampling mode, which lasts 2 hours, a pump module pulled ambient air into a glass elutriator inlet, which is connected to the denuder and the RPF modules, at 10 Lpm maintaining a temperature of 50 °C for the entire system, to avoid moisture. GOM is quantitatively collected onto the KCl-coated quartz annular denuder whereas PBM and GEM continue along the sample line until PBM is collected onto RPF and GEM reaches the 2537 analyzer. Following this sampling step, during which the system provides for 5 minute GEM concentrations, a 1-hour desorption cycle is initiated.

2.3 Alternative techniques for passive monitoring of Hg in air

Filling the gap in the knowledge of mercury temporal and spatial patterns requires accurate monitoring, which extends also to the remote areas worldwide. However, the traditional techniques that have currently been employed are not always suitable for the application in some regions, such as Polar Regions, remote islands, or high summits, which are difficult to reach or provide no adequate conditions (e.g. power supply). Furthermore, current monitoring methods show various limits and artifacts,

directly affecting measurement results [53]. Indeed, some drawbacks are the high costs of maintenance, the constant need for high-energy supply as well as compressed gases, and the demand for well-trained instrument operators [54]. In this scenario, the need for alternative approaches to Hg monitoring appears evident. Thus, the scientific community is working toward the development of new technologies or devices for the Hg monitoring, such as innovative passive air samplers (PASs) which potentially complement traditional active approaches, greatly improving the spatial resolution of measurements. In effect, the strategy behind the use of passive air samplers is that they can be deployed in different locations, without requiring supervision or maintenance. In addition, small dimensions of the whole device are preferred in order to be easily portable and compact. The operation principle is based on the collection of a gaseous pollutant on a sorbent surface via diffusion processes that are regulated by the first Fick's Law ([54,55]):

$$SR = \frac{DA}{L} = \frac{m}{tC}$$

In these equations:

- SR is the sampling rate, which quantifies the volume of air that is effectively stripped of target compound per unit time;
- D is the molecular diffusion coefficient of the target compound in air, namely Hg;
- L is the thickness of the diffusion layer;
- A is the collection surface area;
- m is the mass of sorbed compound;
- t is the deployment time;
- C is the ambient concentration of the target pollutant.

The former equation allows the theoretical sampling rate calculation, involving the molecular diffusion coefficient (that is specific for each compound in a certain medium) and the geometry of the sampler device. Indeed, the target compound migrates onto a collection surface with a rate that is as higher as the area is larger and the length of the diffusive path is shorter. The latter equation is used to determine experimentally the rate at which the chemicals diffuse, by quantifying the mass sorbed during exposure for a certain time period at a known concentration of the pollutants.

Thus, once PAS is calibrated, SR is obtained; PASs can, therefore, be used for outdoor and indoor deployment, and even for occupational purposes [56]. Indeed, passive samplers show various advantages, such as the possibility to be easily deployed, owing to the reduced dimensions (compared to the traditional instruments), simplicity in the handling, independence from the power supply and gas cylinders. Although different passive air samplers exist for Hg monitoring, they all rely on the use of a sorbent material that has a high affinity for mercury species, thus creating a concentration gradient, responsible for the diffusion of the target pollutant from a certain volume of stagnant air to the material itself, while turbulence is reduced. In this case, the target compound is mercury species in the air, being solely Hg^0 (GEM) or the sum of all the gaseous compounds (TGM), depending on the kind of material. Particulate mercury is excluded since it difficultly passes through the diffusion barrier.

Common PASs for Hg monitoring can be either biotic or abiotic. Biotic passive samplers include the leaves of plants, lichens, mosses, and tree rings whereas abiotic samplers include different types of samplers, with radial and axial samplers being the most common commercially. PASs with radial shape commonly consist of a cylindrical sorbent surrounded by a parallel diffusive barrier, which allows increasing the sampling rate by maximizing the surface area. Numerous radial PASs result from the combination of a commercial diffusive barrier, the well-known Radiello, with different sorbent material, e.g. activated carbon or sulfur-impregnated activated carbon. McLagan et al. [57] proposed a passive air sampler for measuring gaseous Hg using sulfur-impregnated activated carbon as sorbent material implemented into a Radiello diffusive barrier. These radial samplers are supposed to have a higher sampling rate than axial design, due to the higher ratio surface to length (A/L), and to be only partially affected by the meteorological conditions since SR slightly increases with both temperature and wind speed across ranges relevant to outdoor deployments [58].

In axial devices, the adsorbing matrix is usually a disk-shaped membrane, with different thicknesses and porosities. A new axial PAS for gaseous elemental mercury has been recently developed in the framework of the GEF-funded UNEP project “Development of a Plan for Global Monitoring of Human Exposure to and Environmental Concentrations of Mercury” by researchers of the Institute of

Atmospheric pollution of the National Research Council (CNR-IIA). Indeed, Macagnano et al. recently developed an innovative sorbent material with a nanostructured pattern, resulting from the deposition of Titania nanoparticles (TiO_2NPs) properly functionalized with gold nanoparticles (AuNPs) [59]. This material is deposited onto a quartz fiber filter in order to obtain a passive membrane that is implemented into a borosilicate glass vessel, similar to the commercially available Analyst [60]. More details about this type of passive material are given in the following chapter.

After PAS is deployed, the collection surface has to be analyzed for the quantification of the sorbed Hg mass, which is then elaborated through the use of the first Fick's Law in order to obtain the time-averaged concentration of the pollutant in the air. The analysis step is achieved by different approaches, which depend on the type of device and sorbent material. The most common techniques involve thermal desorption, which is the release of the target compound after sorbent material is heated, and extraction, which can be achieved by acid or solvent addition and allows the contaminant to be separated from the collection surface. The subsequent quantification step occurs using the common analytical approaches, as CVAAS, CVAFS or ICP-MS [54]. Basically, the thermal desorption keeps the material unaltered, which could be regenerated and reused, whereas acid digestion totally destroys the material, which has to be replaced. Some commercial analyzers exist for the thermal desorption and subsequent quantification of the Hg sorbed onto the collection surface, as Nippon MA3000 (Nippon Instruments Co.) and DMA-80 (Milestone). Nevertheless, also lab-made systems have been implemented to traditional Hg analyzer, for the desorption and quantification of the sorbed Hg mass. For example, researchers from the Institute of Atmospheric Pollution of the National Research Council (CNR-IIA) planned a lab-made furnace, consisting of refractory material, that is capable to reach 550°C for promoting mercury desorption from their passive membrane, contained into a cylindrical gas chamber and connected to the CVAFS analyzer Tekran 2537 (Fig. 2.3). According to the type of passive sampler, meteorological conditions, as temperature, relative humidity, and wind speed, can significantly affect the sampling rate.

Fig. 2.3 Thermal desorption system for the analysis of passive samplers developed by CNR-IIA

For example, McLagan et al. investigated the effect of the temperature and wind speed on a radial sampler, based on a sulfur-impregnated activated carbon sorbent contained into the diffusive body of a Radiello cartridge [58]. Indeed, they tested the uptake rate at different values of temperature and wind speed in order to calculate the correction factor for these parameters. Consequently, it was possible to adjust the SR value, for cases where the actual climatic conditions are different from those set during the calibration procedure. In the same way as radial samplers, axial samplers also experience the effect of meteorological conditions, with SR increasing with both wind speed and temperature.

2.4 Traditional techniques for monitoring of Hg in water

When the analysis of total mercury (THg) in aqueous matrices, like wet deposition or seawater, or any other solid matrix opportunely extracted, is required, one of the traditional instruments, which was also used for the research study herein presented, is the analyzer for liquid samples commercialized by Tekran. This instrument results from three interconnected Tekran subunits: an autosampler (Tekran 2620), a peristaltic pump (Tekran 2610), and a detector (Tekran 2600).

In the same way as the unit 2537, its detector relies on CVAFS for an accurate and sensitive quantification of the mercury trapped with the dual gold amalgamation technique, in accordance to the protocol proposed in the EPA method 1631 “Mercury in water by oxidation, purge, and trap, and cold vapor atomic fluorescence spectrometry” [61]. This method suggests how to treat the aqueous samples, from the initial preparation to the final quantification. Indeed, liquid samples contain mercury

in different forms, which mainly include divalent mercury. Thus, sample preparation covers a key role in the analysis process. According to the protocol, before starting analysis a strong oxidant solution, bromine monochloride (BrCl), has to be added to the sample in the concentration of 1% v/v in order to convert all the mercury compounds, present in the sample, to Hg^{2+}. This step is also necessary to preserve the sample and to avoid mercury losses due to adhesion to the flask walls. Prior to measurement, aliquots of hydroxylamine hydrochloride ($NH_2OH \cdot HCl$) neutralize the excess of BrCl, as well as the free Cl_2 and Br_2 produced by the oxidation reaction. Then, the aqueous sample is located in the autosampler unit Tekran 2620 and is withdrawn from the support of a peristaltic pump equipped with five different channels, allowing the flow of the sample, a reducing agent, ultrapure water (2 channels), and waste. A "Y" fitting connects the sample tube to the reducing agent tube, containing a 3% solution of $SnCl_2$; in this way, the oxidized mercury contained in the sample is quantitatively reduced to volatile Hg^0. Then, the solution containing the volatile mercury species reaches the phase separator (PS), composed of a quartz rod enclosed into a quartz tube, which is necessary to split a solution into gas and liquid. Indeed, along this central rod, the solution containing the newly developed elemental mercury flows whereas argon as carrier gas flows upstream in order to strip the elemental mercury from the solution and carry it into the detector module. Meanwhile, the remaining solution is discarded.

At this point, the elemental mercury undergoes a dual-stage gold amalgamation step to preconcentrate Hg on gold cartridges, as seen for Tekran 2537. In the detector unit, two cartridges are present, with the first being a gold sand cartridge, which serves for pre concentrating Hg while possible interferents (water vapor, organic solvents, halogens) pass through, thus these do not reach the cuvette. A first heating step of this cartridge at 550°C ensures the thermal desorption of the trapped Hg, which is carried to the second cartridge. The second trap is composed of pure gold particles and represents the analytical cartridge, which is responsible for the quantification of Hg present in the sample. Indeed, all the mercury adsorbed onto this cartridge is released by thermal desorption and sent to the quartz cuvette for detection. The cell uses Cold Vapor Atomic Fluorescence Spectroscopy for the quantification of mercury. In the detector, the cuvette is illuminated by a low-pressure mercury-vapor lamp, which

emits radiation at 253.7 nm able to excite any mercury atoms present. Then, Hg atoms re-radiate at the same wavelength, and a photomultiplier tube selectively views the fluorescence produced, which is proportional to the concentration elemental mercury present in the cuvette.

This technique is much more sensitive than atomic absorption and suffers less from positive interferences, resulting in very low detection limits, in the ng L^{-1} range. When operating with these highly sensitive instrumental techniques for the analysis of aqueous samples, a problem of major concern could be the blank contamination, due to the low concentration of mercury that is usually detected in this kind of sample. Indeed, each glassware material and sample flasks, as well as the working environment, has to be well cleaned, in order to avoid biased measurements. A major threat arises from the contamination during the sampling phase, which can compromise the subsequent analyses. Indeed, different precautions should be taken as regards the materials of the sample container, as well as their cleaning. Within the GMOS project, different Standard Operational Procedures (SOPs) were developed to suggest the optimal cleaning procedures for each tool involved in the sample collection and storage, mainly addressed to wet deposition sampling but also applicable to other aqueous matrices [62]. According to these SOPs and to literature findings [63][64], glass and FLPE bottles well fit for the storage of samples with low-pM levels of mercury. In the SOP "Method for the determination of total mercury in precipitation" [62] a revised version of the EPA method 1631 for cleaning sampling bottles suggests the use of acetone, alkaline detergent, 3.5 % HNO_3 at 65-75 ºC for at least 6 hours, and 1% BrCl for at least 24 hours for a complete removal of any Hg trace. After the cleaning procedure, the addition into the bottles of 20 mL L^{-1} of 0.8% high purity HCl preserve the sample while it is in the field. It is also important to seal the bottles and place them inside three brand-new zip-lock bags.

2.5 Sample preparation protocol alternative to EPA 1631 for Hg in biota

As previously mentioned, the analysis and quantification of total mercury in solid samples is not much different from that of liquid ones, except for a pre-treatment process necessary to convert the matrix from solid to liquid. Indeed, once the

conversion to liquid occurs, the analysis and quantification of total mercury can be performed by CVAFS, as previously described, following EPA method 1631. The appendix of this method provides for the sample preparation procedures necessary for the oxidation of total mercury (Hg) in solid and semi-solid sample matrices [65]. These procedures may be used in conjunction with EPA method 1631 for the determination of mercury in tissue, sludge, sediment, soil, industrial samples, and certified reference materials. In detail, for matrices containing organic materials, such as sludge and plant and animal tissues, the digestion of 0.2 - 1.5 g is achieved with a mixture of HNO_3/H_2SO_4 and is completed with a BrCl solution, which destroys the remaining organic material and converts methylmercury to inorganic mercury, Hg^{2+}. After preliminary digestion at room temperature, the sample has to be heated on a hot plate and refluxed for 2-3 hours to fully oxidize the remaining organic matter.

For geologic material, a portion of the sample (0.5 - 1.5 g) is digested with aqua regia (HCl/HNO_3) to solubilize inorganic materials. The dissolution reaction generates nitrosyl chloride (NOCl) and free Cl_2, which are both strong oxidants for Hg-containing compounds, including cinnabar (HgS), which is otherwise more slowly attacked by BrCl. Aqua regia also converts all methylmercury to Hg^{2+} but is not strong enough to dissolve silicate minerals. This step requires at least 4 hours to complete.

It seems clear that both these procedures require very long analysis time, which can be tedious when a great number of samples have to be analyzed. In addition, they can be subject to Hg losses, contamination as well as reagents consumption and waste production. Therefore, alternative sample preparation approaches become necessary. One of the best strategies to reduce all the disadvantages previously mentioned is to speed up the oxidation of organic compounds and promote the rupture of chemical bonds by microwave-assisted heating of the sample, into a closed system containing the sample. Indeed, microwave digestion has revealed a good technique for the degradation of a great variety of sample matrices, being tissues, soils or sediments. It relies on the use of electromagnetic radiations, interacting with polar molecules in order to cause intermolecular collisions that produce heat and dissolve samples [66]. Compared to conventional heating, as for EPA method 1631, where the reaction mixture is heated in a conductive way, microwave irradiation results in a more efficient internal heating by direct coupling of microwave energy with dipoles and/or ions that

are present in the reaction mixture. Thus, the conversion of electromagnetic energy into heat energy works efficiently and results in extremely fast heating rates – not reproducible with conventional heating.

Solid samples are therefore converted into representative liquids using the appropriate digestion solution, which can be one or a mixture of reagents, usually strong acids and/or strong oxidants, according to the type of the matrix in question. The most commonly used acids for digestion include nitric acid (HNO_3), hydrochloric acid (HCl), hydrofluoric acid (HF), sulfuric acid (H_2SO_4), perchloric acid ($HClO_4$), and aqua regia (HCl/HNO_3 3/1). Strong oxidant reagents, as hydrogen peroxide (H_2O_2), can also be added to the acid mixture to enhance the digestion power.

By using microwave technology, it is possible to heat up the sample solution extremely fast and perform digestions at high pressures and temperatures, due to the applied pressure vessels even far above the boiling point of the used acids. The possibility to set temperature gradients reduces the digestion time down to only a few minutes. In addition, issues related to contamination and losses through volatilization are minimized. This all results in improved reproducibility if compared to the traditional sample preparation methods.

Chapter 3

Application of Hg monitoring techniques to different case studies

3.1 Introduction

Some of the research studies carried out during my Ph.D. were achieved through the application of the techniques previously described:

1. monitoring of Hg species in the marine atmosphere as well as the aquatic environment of the Mediterranean Sea;
2. field application of newly-developed passive devices through the comparison with the conventional active techniques;
3. development of an appropriate sample preparation strategy for the monitoring of total Hg and other heavy metals in fertilized soils and in the carabid beetles *Harpalus (Pseudoophonus) rufipes*.

These investigations will be presented in three case studies. In the first case study, the results of the measurements performed during an oceanographic cruise campaign organized by CNR-IIA to which I took part in summer 2017. The findings reported in the second case study are a small part of a wider intercomparison campaign exercise carried out from February to April 2019 among different passive air samplers. In this intercomparison campaign, I focused on the deployment, quantitative analysis and data elaboration of the passive devices developed by CNR-IIA in recent years, whose structure has undergone improvements during my Ph.D. studies. The third case study deals with the monitoring of Hg and other metals in fertilized crop fields and in insect specimen living in them, *Harpalus (Pseudoophonus) rufipes*, exploiting sample preparation protocol alternative to that suggested in EPA method 1631. In this study, which was carried out in collaboration with researchers from the Department of Ecology of the University of Calabria, I was concerned with the assessment of a plausible protocol for sample preparation, analyses and evaluation of the results from a chemical point of view.

3.2 Case study 1: Oceanographic Campaign in the Mediterranean Sea Basin

3.2.1 Project aim and study area

In the framework of the MED-Oceanor measurements program ”Atmospheric Mercury Chemistry in the Marine Boundary Layer”, funded by the Italian National Research Council (CNR) [67], a cruise campaign was carried out onboard the Research Vessel "Minerva Uno" from August 18th to September 7th 2017 in the western Mediterranean Sea. The aim of this campaign was to investigate the influence of volcanic sources on the pattern of speciated mercury in the Marine Boundary Layer (MBL).

The Mediterranean Sea basin is among the most interesting semi-enclosed areas in the world owing to its unique geographic position and its peculiar meteo-climatic conditions have experienced a relevant pollution load [68]. Natural sources, as Saharan dust outbreaks, wildfires, volcanoes, and related geological activities, as well as anthropogenic ones, like dense ship traffic and highly industrialized sites, account for the increasing pollutant levels in the atmosphere [69]. From a geological point of view, the Mediterranean Sea presents various structures tectonically active; consequently, the emissions from volcanic activity could impact on human health and ecosystem. Compared to other areas in the world, a considerable concern is addressed to the Mediterranean Sea since numerous volcanoes, as well as solfataras and fumaroles, are present, some of them being among the most active in Europe, like Etna, Stromboli and Vulcano.

In this scenario, it is extremely important to know their mercury contribution to the atmosphere. This was the driving force behind the choice of the monitoring sites throughout the campaign, which therefore included 13 marine sampling stations near volcanoes. The cruise campaign consisted of scheduled stops and route legs, starting from the Brindisi Harbor on August 18th, and going southward to Sicilian coasts, then northward to the Gulf of Naples, passing from Marsili, and then back southward to the Aeolian Archipelago on September 7th. In particular, the scheduled stops included Acireale, Acicastello, Marsili, Ischia, Phlegraean Fields, Gulf of Naples, Panarea, Vulcano, and Stromboli (Fig. 3.1). A brief description of each sampling site is given below.

- Mount Etna is one of the most active volcanoes worldwide, which has shown frequent paroxysmal episodes as well as passive degassing periods. Considering that the atmospheric circulation in the Etnean area is usually

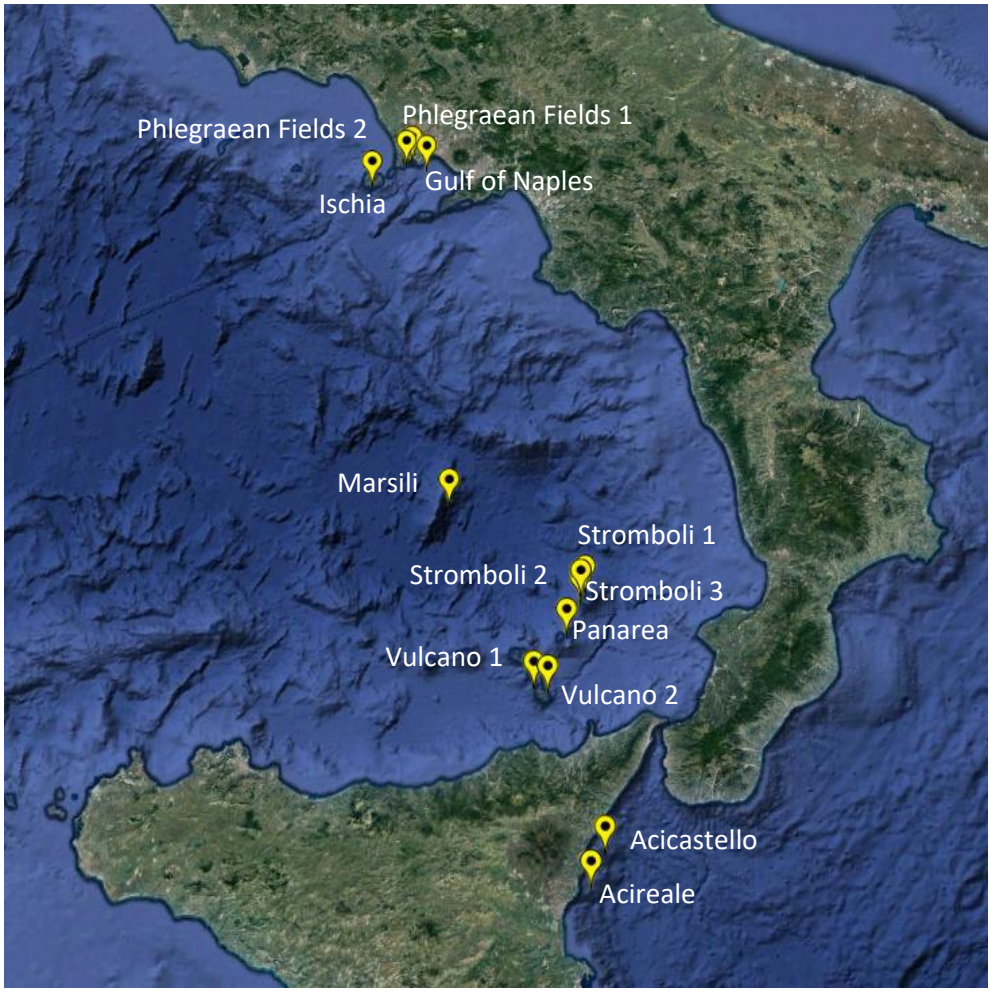

Fig. 3.1 Sampling sites selected for the Hg monitoring during the MED-Oceanor 2017 campaign

predominantly westerly to northwesterly, sampling sites in this area were chosen in front of the Acireale and Acicastello coasts.

- Part of the Aeolian volcanic arc, Stromboli is characterized by permanent activity and continuous gas emissions. Indeed, it has a significant hydrothermal system [70], as well as "open-conduit" volcanoes able to degas very large quantities of unerupted magma directly into the atmosphere. Three different sampling sites around the island of Stromboli were monitored, labeled as Stromboli 1, 2 and 3.

- Marsili Seamount is an underwater explosive volcano (3.5 Km depth), which has an active magmatic chamber at about 2.5 km below the summit. This area was monitored by a sampling stop above the crater of the volcano.
- Phlegraean Fields are a complex volcanic area located west of the city of Naples, which comprises numerous craters e volcanic structures, such as the Solfatara volcano, each contributing with several explosive vents having predominant ENE and NNW trends. In this area, sampling was performed at a distance of about 1 Km at two different sites, namely Phlegraean Fields 1 and 2.
- Vulcano is the southernmost of the seven islands forming the Aeolian Archipelago in the Tyrrhenian Sea. Its activity is characterized by vigorous fumarole emissions around the summit crater, known as La Fossa. In Vulcano, the sampling was performed at two sites, labeled as Vulcano 1 and 2.
- Ischia is the westernmost active volcanic complex of the Campania area and belongs to the Phlegraean volcanic district, which also includes Phlegraean fields. Thermal manifestations characterize Ischia as thermal waters and fumaroles, most of which are concentrated along the faults affecting Mt. Epomeo. In this area, sampling was performed in a site labeled Ischia.
- Panarea Island lies in the western sector of a submarine 120 m deep platform in the Aeolian Archipelago. It has long been considered extinct and it only shows manifestations of secondary volcanism, mainly submarine (fumaroles and gas emissions). One sampling site was chosen in this area.

With the overall aim to understand the chemical-physical mechanisms occurring in the marine boundary layer (MBL), both air and water compartments were investigated by means of conventional techniques. Indeed, the different species of mercury in air were continuously measured using the Tekran speciation unit along the route. In addition, in each site seawater samples were collected at different depths in order to obtain information about the horizontal and vertical distribution of total mercury.

Moreover, meteorological parameters were acquired during the whole campaign in order to take into account the different climatic conditions. In detail, air temperature, wind speed, wind direction, and atmospheric radiation were monitored using the

automatic meteorological station placed on the research vessel. Moreover, navigation data, namely coordinates of the vessel position, navigation direction, and the shipping speed, were supplied with 1 min time resolution.

3.2.2 Air sampling and measurements

In each site, continuous atmospheric measurements were performed using the conventional integrated system by Tekran, composed of the three units 2537A, 1130, and 1135 [71] for the simultaneous collection and analysis of the different Hg species, GEM, GOM, and PBM, respectively. The speciation units were positioned on the rooftop of the research vessel at about 10m above the sea surface and connected to the GEM 2537A analyzer through a heated PTFE line (50°C, 10 m in length). The whole system was configured to collect 2 hours GOM and PBM samples on a quartz KCl-coated annular denuder and quartz filter assembly, respectively, with a 1-hour desorption step, while GEM was sampled and detected every 5 minutes. Different precautions were taken to allow the speciated system working properly during the whole campaign; for example, KCl-coated denuder was replaced after 15 days to avoid passivation. In addition, an external heated boot was placed around the impactor to reduce the RH influence. Following the SOPs within the GMOS project [51] the Tekran analyzer was calibrated on a 71 h basis using the internal permeation source. With a flow rate of 1 L min^{-1}, the detection limit for GEM was 0.1 ng m^{-3}, whereas the method detection limit (MDL) for GOM and PBM, calculated as three times the standard deviation of field blanks (3σ), was 0.7 pg m^{-3}.

In addition to the measurement of the three Hg species, ancillary parameters were continuously recorded, namely O_3, NO_x, and SO_2 using the Teledyne analyzers API Model 400E, 200E, and 100E, respectively, located on the top deck (about 10 m a.s.l.). All these instruments were calibrated at the beginning of the campaign and regular zero and span checks were carried out every 2-3 days. O_3 analyzer operated with a sampling resolution of 1 min at a flow rate of 0.8 L min^{-1}, whereas NO_x and SO_2 analyzers had a sampling flow rate of 0.5 and 0.6 L min^{-1}, respectively; all the detectors provided data with 1 min time resolution. Unlike O_3, which uses the absorption method, and SO_2, which uses the fluorescence method, the NO_x analyzer relies on the chemiluminescence method coupled with state-of-the-art microprocessor technology

to provide the sensitivity and stability necessary for the ambient detection of the total nitrogen oxides NO_x. The monitoring of these parameters revealed useful for the investigation of the possible sources of each Hg species in the MBL. Indeed, high Hg concentrations could result in the Mediterranean basin due to the intense solar radiation, which initiates photochemical reactions resulting in high O_3 levels [30]. This is typically true for the Mediterranean area, due to its peculiar climatic summer conditions, characterized by high temperature and high synoptic pressure values [72]. As regards the nitrogen oxides, their spatial distribution allows distinguishing sites affected by anthropogenic sources from sites with a predominance of natural sources, while sulfur dioxide is commonly used as a tracer of volcanic emissions [73].

3.2.2.1 Data treatment and backward trajectory model

Meteorological data were treated in order to consider the movement of the research vessel: in particular, data obtained when the shipping speed was smaller than wind speed and the difference between wind direction and ship course was less than 30° were neglected since they could be affected by the stack emissions of the ship. In addition, at each sampling site, special care was taken to anchor the research vessel in the opposite direction of the wind, in order to avoid the contamination from the ship plume.

In this regard, in conditions of calm wind (lower than 1 m s^{-1}), which occurred for the 7% over the total campaign, short transepts were run around the selected site, moving at low velocity (< 1 knot).

Other than meteorological data, also the results of the automatic instruments were processed for quality issues, above all those for Hg monitoring.

Following the SOPs and the GMOS-Data Quality Management (G-DQM) system, developed within the GMOS project, it was possible to check the quality of the data resulting from the Tekran speciation unit [48].

The evaluation of the measurements was accomplished using different complementary tools. In particular, the Hybrid single-particle Lagrangian integrated trajectory model (HYSPLIT), available at the NOAA Air Resources Laboratory [74], was used to calculate 72 h backward trajectories to check the origin and pathway of the air masses collected aboard the RV at midday, at midnight and when the RV was stopped at each

station. The analysis was performed using the READY website with the GDAS meteorological dataset, characterized by a grid-scale of 0.5 degrees.

In addition, daily maps from NCEP (National Centre for Environmental Prediction) /NCAR (National Center for Atmospheric Research) Reanalysis data were obtained at a geo-potential height equal to 850 mbar and 1000 mbar to show the air mass circulation (cyclone or anticyclone) in the Mediterranean region, delimited by the coordinates 15°- 70° N and 15° W – 50° E.

3.2.3 Air measurements results

3.2.3.1 Meteorology

During the cruise campaign, local weather conditions were mainly characterized by the absence of precipitations, sunny and quite hot days, in line with seasonal climatology. Indeed, low wind speed and stable average daily values of temperature and pressure were registered. In detail, the average wind intensity was 3.8 m s^{-1}, ranging between 0.3 and 13.5 m s^{-1}. As regards the synoptic pressure, it varied in the range 1008.8 - 1019.6 hPa, with a mean value of 1014.1 hPa. The average temperature was 26.1 °C and varied between 22.1 and 31.2 °C during the entire campaign, with the maximum at Vulcano 1. From the NCEP/NCAR Reanalysis maps, these conditions find confirmation in the expansion of the Azores Anticyclone over the Mediterranean basin, which persisted throughout the sampling campaign, until September 2nd, when the anticyclone moved northeastward up to Central Europe (Fig. 3.2). This favored the development of low-pressure systems, which resulted in a strong negative pressure anomaly. Indeed, rough seas and strong wind were encountered, forcing a stop in the Lipari harbor. A summary of the meteorological conditions is reported in Table 3.1.

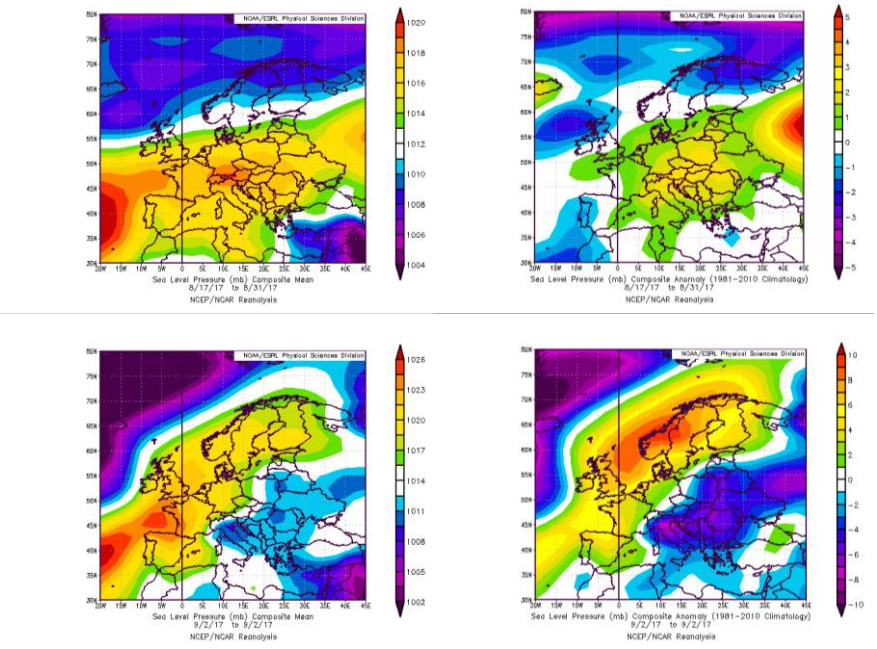

Fig. 4.2 NCEP/NCAR reanalysis maps (mean and anomaly) of August 31st (up) and September 2nd (down)

	Average ± SD (Range)
Air Temperature (°C)	26.1 ± 1.2 (22.1 - 31.2)
Wind Speed (m s^{-1})	3.8 ± 2.5 (0.3 – 13.5)
Air pressure (hPa)	1014.1 ± 2.5 (1008.8 - 1019.6)

Table 3.1 Meteorological parameters measured during the campaign

3.2.3.2 Hg species and O_3, NO_x, SO_2 trends

With the aim to obtain comparable values of the different Hg species, the values of GEM, GOM and PBM concentration were averaged over 2 h corresponding to the sampling duration of both GOM and PBM, as set in the Tekran integrated system configuration.

As regards the GEM values, it showed a quite large variability from 0.66 ng m^{-3} to 4.32 ng m^{-3}, with a mean value of 1.08 ± 0.29 ng m^{-3}. This result is slightly lower than the background levels observed in the Marine Boundary Layer (MBL) of the Western Mediterranean Sea detected during previous oceanographic campaigns [30,67].

Indeed, during the 2003 summer cruise campaign the detected GEM value was 1.7 ng m^{-3} for the western sector of the Mediterranean area whereas, during the 2010 summer campaign, it was 2.0 ng m^{-3}.

During the 2017 campaign, the maximum GEM values, 4.32 and 3.41 ng m^{-3}, were recorded in the Campanian area, at Phlegraean Fields 1 and 2, respectively.

As regards the gaseous oxidized Hg compounds, the average concentration over the whole campaign was 15.38 ± 12.65 pg m^{-3}, showing a broad range from 1.98 to 76.40 pg m^{-3}. The highest peak was detected in the Aeolian area, in Vulcano 1, where volcanic degassing and/or eruptions can have a significant impact on the Hg emission levels [75]. Later on, this peak will be evaluated with the support of backward trajectories, in order to seek any possible sources and confirm the role of volcanic emissions. From the plot of GOM trend during the cruise campaign, it can be seen the typical diurnal cycle with maxima during daylight, typically between 11:00-17:00, and minima during nighttime hours (Fig. 3.3) [30,76].

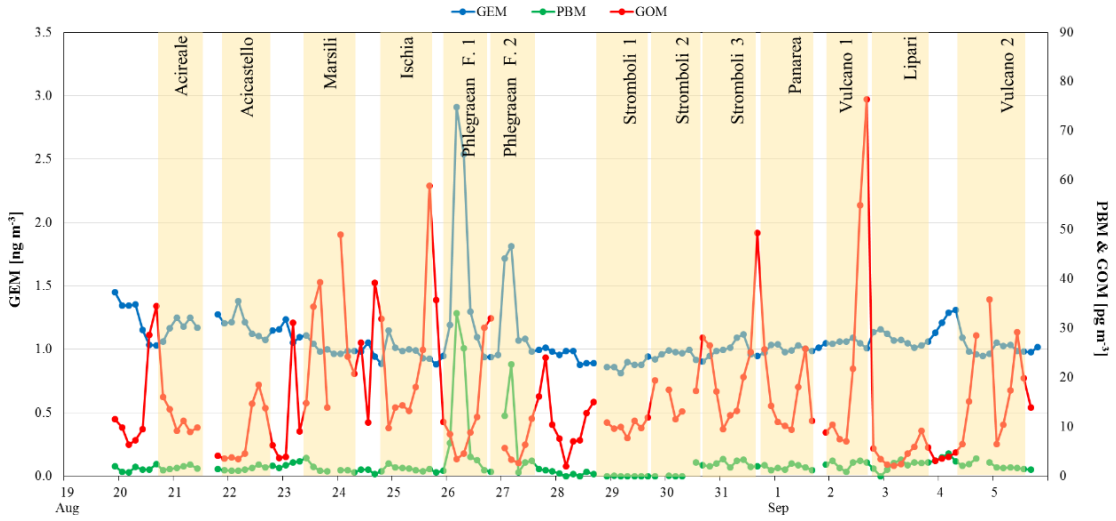

Fig. 3.3 GEM, GOM, and PBM trends detected throughout the campaign

Indeed, the maximum GOM concentration, in absence of anthropogenic influence, usually coincides with the maximum of the solar irradiation, indicative of photolytically produced oxidants, which in turn are responsible for the gas-phase oxidation of GEM to GOM. Apart from gas-phase oxidation processes, also direct emission from anthropogenic or natural sources and out-gassing of $HgCl_2$ from

deliquesced aerosol particles [77] are generally considered the main responsible for the GOM production. Anyway, it has been commonly accepted that the in situ oxidation reactions and $HgCl_2$ out-gassing from aerosol are the main sources of GOM in the MBL, due to the short atmospheric lifetime of GOM species, which makes transport from nearby anthropic sources a minor contributor in the marine atmosphere [30].

Regarding PBM levels, the mean value for the entire campaign was 2.42 ± 4.20 pg m^{-3} varying in the range between 0.70 and 33.02 pg m^{-3}. Its maximum values, 33.02 and 22.69 pg m^{-3} were registered in the Phlegraean Fields area, in both monitoring stops (1 and 2), where, as already seen, the GEM showed a concomitant increase, probably due to anthropogenic influence.

It is noteworthy keeping in mind that the integrated system by Tekran actually measures only the Hg bound to the finer fraction of particulate matter that is $PM_{2.5}$. Thus, the collected data mostly underestimated the marine as well as the volcanic contribution to particulate bound mercury, considering that numerous natural sources (i.e. sea spray, dust, volcanic ashes) in the Mediterranean area are known to contribute to high levels of atmospheric particulate matter mainly in its coarser fraction [76]. Considering that in the marine environment, sea spray provides for sea-salt particle surfaces on which pre-existing GOM can adhere, in ideal conditions, one might expect a correspondence between the GOM and the PBM diurnal cycle.

During the cruise campaign, the typical PBM diurnal cycle was not so clear, probably due to the coexistence of a mixture of various influences, thus hiding the expected PBM profile in the marine environment. As previously mentioned, further to the monitoring of Hg speciation in the MBL, also ozone, nitrogen oxides, and sulfur dioxide were acquired (Fig. 3.4). Regarding O_3, the mean value was 50.01 ± 9.26 ppb ranging between 1.16 and 77.80 ppb. As known from literature studies, the observed O_3 level increased during the day, due to the photochemical production, and reduced at night [78].

The spatial distribution of NO_x allows distinguishing sites affected by anthropogenic sources from sites with a predominance of natural sources. The mean value of NO_x recorded for the whole cruise campaign was 8.77 ± 13.59 ppb with the maximum values being 181.00 ppb. As it will be explained later, sites with a massive contribution

of NO_x, such as Phlegraean Fields 1 and 2, were considered as potentially affected by anthropogenic sources.

Regarding SO_2, the mean value was of 9.70 ± 1.88 ppb, showing quite a high variability in the range 6.39 - 28.79 ppb. The highest was recorded in Vulcano 1, maybe due to the interception of volcanic emissions. Indeed, SO_2 is used as a tracer of the degassing processes by geothermal sources, such as fumaroles and volcanoes.

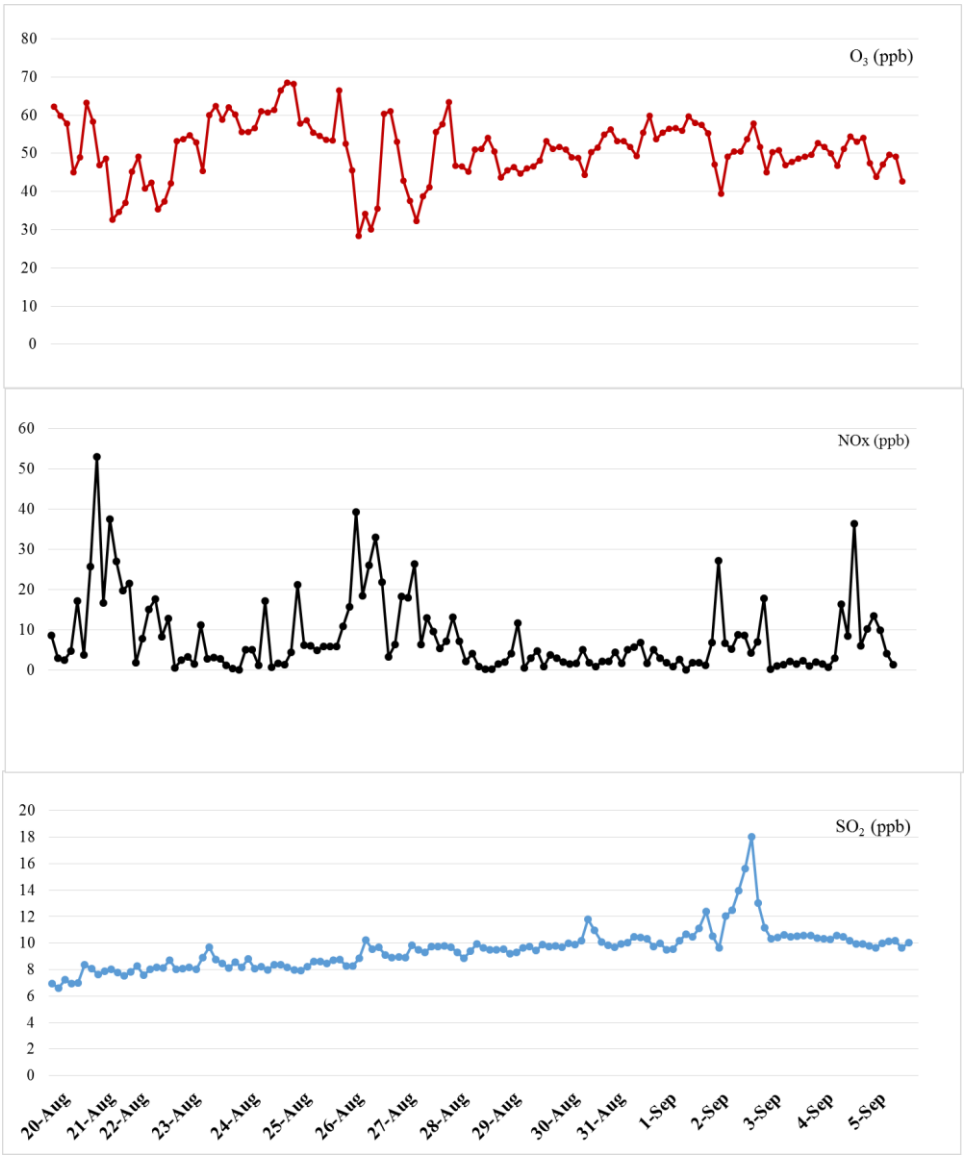

Fig. 3.4 O_3, NO_x, and SO_2 trends detected throughout the campaign

3.2.3.3 High Hg concentration events

During the measurement campaign, remarkable peaks of Hg were detected, and a thorough discussion about these specific events will follow in the next sections. Some Hg concentration peaks, as GOM peaks on August 24th at 16:50 UTC and on August 31st at 17:10 UTC, were neglected from the subsequent analysis since detected while the research vessel was moving to another monitoring site.

High GOM event in Marsili

The first high GOM peak of 48.95 pg m^{-3} was detected in Marsili at 01:50 UTC of August 24th. The increase in GOM concentration was not accompanied by an increase in PBM or GEM levels. The backward trajectory calculated at the vessel's position showed that air masses were coming from the sea surface over the open Mediterranean in the previous hours (Fig. 3.5-left), thus allowing us to exclude, for this specific event, any anthropogenic influence.

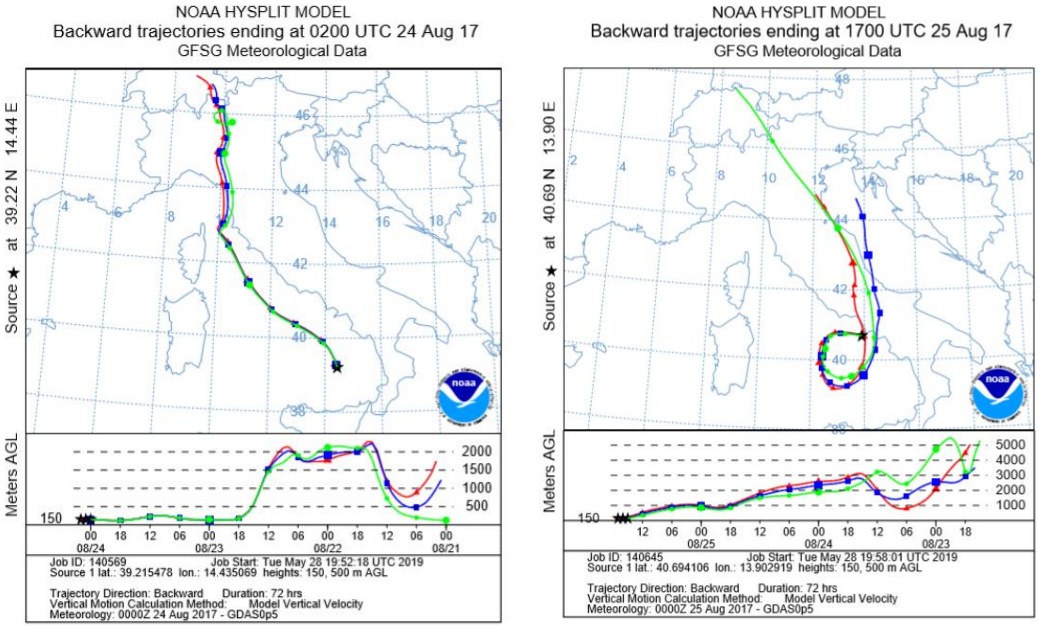

Fig. 3.5 Backward trajectory of air masses in Marsili (left) and Ischia (right)

The fact that this value was registered in the nighttime hours allows to exclude the association with photo-production processes and suppose that it could be due to an influence of volcanic emissions. However, this hypothesis is not supported by an

increase in SO_2 concentration. In addition, the possibility that this value results from the atmospheric transport from nearby sources can be excluded for the absence of neighboring sources and even for the meteorological conditions prevailing during that day, characterized by high temperatures and modest wind speed. Thus, maybe transport was not a major factor in determining the observed GOM concentration since it can be transported only for short distances from its point of production. A further attempt to explain the GOM peak results from the observation of the ozone levels within the daytime hours of August 23rd. Indeed, during this day the highest O_3 values of the entire campaign were registered in Marsili, in accordance with the high-pressure meteorological conditions, clear skies and high temperatures which are known to lead to photo-chemical ozone formation. The high ozone levels are most probably the main responsible of the photo-oxidation of elemental mercury to GOM, which persisted in the MBL, due to the low wind speed. Thus, wind speed, which controls the deposition velocity rates, avoids the removal of GOM, in conjunction with the high radiation, which controlled the presence of photochemically induced oxidants able to convert GEM into GOM [79–81].

High GOM event in Ischia

Another GOM peak, up to 58.86 pg m^{-3}, was registered at 16:50 UTC of August 25th, when the research vessel was stopped in Ischia. The backward trajectory (Fig. 3.5-right) also, in this case, showed that air masses traveled on the sea surface, away from the mainland. Thus, anthropogenic sources could be reasonably excluded. However, in this day very high levels of O_3 were registered, suggesting the possible relation with the GOM concentration. Therefore, the peak could arise from in situ oxidation of elemental mercury by photochemically driven reactions within the MBL, involving tropospheric ozone as one of the main oxidants, in accordance to the high values of the solar radiation (up to 743 W m^{-2}) [30]. This is also supported by the time of the GOM peak, which well fits with the diurnal trend of GOM, being maximum during daylight.

High PBM and GEM event in Phlegraean Fields 1 and 2

In the nighttime/early daylight hours of August 26th, a concomitant increase of GEM and PBM was measured in the Phlegraean Fields 1 site, up to 2.91 ng m^{-3} and 33.03 pg m^{-3}, respectively. The calculation of the backward trajectory (Fig. 3.6-left)

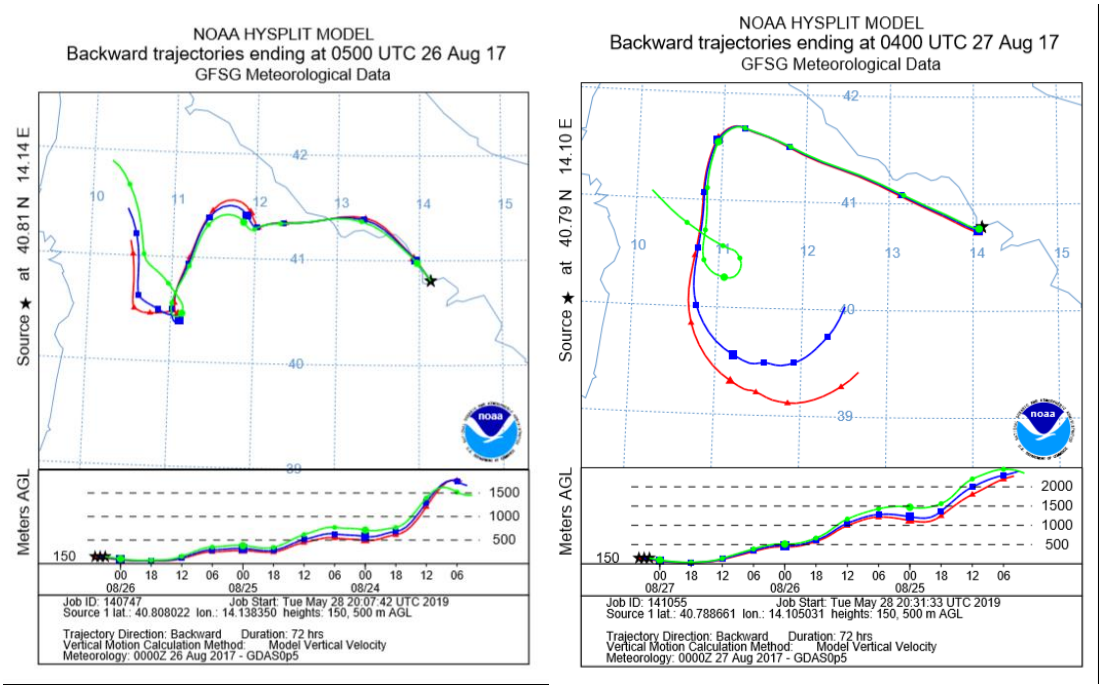

Fig. 3.6 Backward trajectory of air masses in Phlegraean Fields 1 (left) and Phlegraean Fields 2 (right)

immediately showed that air masses during the previous hours crossed the industrialized coast, northwesterly from the sampling area. This suggested that the most likely source of GEM and PBM is the anthropogenic activity in the Campanian area, which results in significant releases of Hg into the troposphere, in the form of GEM as well as PBM, due to the general pollution level, which contributed to increase particulate matter. Indeed, the Campanian mainland near the area under investigation experiences a high pollution load due to the intense traffic and industrial activities. As a confirmation, also nitrogen oxide concentration, which is commonly used as tracer of the anthropogenic sources, reached 56.93 ppb (Fig. 3.4). In correspondence, a decreasing in O_3 levels (average 43 ppb), suggests the influence of O_3 titration by shipping emissions, which reduce O_3 concentrations, as modeling studies reported [82].

In the same way, the subsequent day, in Phlegraean Fields 2, a slighter increase in GEM and PBM concentrations, up to 1.81 ng m^{-3} and 22.69 pg m^{-3}, respectively, was

detected. Even in this case, the path of the air masses (Fig. 3.6-right), traveling at low heights, crossed the industrialized coast, enriching with Hg species released by anthropogenic activity, as industries and shipping emissions.

High GOM concentration event in Vulcano 1

In Vulcano 1, on September 2nd, the highest GOM peak of the whole campaign was registered, namely 76.4 pg m^{-3}. Considering the intense volcanic activity of the Aeolian Islands, this peak was supposed to have a geothermal origin. Indeed, this peak was accompanied by a slight increase in the PBM concentration, up to 3.15 pg m^{-3}, maybe due to the rapid conversion of the GEM emitted from volcanoes or fumaroles into GOM and PBM [75].

Moreover, an intense peak in the SO_2 concentration was registered, supporting the hypothesis that the volcanic plume had been intercepted by the instruments onboard the research vessel. As a confirmation, the HYSLPIT trajectory (Fig. 3.7) showed the air masses crossing the Aeolian archipelago, specifically near Vulcano Island. In addition, the calculation of the Hg/SO_2 ratio in this area was about $2.9 \cdot 10^{-5}$, which is compatible with the classification of the passively degassing volcanoes reported in Pyle and Mather [73].

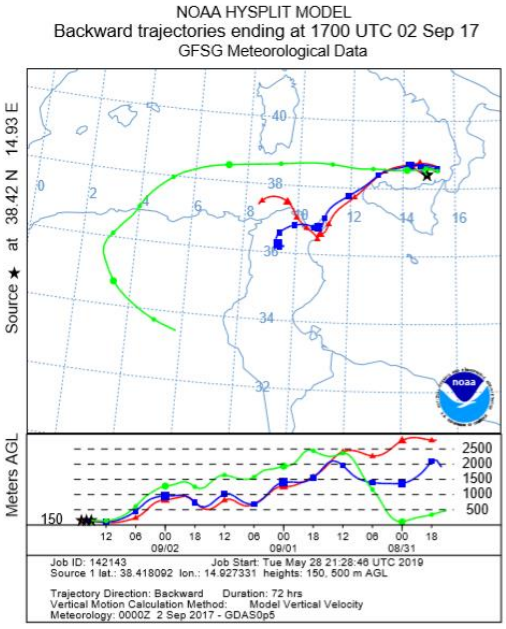

Fig. 3.7 Backward trajectory of air masses in Vulcano 1

3.2.3.4 GOM relation with the solar radiation

It has been previously said that, except for few cases, the GOM concentration during the oceanographic campaign mainly followed the typical diurnal cycle with maximum values being detected after sunrise and minima towards the evening hours. This suggested the absence of anthropogenic sources affecting GOM levels within the MBL, in accordance with its short atmospheric lifetime. Therefore, it is commonly accepted that the in situ gas-phase oxidation of Hg^0 and the out-gassing of $HgCl_2$ from aerosol particles are the main source of GOM production in the MBL, with the second process being favored by rough seas, but this was not the case of our campaign. The diurnal variation, therefore, could be attributed to greater daytime production favored by the photochemical reactions within the MBL. The Mediterranean Sea is an enclosed basin connected to the Atlantic Ocean by the narrow strait of Gibraltar through which water flow is driven by salinity and heat gradient. Therefore, the intense solar radiation over several months of the year, as well as the high temperature and extended periods with little or no precipitation strongly affect the distribution of the mercury species within the MBL. The influence of sunlight on the GEM oxidation can be deduced from the plot reported in Fig. 3.8 where the GOM concentration and the solar radiation in the PAR-UVA-UVB region, averaged over 3 hours, are reported.

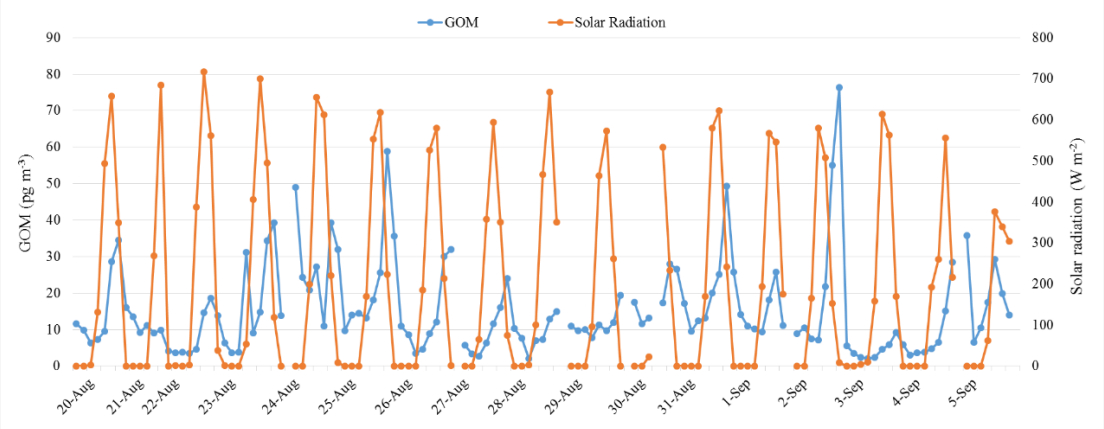

Fig. 3.8 Relationship between GOM concentration and solar radiation

Indeed, this graph, immediately illustrates the correspondence between the maximum GOM concentrations with the peak of the solar radiation, supporting the hypothesis

that the solar radiation indirectly rules the in situ oxidation of elemental mercury controlling the formation of oxidants like O_3 in the atmosphere.

3.2.4 Seawater measurements

3.2.4.1 Sampling and analysis

As previously mentioned, in addition to the atmospheric monitoring, also seawater samples were collected with the aim to investigate the horizontal and vertical variability. A number of 14 monitoring sites were selected which were quite the same as those selected for the atmospheric measurements; sampling points were added in Ischia, Gulf of Naples, and Vulcano whereas Stromboli 2 and Lipari was not performed. A list of all the monitoring sites is reported in Table 3.2. For each of them, a seawater sampler, commonly known as "CTD" allowed the collection of samples at a different depth, from the surface to bottom. This sampler (Fig. 3.9) consists of stainless steel rosette which hosts 24 Niskin bottles with a volume of 10 L and is also equipped with sensors for the simultaneous monitoring of conductivity, temperature, depth (hence the name CTD), as well as turbidity, fluorescence, and oxygen concentration. In addition, four field blank samples were collected in Acireale, Marsili, Ischia 1 and Vulcano 3, as representative of the area surrounding Etna (referred to as Sicily), Marsili, Campania, and the Aeolian Islands, respectively. While going underwater, these sensors allowed the acquisition of all the necessary parameters to select the depth levels at which sampling had to be performed. Conversely, while moving back toward the surface, each Niskin bottle opened and sampled the water corresponding to the selected depth level. Once back on the board, seawater samples were transferred from Niskin to FLPE 1L bottles, which were acid pre-cleaned in the laboratory following the procedure described in GMOS SOPs [62]. Immediately after filling, samples were acidified with 20 mL HCl 0.8 % V/V.

In the laboratory, total Hg (THg) was determined by CVAFS after oxidation of all the mercury species present in the sample by BrCl. Then, divalent Hg was reduced by $SnCl_2$, and amalgamated in the dual gold traps system, as described in the previous chapter. It followed the thermal desorption at 550°C and the detection by CVAFS. Quantification was obtained after calibration of the instrument through the analysis of standard solutions containing known Hg, in the range 0.5 - 25 ng L^{-1}. The limit of

detection, resulting as three times the standard deviation of the reagent blank, was 0.03 ng L^{-1} (0.15 pM), whereas repeatability and reproducibility were 4% and 10%, respectively.

Total Samples	Site	Date	Time	Bottom depth (m)	
8	Acireale	20 Aug	19:00	589.0	1 Field blank Sicily
6	Acicastello	21 Aug	20:40	370.5	
13	Marsili	23 Aug	11:30	2547.5	1 Field blank Marsili
7	Ischia 1	24 Aug	18:45	211.6	1 Field blank Campania
4	Ischia 2	25 Aug	19:00	136.0	
4	Phlegraean F. 1	25 Aug	21:30	62.0	
4	Phlegraean F. 2	27 Aug	20:10	45.7	
5	Gulf of Naples	27 Aug	22:45	155.5	
6	Stromboli 1	28 Aug	16:45	300.0	
11	Stromboli 3	30 Aug	17:30	1512.5	
4	Panarea 2	01 Sep	19:15	20.0	
4	Panarea 1	01 Sep	21:30	23.0	
4	Vulcano 1	02 Sep	16:00	35.5	
5	Vulcano 2	04 Sep	14:45	87.5	
6	Vulcano 3	04 Sep	19:40	88.3	1 Field blank Aeolian Islands

Table 3.2 Selected monitoring sites for seawater measurements

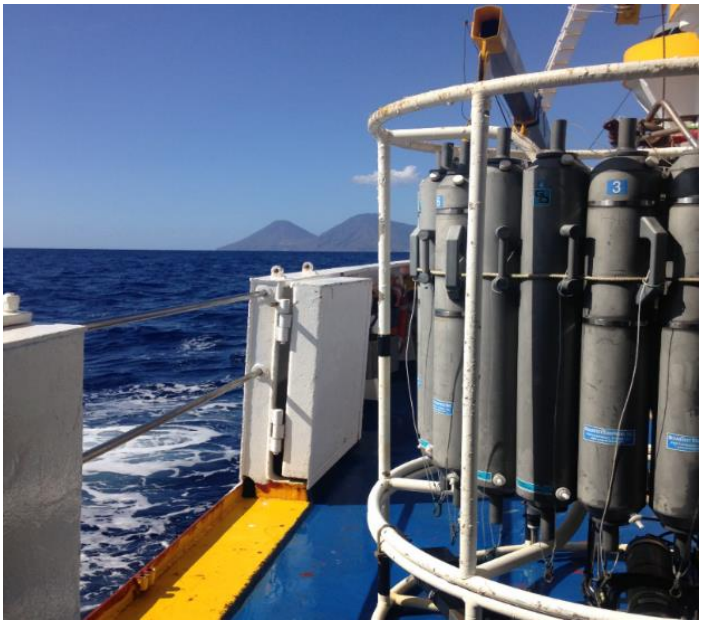

Fig. 3.9 CTD seawater sampler

3.2.4.2 Results and discussion

The mercury concentrations in the samples from different sites showed a relatively low Hg concentration with a slight variability among sites. Generally, the average surface value of THg for the 83 samples was 0.70 ± 0.43 pM, varying in the range 0.31 -1.88 pM. Its maximum value was detected in Marsili, maybe due to atmospheric deposition. Indeed, atmospheric measurements performed in Marsili revealed a high GOM concentration, as previously discussed, which is delivered to the sea surface due to its high water solubility and high deposition velocity [25]. If the vertical distribution is also considered, then THg concentration values ranged between 0.15 – 4.65 pM, with the maximum being detected in the bottom sample of Phlegraean Fields 1. A preliminary attempt to explain this maximum value on the bottom is related to the geothermal activity of the site.

The values obtained for THg in this study are in agreement with the study reported in the literature. In detail, Horvat et al. (2003) [27] reported THg values from 0.81 to 2.33 pM for surface waters of the Mediterranean whereas Cossa et al. [83] found concentrations for THg within the range 0.8 - 6.4 pM. Even the values for the western sector of the Mediterranean Sea reported in Kotnik et al. [84] are in good agreement

with the data obtained by our investigation. Indeed, they reported a mean THg concentration of 1.26 pM, with values comprised between 0.41 and 2.65 pM.

In Fig. 3.10, the THg concentrations obtained for each site are reported. The surface THg values for Gulf of Naples and Vulcano 1 are not reported since these resulted lower than the detection limit. Anyway, from the plot, it can be immediately seen that the most polluted site was the Campanian area of the Phlegraean Fields, due to the detection of high concentration along the water column.

The high level of GOM concentration relates with the high surface values, due to the atmospheric deposition processes.

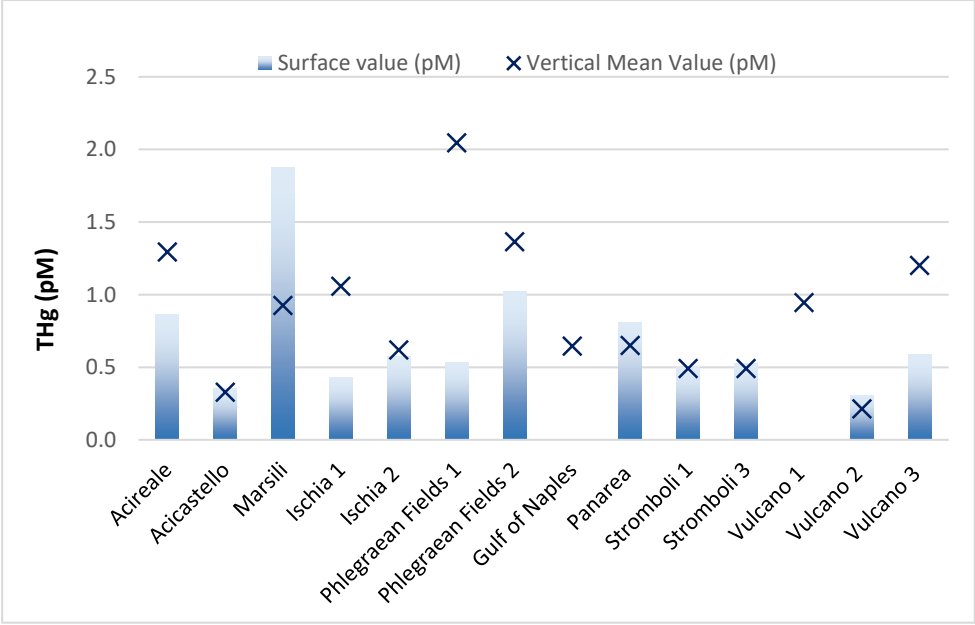

Fig. 3.10 Total mercury (THg) concentration at each site. Histogram bars represent the THg value of the sea surface; the X symbol represents the mean THg concentration along the water column

Vertical distribution profiles of THg concentration and water temperature for each site are shown in Fig. 3.11. In accordance with literature studies, the profiles showed a maximum of THg just below the thermocline, as a consequence of the accumulation of mercury adsorbed to organic matter in the thermocline layer [83]. Some exceptions to this evidence are for example Panarea, Phlegraean Fields and Vulcano 3, which are shallow sites, where a thermal stratification is not expected, and results in a homogeneous water column. However, in these sites, below the thermocline, was

obtained a THg concentration higher than the overlying depth levels. Clearly, the analysis of THg itself hinders a deep analysis of the various sources affecting its distribution along the water column. On the contrary, a more accurate analysis could be provided by the speciation analysis at different depths. Therefore, the obtained data are going to be integrated with the speciated Hg quantification, namely of DGM, RGM, and $MeHg^{+}$, obtained by other research groups who took part in the same oceanographic campaign.

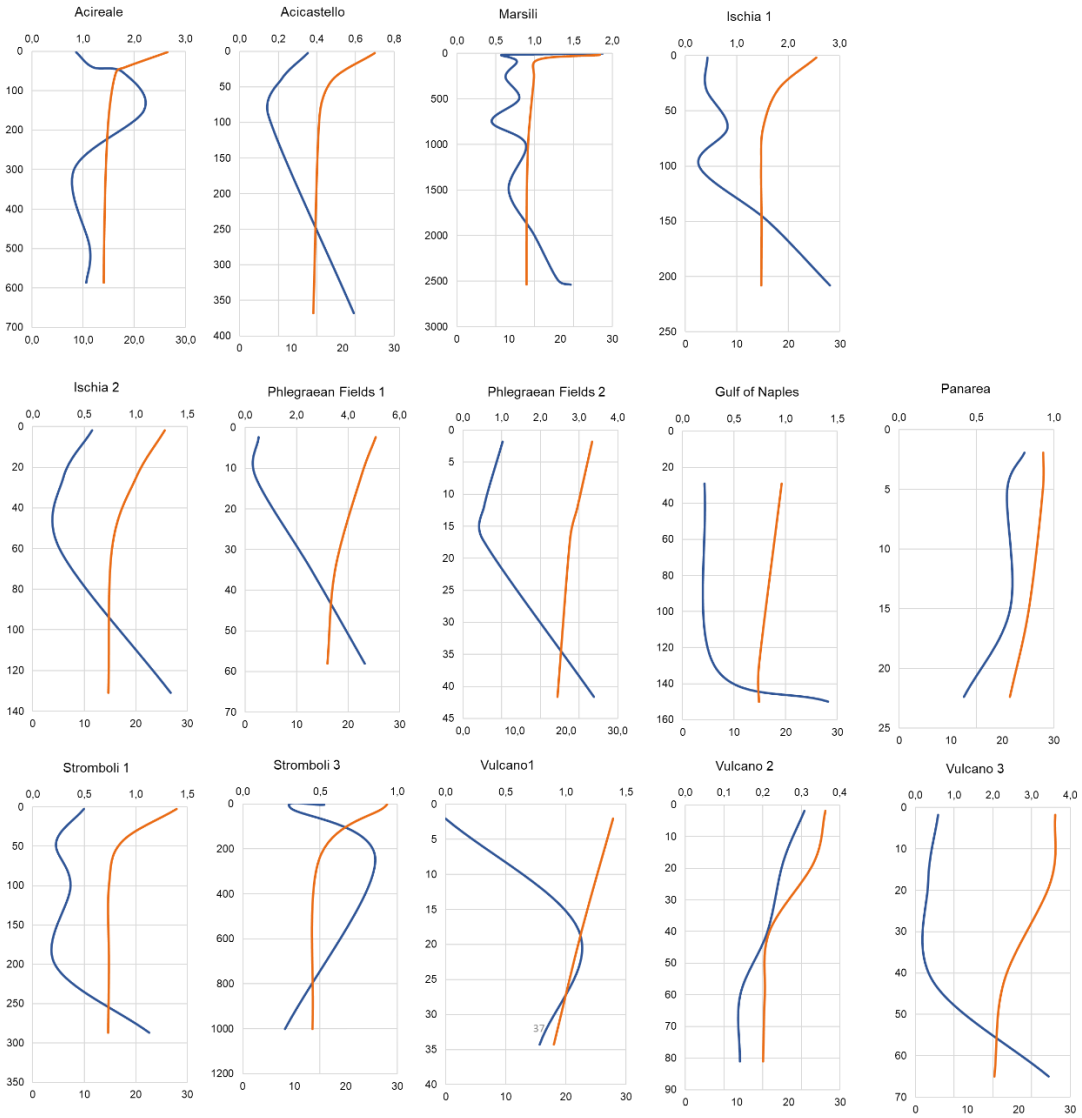

Fig. 3.11 Vertical distribution profiles of THg concentration and water temperature at each site

3.2.5 Conclusion

In the framework of the ongoing MED-Oceanor measurement program, an oceanographic campaign was carried out in the Mediterranean Sea basin to investigate the Hg species distribution in the proximity of different volcanoes, like the Etna, the Phlegraean Fields, and the Aeolian Islands. The investigation concerns measurements in both atmosphere and seawater for the determination of speciated Hg (GEM, GOM, and PBM) and total Hg, respectively. As regards the atmospheric Hg, the obtained mean concentrations are 1.1 ± 0.3 ng m^{-3}, 15.4 ± 12.6 pg m^{-3}, and 2.4 ± 4.2 pg m^{-3}, respectively for GEM, GOM, and PBM.

The influence of the volcanic emissions in terms of peaks in the GOM concentration, up to 76.4 pg m^{-3}, is evident in the Vulcano 1 measurements site, as also supported by the registration of the highest SO_2 concentration. Moreover, for this site, the calculation of the Hg/SO_2 is compatible with the data reported in the literature for the passively degassing volcanoes. An overall evaluation of the results obtained through this investigation suggests that the natural contribution of sources on Hg levels within the Mediterranean basin should not be considered negligible. Anyway, further measurements closer to the volcanic plume emissions are necessary for a better comprehension of the mechanism of Hg species. As regards the seawater investigation, the analysis of the collected samples yields to average THg concentrations in the range 0.15 – 4.65 pM, well-matched with values already reported in the literature for the western sector of the Mediterranean. Moreover, the analysis of the vertical distribution profile shows a correspondence between the maximum THg and the thermocline, in accordance to Cossa et al. [83]. Anyway, further investigations regarding the speciation analysis in seawater should be accomplished in order to completely evaluate the influence of the different sources on Hg distribution.

3.3 Case study 2: Passive Air Samplers (PASs)

3.3.1 Overview of the PASs: Structure and improvements over time

During the Ph.D. work, the use of passive sampler devices has been investigated as an alternative approach to traditional sampling methods. Indeed, as previously mentioned, passive sampling can result in various advantages over the traditional

active sampling: it does not involve the use of cumbersome instrumentation, but passive devices typically have small dimensions, thus can be easily transported to remote sites, without needing for electrical power or pumps. In addition, due to the very low cost, passive samplers can be placed at multiple points of a given area, allowing a spatial mapping of Hg concentration (not just in a single point as with an automated analyzer) avoiding supervision or maintenance. This innovative approach has been explored within the project "Development of a Plan for Global Monitoring of Human Exposure to and Environmental Concentrations of Mercury" funded by the GEF (Global Environment Facility) at the end of 2014. This project was agreed by the Chemicals and Health Branch of the United Nations Environment Programme (UN Environment) in collaboration with the National Research Council of Italy – Institute of Atmospheric Pollution Research (CNR-IIA) and the World Health Organization – European Centre for Environment and Health (WHO – ECEH), in order to develop a global Mercury Monitoring Plan for the future implementation of the International Convention of Minamata on Mercury. The overall aim of this project was to harmonize approaches as well as to strengthen the analytical capacity, at a global level, for the accurate monitoring of mercury concentrations, both in ambient air and in human biological components. In particular, CNR-IIA was involved in the monitoring of mercury in ambient air (Component 1), whereas the World Health Organization (WHO) in the bio-monitoring of mercury (Component 2). To achieve the goals of component 1 for the environmental monitoring, CNR-IIA, with the cooperation of the GMOS network partners, designed and tested an innovative prototype of passive sampling, exploiting the nanostructured pattern of a sorbent surface for the unassisted collection of atmospheric mercury [59]. The first prototype of these passive devices comprised a sorbent membrane, kept at the bottom of a borosilicate glass vessel through the use of a locking ring, and a cap for sealing the device. For the environmental exposure, this cap had to be replaced with a perforated cap hosting a nylon diffusive membrane. This last membrane consisted of an anti-convection micro-porous nylon screen useful for gas diffusion and particulate stopping.

As regards the sorbent material, it consisted of densely packed titania nanoparticles ($TiO_2 \leq 25$nm diameter) finely decorated with gold nanoparticles (AuNPs). The functionalization step was achieved by exploiting the photocatalytic properties of the

titania-anatase, which under UV irradiation is able to reduce $HAuCl_4$ into elemental gold, in the presence of polyvinylpyrrolidone (PVP) as capping reagent. In detail, commercially available Titanium (IV) oxide nanoparticles, in the anatase phase, were suspended into an aqueous solution of PVP/$HAuCl_4$ (0.1 M PVP, 0.5 mg mL^{-1} $HAuCl_4$). This suspension was irradiated with UV light for 1 hour: the yellow-colored aqueous suspension of TiO_2NPs containing $HAuCl_4$ and PVP under UV-light irradiation turned into a blue-purple color, suggesting the formation of gold nanoparticles. Such a functionalization of the TiO_2NPs was checked by UV-Vis spectrophotometry (UV-Spectrometer Shimadzu 2600). Later on, it was centrifuged and rinsed with ultrapure water in order to remove PVP excess. The resulting precipitate was vortexed, diluted with ultrapure water, and deposited on thin quartz slices by drop-casting. In this way, about 10 mg of material was deposited onto the quartz substrate. The whole membrane was then heated to 80 °C in a first stage, and then to 450 °C under clean airflow, in order to remove possible traces of polymer and mercury, respectively, eventually collected during preparation. As reported in [59], the morphological characteristic of the sorbent material was deeply investigated using different techniques, namely Scanning Transmission Electron Microscopy (STEM), High-Resolution Transmission Electron Microscopy (HR-TEM), Atomic Force Microscopy (AFM), and Optical Microscopy (OM). Thus, it was possible to confirm the homogeneity of the layer, showing a good nanoparticle distribution onto the support with size ranging between 5 to 40 nm, centered around the mean value of 32.6 nm [59]. This novel sorbent material showed very good performances for mercury collection, due to the strong affinity with gold, to the high adsorbing capability resulting from the nanostructured pattern of the layer, and to the reusability of the whole device after thermal desorption analysis. For the environmental deployment, CNR-IIA also developed a housing shelter where the passive devices had to be hooked for the desired sampling period. It is worth noting that the passive devices are to be deployed with the passive membrane facing downward, in order to allow the axial diffusion from the diffusive nylon membrane to the sorbent surface. The average concentration sorbed over the time period in which the sampler is exposed to ambient conditions is determined by chemical analysis of the passive membrane. To achieve this goal, a lab-made system, still in use, was planned by CNR-IIA in order to be

linkable to the most common analytical systems for mercury determination. It consists of a quartz housing for the sorbent membrane, a furnace for the thermal desorption linked to a mercury analyzer Tekran 2537. The great advantage of such a system is that it exploits filtered ambient air to flow the desorbed Hg vapors to the mercury analyzer instead of the argon carrier customarily required by the Tekran 2537. Indeed, the membrane contained into the prototype is taken out of the glass vessel and placed into the quartz cylindrical housing (Spaziani, Italy), which in turn is subjected to 550°C into furnace (De Marco, Italy) for the desorption of the sorbed Hg. Later on, the mercury vapor contained into the air stream is quantified by CVAFS in the Tekran analyzer.

After desorption is complete, (usually two or three 5-minutes cycles of the analyzer are necessary to give back a blank membrane) the passive disc can be re-assembled into a cleaned glass vessel, for another environmental deployment. In this way, also environmental waste is reduced and consequently, the total cost of their production is lower.

The functioning of these preliminary devices was tested during different field campaign exercises in various sites of the GMOS network (Mount Curcio Station, EMMA station, Cape Point Station, Mount Ailao, Listvyanka Station), which agreed to compare the results of these passive sampling with Hg measurements by conventional instruments. Although acceptable results were obtained in most sites, during my Ph.D. studies some improvements have been carried out from the production to the deployment steps, in order to avoid issues related to both contaminations of the sampler and Hg losses from the sampler cap.

Indeed, the assembling of the devices has been accomplished into a glove box in order to avoid any contamination after the cleaning step, which involved the use of diluted $HClO_4$ as an oxidizing agent, and ultrapure water, successively, for each component of the device. Moreover, a double cap system was introduced to reduce contamination in the vessel due to the opening of the cap: the bottom cap is always screwed to the glass vessel and contains the diffusive membrane, whereas the top cap is only used when the device is not deployed.

Fig. 3.12 PAS structure before (left) and after (right) improvements. The double cap system is also reported

In such a way, the passive membrane never gets in contact with the surrounding air in favor of the diffusion processes into the glass vessel. The use of two O-rings – one between the vessel and the bottom cap and another between the two caps – makes the whole device air-tight. In Fig. 3.12 a comparison of the two PASs, the prototype and the most recent one with the double cap, is reported.

As regards the shipment of the passive sampler to the monitoring site station, a new strategy for the storage involved the use of heat- and zip- sealed aluminum bags, which also contained a lab-made cartridge. This cartridge acted as scrubber for the collection of any mercury traces eventually present into the bag; it was realized by merely perforating a common laboratory sample-holder, containing the same passive membrane used in the prototypes. The shelter housing for the environmental deployment was improved by replacing the metallic material previously used for the circular top structure (Fig 3.13) with a non-conducting material, namely Teflon, in order to better protect the samplers from the solar irradiation, which could potentially affect the sampling step. Moreover, a Teflon bell around the samplers was added to the top structure for shielding the samplers from wind and rain.

3.3.2 PASs calibration

Before field-testing, these PASs need to be calibrated in order to determine an experimental value of the sampling rate, SR, which represents, as previously reported, the volume of air that is effectively stripped of mercury. Calibration of the PASs is accomplished by injecting under dry air increasing amounts of mercury vapors, withdrawn from the Tekran 2505 Primary Calibration Source with the help of a gas-

tight syringe, into a quartz chamber, suitable to contain the passive air sampler (Fig. 3.14).

Fig. 3.13 PASs holder for the outdoor deployment before (left) and after (right) improvements

Fig. 3.14 Customized quartz chamber for the controlled exposure of PASs during calibration

Numerous tests were performed, involving different deployment times, while continuously measuring Hg concentration into the chamber with an active instrument (Tekran 2537). After desorption of the passive membrane, results were elaborated using the first Fick's Law [56]. The average experimental value of the SR obtained at 20 °C was 0.0147 ± 0.0007 m^3 day^{-1}.

In addition, meteorological conditions, namely ambient temperature, and relative humidity were investigated in order to determine their effect on the sampling rate of the gaseous mercury. Therefore, to investigate the effect of humidity and temperature,

adsorption at different Hg^0 vapor concentrations was studied by exposing the passive membrane to the pollutant just for 15 min. The relative humidity changes were controlled and generated by a mass flow controller flowing dry air and increasing the concentrations of water vapors throughout the measuring chamber. Temperature values were provided by dipping the measuring chamber into a thermal bath. In particular, RH was investigated in the range of 0 – 70 %, whereas temperature was varied within -20 – 60 °C, with the temperature -20 °C reached by placing the measuring chamber into a refrigerator. Experimental results reported only slight effects due to both temperature (+0.1 % per Celsius degree) and relative humidity (+0.06 % per % RH unit). Nevertheless, a thorough calibration, including also the study of the effect of wind speed, is still matters of investigation.

3.3.3 Field testing of the analytical performances of the Passive Air Samplers

The analytical performances and the potential influence of different meteorological conditions on Hg behavior have been evaluated during an intercomparison field exercise that involved two different sites. These monitoring sites were located in the area surrounding the CNR-IIA in Rende (Italy) and the Ontario Environmental Science Centre in Downsview (Canada). These locations were selected as monitoring sites because they are mostly background sites, where the mercury concentrations as total gaseous mercury (TGM) are continuously monitored by means of the conventional active Tekran 2537.

The area surrounding the CNR-IIA in Rende is a suburban site, which is not affected by local sources, except for a small industrial area. Anyway, mercury concentration in the atmosphere mostly remains in the range of background values, typically oscillating between 1 and 2 ng m^{-3}. The deployment set-up in this site consisted of the metallic support where the sampler holders were mounted, parallel to the ground, at a height of about 3 meters. The meteorological parameters were continuously acquired using all the sensors provided within the meteorological station located close to the sampling point. In detail, LSI LASTEM DMA875 thermo-hygrometer was used for the temperature and the relative humidity, whereas LSI LASTEM DNA821 anemometer for the wind speed and direction. Data were acquired with a 30 s resolution.

Ontario Environmental Science Centre in Downsview is a background site not affected by local sources. At this site, the deployment set-up was quite similar to that equipped in Rende, with metallic holder structures suitable for the outdoor deployment of the passive samplers. Also in this case, meteorological parameters were continuously acquired using all the sensors provided within the meteorological station, but the resolution was 1 hour.

Thus, at these sites, passive air samplers were co-exposed for several rounds of 2, 4, 6, 8, 12 weeks, covering a total period of 3 months, from February to April 2019. The sampling plan, reported in Table 3.3, specifically included four rounds lasting 2 weeks each, three rounds of 4 weeks, two rounds of 6 weeks, one round of 8 weeks, and one round of 12 weeks.

Round-Duration	w1	w2	w3	w4	w5	w6	w7	w8	w9	w10	w11	w12
1st 2-week	■	■										
2nd 2-week			■	■								
3rd 2-week					■	■						
4th 2-week									■	■		
1st 4-week	■	■	■	■								
2nd 4-week					■	■	■	■				
3rd 4-week									■	■	■	■
1st 6-week	■	■	■	■	■	■						
2nd 6-week							■	■	■	■	■	■
1st 8-week	■	■	■	■	■	■	■	■				
1st 12-week	■	■	■	■	■	■	■	■	■	■	■	■

Table 3.3 Sampling Deployment Scheme for PASs in Rende and Downsview

For each round, three replicates and a blank field were deployed; thus, it was possible to determine the repeatability and the lower detection limit of the samplers, which was calculated as 3 times the standard deviation of the blanks of each time-period, respectively. In addition, five PASs for each type were used as storage blank, in order to check for any possible contamination from shipment, storage, or laboratory

contamination. After sampling, PASs were placed back in the corresponding bags and stored in a dark and cool environment, before shipping to each laboratory.

At the same time, mercury was also monitored in continuous by means of the Tekran Hg analyzer, in order to evaluate the performance of the PASs in terms of comparison with Tekran active measurements, strengthening the capacity in providing globally comparable data. Nevertheless, active measurements in Downsview are still not available, therefore the results of the campaign will be evaluated in terms of comparison between the PASs in the two sites, as well as in terms of comparison with the active Hg analyzer, as concerns Rende monitoring site.

It should be emphasized that they provide time-integrated concentrations with continuous-time coverage, with the averaging time determined by the period they are deployed to ambient air. Therefore, they are obviously not well suited for monitoring temporal variations over short time intervals neither for the detection of individual peak values nor when real-time measurements are needed. On the contrary, the most common applications include long-term monitoring of atmospheric Hg levels in remote regions and in developing countries, atmospheric mercury source identification and characterization through finely resolved spatial mapping and personal Hg exposure monitoring for compliance and exposure assessment [54].

3.3.3.1 Results and discussion

In this section, the results of the field application will be reported, focusing on the analytical performances of the PASs in terms of linearity, precision, accuracy, and method detection limit. In addition, the influence of meteorological conditions, as temperature, relative humidity and wind speed, will be described.

A brief overview of the results from the chemical analysis of the CNR passive samplers in the two monitoring sites is summarized in Table 3.4.

For the passive sampling, the reported value refers to the time-averaged concentration of mercury adsorbed during the whole campaign period, that is 12 weeks, whereas the active sampling values result from the averaging of the 5-minutes monitoring of mercury in the ambient air through the continuous Tekran Hg analyzers.

Fig. 3.15 shows the results from the chemical analysis of the passive samplers developed by CNR and deployed in both Rende and Downsview in terms of the net Hg mass (i.e. after subtraction of the field blank Hg mass).

Deployment site	Sampling Method	Mean Hg concentration (ng m^{-3})	± SD	Mean Normalized Difference
Rende	Active	1.71	0.32	7.68
	Passive	1.58	0.28	
Downsview	Active	N.A	-	
	Passive	1.38	0.08	

Table 3.4 Summary of the results of the chemical analysis of the PASs in the selected monitoring sites

It can be clearly seen that satisfactory linearity among the responses of the PASs for the different deployment periods was achieved, with the sorbed Hg mass increasing with the deployment time.

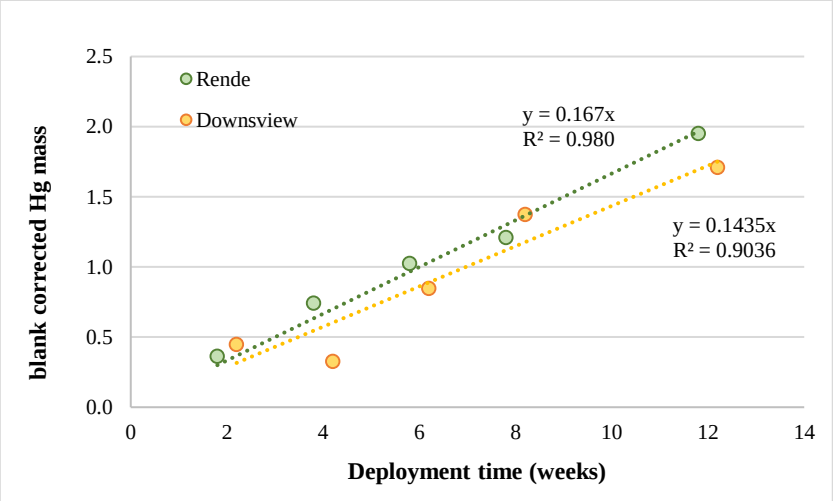

Fig. 3.15 PASs Hg mass for each deployment period

In particular, very good linearity was obtained for the PASs deployed in Rende. In Downsview, the sorbed Hg mass from the PASs deployed for 4 weeks is lower than expected, affecting the overall linearity. This is also evident from the box and whiskers plot (Fig. 3.16) which shows the distribution of the results obtained at all sites.

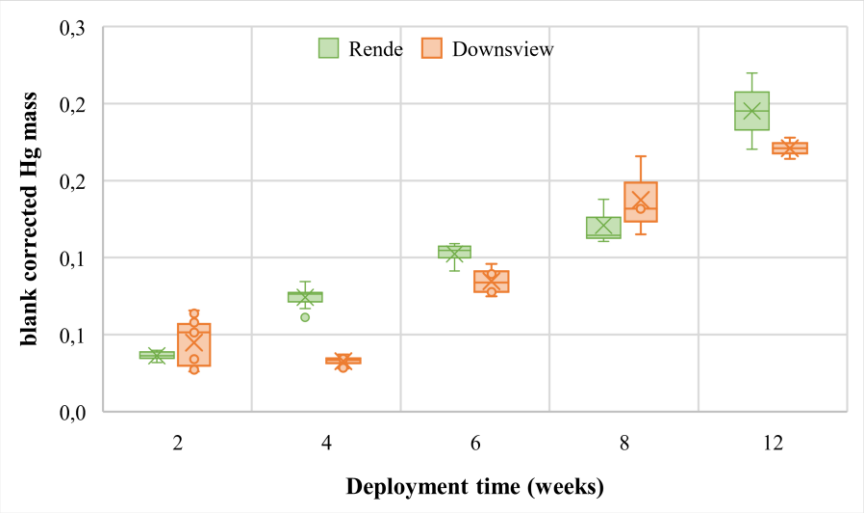

Fig. 3.16 Distribution of the results obtained for the samplers in the two sites

This plot repeats the linear trend for the PASs deployed in Rende and for those deployed in Downsview, except for the 4-week rounds, which are consistently lower than expected. Moreover, the width of the box for each deployment period suggests a good precision among the replicates of each round. Indeed, in Table 3.5 it can be seen that precision, expressed as percentage relative standard deviation (RSD%), is always lower than 15%, except for the 4-week and 12-week deployment in Rende and the 8-week deployment in Downsview, where RSD% is 17.07%, 17.92%, and 18.76 %, respectively. Probably, the decreased precision for these rounds was due to the occurrence of anomalies during the operational procedures as well as during the handling and storage of the samplers. The use of field blanks (FBs) for each deployment round allowed the determination of the method detection limit (MDL), expressed as three times the standard deviation of the blanks. In detail, a total of 11 field blank samplers was used, one for each deployment round:

- 4 field blanks for the 2-week deployment;
- 3 field blanks for the 4-week deployment;
- 2 field blanks for the 6-week deployment;
- 1 field blank for the 8-week deployment;
- 1 field blank for the 12-week deployment.

The mean Hg concentration detected in the field blanks was 0.16 ng and 0.21 ng in Rende and Downsview, resulting in 0.06 ng and 0.13 ng as MDLs, respectively.

With the aim to establish PASs as an alternative strategy to Hg monitoring, the passive sampler performances were compared to those of the Tekran continuous monitoring. The active Hg concentration in ambient air showed a quite constant trend over the whole campaign period in Rende, with values ranging from 0.88 to 4.21 ng m^{-3}. Fig 3.17 shows the Hg concentration trend over the 12 weeks exposure in Rende.

	Rende			Downsview		
Deployment round	**Passive**	**± SD**	**RSD%**	**Passive**	**± SD**	**RSD%**
1st 2-week	1.64	0.08	4.79	1.46	0.17	11.51
2nd 2-week	1.71	0.11	6.33	2.82	0.30	10.58
3rd 2-week	1.82	0.12	6.66	2.62	0.33	12.59
4th 2-week	1.88	0.07	3.74	1.37	0.13	9.38
1st 4-week	1.72	0.29	17.07	0.81	0.03	4.19
2nd 4-week	1.88	0.05	2.84	0.86	0.03	3.99
3rd 4-week	1.82	0.07	4.06	0.73	0.07	9.13
1st 6-week	1.60	0.18	11.01	1.40	0.15	10.56
2nd 6-week	1.72	0.07	4.27	1.34	0.13	9.55
1st 8-week	1.47	0.18	12.18	1.66	0.31	18.76
1st 12-week	1.58	0.28	17.92	1.38	0.08	5.64

Table 3.5 Precision values of the PASs deployed in the two sites

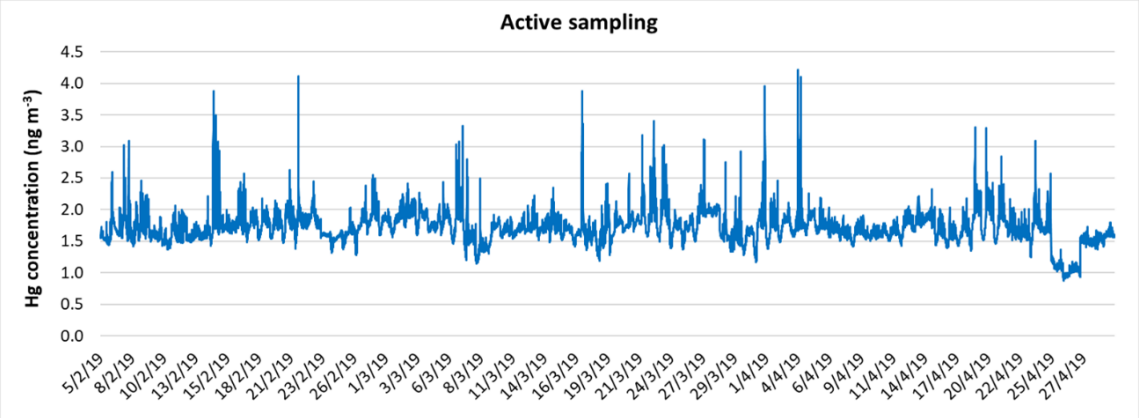

Fig. 3.17 Hg concentration profile in Rende measured using a Tekran 2537 Hg analyzer

This was confirmed by the plot in Fig. 3.18 which shows the average concentration values for the active Hg measured over each deployment round.

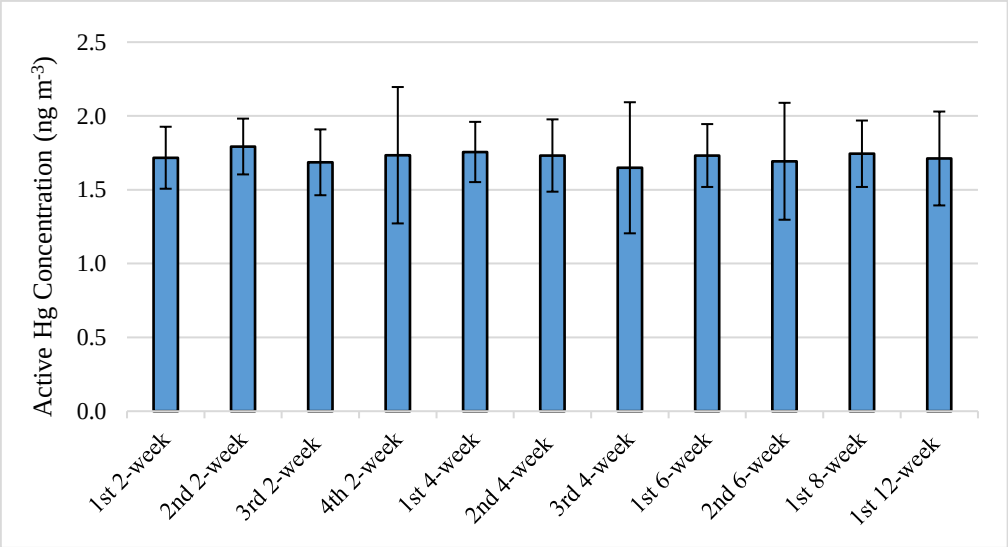

Fig. 3.18 Average Hg concentration sorbed during each deployment round

When compared to the passive sampling concentrations, it can be clearly seen that there was an acceptable agreement among active and passive sampling strategies in Rende (Fig. 3.19).

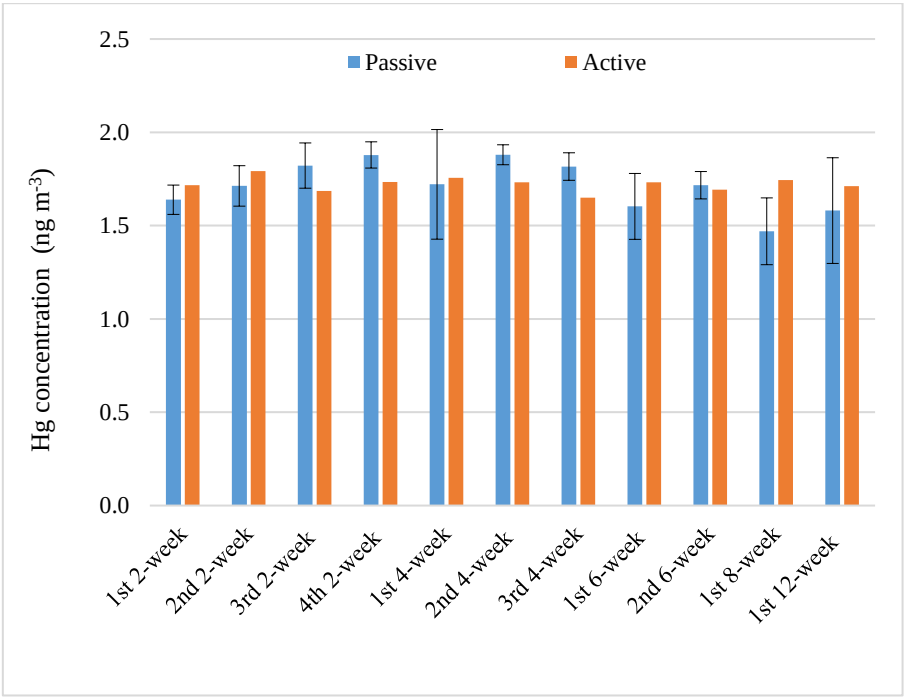

Fig. 3.19 Comparison between active and passive Hg concentration for each deployment round

Indeed, the mean normalized difference among the active and passive sampling approaches, which resulted to be 7.12%, confirmed that PASs represent a good alternative to the traditional monitoring techniques, allowing to fill the gaps in the monitoring of Hg worldwide.

In particular, a more accurate analysis of the MND values for each round shows that very good results were obtained for deployment periods up to 6 weeks in Rende, where the MND is lower than 7% (Table 3.6). Conversely, longer deployment times maybe lead to passivation of the membrane, as supported by the increased MND value, up to 16%. Indeed, for 8-week and 12-week rounds, passive concentration is lower than active concentration.

3.3.3.2 Influence of the meteorology

As previously mentioned, meteorological conditions, as temperature, wind speed, rain, and humidity can potentially affect the diffusion rates of the mercury species [58]. Continuous monitoring of these parameters was, therefore, necessary to seek for any relation between the sorbed Hg mass and the sampling rate. As regards the temperature, Rende exhibited a mean value of 12.04 ± 4.64 °C whereas in Downsview, the mean temperature was 6.62 ± 4.28 °C. Wind speed in Rende ranged from 0 and 6.91 m s^{-1}, with a mean value of 1.18 ± 0.93 m s^{-1} whereas in Downsview it ranged between 0 and 8 m s^{-1}, with a mean value of 2.01 ± 1.44 m s^{-1}. Relative humidity varied between 13.59 and 97.89 %, being 60.38 ± 18.08 % the mean value in Rende, whereas in Downsview the mean value was 64.16 ± 17.59 %, varying in the range 26.20 - 90.80 %. Fig.3.20 summarizes the mean value for each deployment round.

Preliminary laboratory tests [59] showed that Hg sorption by PASs is only slightly affected by temperature and relative humidity, with sorbed Hg mass varying 0.62 pg per Celsius degree over a thermal range of -20 – 60°C and by 0.40 pg per RH% unit over a range of 10 – 70%. In our case, from the plot in Fig. 3.21 regarding the monitoring in Rende, it can be noticed that passive Hg concentration increased with temperature, except for the 4th 2-week deployment and 3rd 4-week deployment. Moreover, the Hg concentration retrieved from passive samplers was independent of the wind speed and relative humidity.

	PASs			Tekran 2537X		Active vs Passive	
Weeks	**Passive**	**± SD**	**RSD%**	**Active**	**± SD**	**|Difference|**	**MND per period**
1st 2-week	1.64	0.08	4.79	1.72	0.21	4.56	6.36
2nd 2-week	1.71	0.11	6.33	1.79	0.19	4.47	
3rd 2-week	1.82	0.12	6.66	1.69	0.22	8.06	
4th 2-week	1.88	0.07	3.74	1.73	0.46	8.35	
1st 4-week	1.72	0.29	17.07	1.76	0.20	1.99	6.90
2nd 4-week	1.88	0.05	2.84	1.73	0.24	8.54	
3rd 4-week	1.82	0.07	4.06	1.65	0.44	10.17	
1st 6-week	1.60	0.18	11.01	1.73	0.21	7.44	4.42
2nd 6-week	1.72	0.07	4.27	1.69	0.40	1.39	
1st 8-week	1.47	0.18	12.18	1.74	0.22	15.73	15.73
1st 12-week	1.58	0.28	17.92	1.71	0.32	7.68	7.68

Table 3.6 Mean normalized differences between active and passive Hg concentration in Rende

In the same way, the trend of the meteorological parameters in Downsview apparently did not affect the Hg concentration sorbed by PASs.

Anyway, a more accurate analysis can be performed to evaluate quantitatively any possible influence of the temperature on the sampling rate. Indeed, as previously reported by Mc Lagan et al. [56], it is possible to adjust the sampling rate value by calculating a correction factor, which accounts for the actual temperature experienced by the passive samplers during the environmental deployment. This correction factor needs to be calculated as the slope of a linear regression of SR for each round against temperature, in accordance with Mc Lagan et al. [56].

Once obtained, the adjusted value of the sampling rate, named SR_{adj}, is derived as follows:

$$SR_{adj} = SR_{cal} + slope * (T_{exp} - T_{cal})$$

For example, this was applied to the data obtained for the monitoring in Rende. The slope of the linear regression attained by plotting the sampling rate for each deployment round versus temperature was $1 \cdot 10^{-6}$ m^3 day^{-1} $°C^{-1}$. This slope had a very low impact on the SR value, accounting for a variation from 0.01470 to 0.01469 m^3 day^{-1}. This confirms that temperature values only slightly affected the Hg sorption

process through the PASs membrane. The effect of both wind speed and relative humidity needs further laboratory tests in order to be critically evaluated.

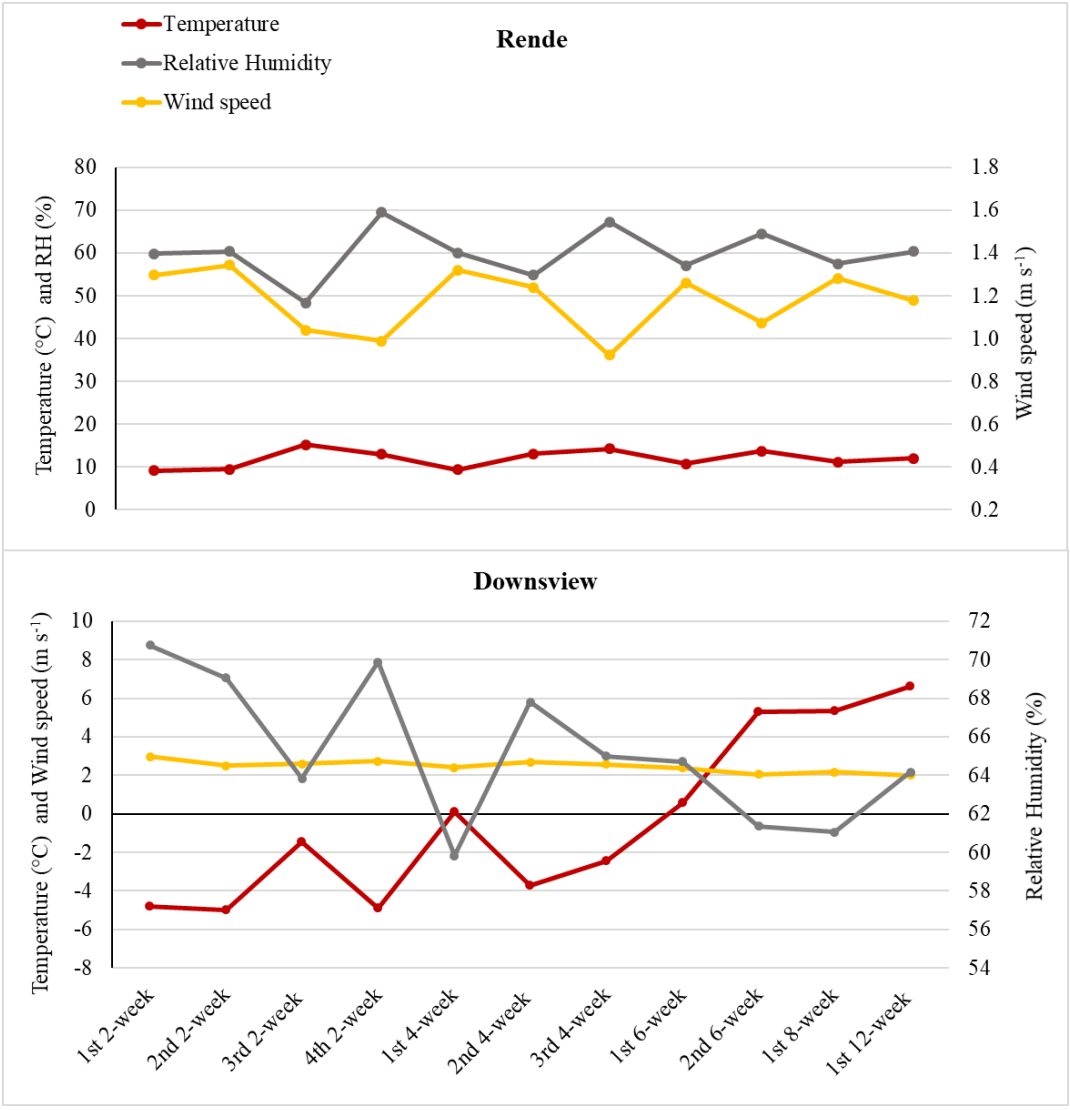

Fig. 3.20 Average values of meteorological conditions for each PASs deployment round in Rende (up) and Downsview (down)

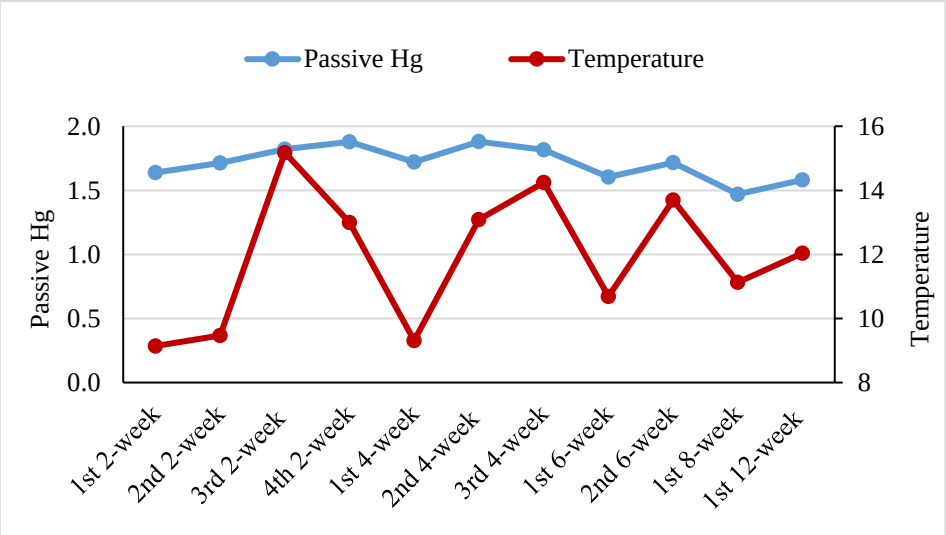

Fig. 3.21 Trend of the passive Hg concentration in relation with temperature in Rende

3.3.4 Conclusion

In the framework of the project "Development of a Plan for Global Monitoring of Human Exposure to and Environmental Concentrations of Mercury", a novel nanostructured material potentially capable of adsorbing gaseous mercury has been developed. This material consists of a layer of titania nanoparticles (TiO_2NPs, ≤25 nm diameter) finely functionalized with gold nanoparticles (AuNPs) and drop-casted on a thin quartz slice, which is incorporated into a common axial sampler. Such a system acts as a passive air sampler since it only relies on the unassisted molecular diffusion of the volatile elemental mercury onto an adsorbent material, without the need for electricity or pumps. Moreover, the whole device has the advantages of being compact, cheap, simple to operate and portable, thus allowing mercury monitoring also in remote areas. During my Ph.D. studies, the structure of the axial sampler, as well as the holder for the outdoor deployment, were improved and tested on the field through intercomparison campaign aimed at evaluating their analytical performances in two sites, Rende and Downsview. At these sites, PASs were exposed for time periods from 2 to 12 weeks, and quantitative analysis of adsorbed Hg was carried out by lab-made equipment for thermal desorption and determination by CVAFS. The use of field blank samplers allowed to assess the detection limit of the PASs, which resulted in 0.06 ng and 0.13 ng at Rende and Downsview, respectively. In addition, PAS repeatability,

evaluated as precision among triplicate samplers for each round, was always lower than 15 %, except for few cases. Meteorological conditions, including wind speed and direction, temperature and relative humidity, were simultaneously monitored and the values of the temperature was used to quantify the influence on the sampling rate value, which resulted not significant.

The performances of the passive samplers were compared to active measurements performed by means of Tekran Mercury Analyzer. The comparison shows an acceptable agreement between active and passive sampling in Rende, since passive Hg concentration only deviates by 7.12% from active measurements. This confirms that PASs represent a good alternative to the traditional monitoring techniques, allowing them to fill the gaps in the monitoring of Hg worldwide.

3.4 Case study 3: *Harpalus (Pseudoophonus) rufipes* as a bioindicator of environmental contamination

3.4.1 Introduction

Monitoring studies in the different environmental compartments are of fundamental concern for the assessment of the pollution level and the distribution of pollutants across the consecutive levels of the trophic chains in various ecosystems. They provide significant information on the transport vectors and bioavailability of pollutants. Indeed, for Hg, as well as other classes of toxic compounds, emissions from various sources, transport through the atmosphere, deposition into ocean and soils, potential conversion into toxic forms and subsequent incorporation into the food webs represent important components for the cycle of the pollutants worldwide. In this context, increasing attention has been given to heavy metals as components of the pollution load in the environment. Because heavy metals are non-degradable, they tend to accumulate in tissues and can be passed along the food chain [85,86]. Thus, one of the important challenges in ecotoxicology is assessing the effects of pollutants transferred to higher levels of food-webs and their wider consequences [87]. Usually, this is accomplished through quantification of the heavy metals bioaccumulated in animal tissues, in respect of the soil they are living in or a lower trophic level they feed on. Indeed, organisms can take up metals via different mechanisms, as biomagnification

along the food chain or direct absorption from the environment. However, not all animal specimens can be used for this purpose, but they must behave as a bioindicator, that is they have to be taxonomically and ecologically well known, widely distributed and easy to collect.

During the Ph.D. studies, an investigation of Hg and other heavy metal levels in fertilized soils and their bioaccumulation in a secondary generalist predator, *Harpalus (Pseudoophonus) rufipes* (DE GEER, 1774), was carried out with the aim to evaluate the transfer along the food chain in agroecosystems. For comprehensive monitoring, the concentration of metals in samples of non-fertilized soils used as a control, fertilized soils, and beetles was also determined.

Fig. 3.22 *Harpalus (Pseudoophonus) rufipes*

In this scenario, *Harpalus (Pseudoophonus) rufipes* (Fig. 3.22) was evaluated as a potential biological indicator of the quality of the environment it is living in.

Indeed, this beetle is a generalist predator well known to be involved in the pest control as predators of seeds [88] and invertebrates [89]. Moreover, it is one the most frequent epigean species in agricultural ecosystems [90,91], is extremely sensitive to several abiotic and biotic factors, responds quickly to habitat alteration and can be easily and cost-effectively collected by using classic pitfall traps. Among various carabid, these beetles represent an important group of bioindicators that are broadly used to quantify environmental impacts such as the effects of anthropogenic activities. One of these activities is represented by the use of fertilizers in croplands to enhance the agricultural yield. Although the metal concentration in the fertilizers that are commonly employed

is low and is not thought as a considerable contributor to environmental contamination, the renewed use of fertilizers over the years may lead to the accumulation of metals in the receiving soils with consequent relevant risks for human and ecosystem health [92]. Metal accumulation in carabids (BAF) was estimated as the ratio between the metal concentration in the beetle body and that in the soil [93].

3.4.2 Beetles and soil sampling

Samples of *H. rufipes* were collected from mid-May to the end of June 2018, in accordance with the period of activity of this species in the sampled area. All beetles were collected from two sites (Fig. 3.23) with a sandy loam in the Sila Mountain (Calabria, Southern Italy) using in vivo pitfall traps (plastic jars, 9 cm in diameter) containing fruit as an attractant; all traps were emptied every 7 days. In the first site, two crop fields, each approximately of 4.7 ha, were selected from a conventional farm of San Giovanni in Fiore, named Torre Garga and located at 1240 m a.s.l., (39°16′58.05″N, 16°38′43.26″E). These crop fields labeled as TA and TB (Treated fields A and B), have a typical crop rotation of potatoes, wheat and lettuce in 3 years. The second site, chosen as control, was an organic potato field (hence the label O) of

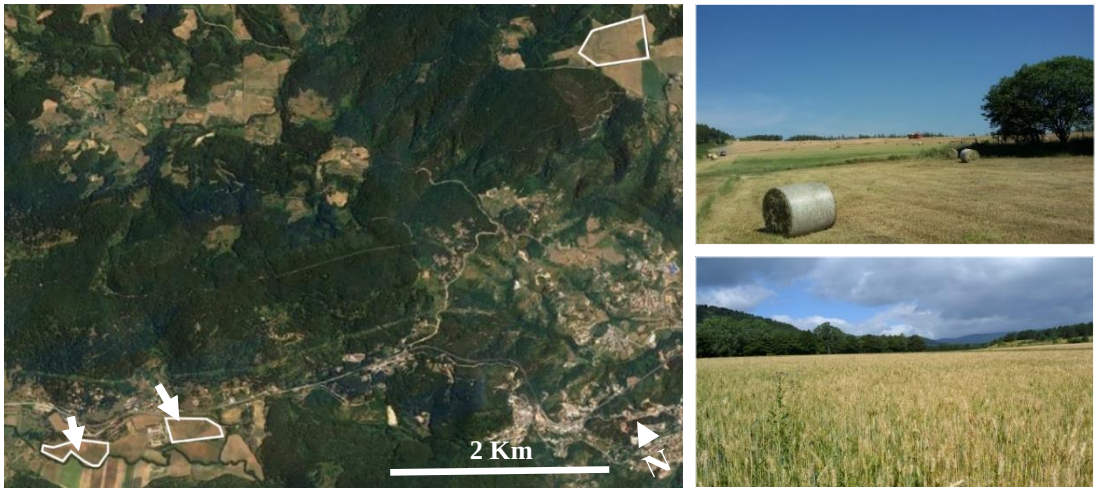

Fig. 3.23 Map of the selected monitoring sites, Macchia di Tuono (up) and Torre Garga (down)

area approximately 6 ha in a biological farm of San Giovanni in Fiore, named Macchia di Tuono and located at 1150 m a.s.l. (39°17′10.28″N, 16°42′28.33″E), 5.5 Km north-east of the sampled conventional field. From TA, TB, and O, a number of 15, 15, and

16 beetles were collected, respectively, and kept into polypropylene tubes for transport. Soil cores (n= 6, 6, 12) were simultaneously taken to a depth of about 15 cm from each field TA, TB, and O, respectively. Then, they were transferred to polypropylene tubes for storage and transport.

3.4.3 Analytical protocol

The chemical analysis of the metals contained in both beetle and soil samples was accomplished using a Tekran 2600 Hg analyzer, for Hg quantification, following the EPA method 1631, and an inductively coupled plasma-mass spectrometry (ICP-MS), for the multielement analysis. This choice was taken due to the higher sensitivity and selectivity of the CVAFS technique over the MS as concerns Hg quantification. Considering that both instruments need a liquid matrix, a proper sample preparation step had to be carried out.

In the Appendix to EPA method 1631 "Total Mercury in Tissue, Sludge, Sediment, and Soil by Acid Digestion and BrCl Oxidation" [65], it is provided for a digestion procedure for oxidation of total mercury in solid and semi-solid sample matrices. In particular, biota samples are digested with HNO_3/H_2SO_4 and then diluted with BrCl solution to destroy the remaining organic material whereas for geological samples aqua regia (HCl/HNO_3) is suggested to solubilize inorganic materials. In both cases, samples are slowly digested by hot re-fluxing for at least 8 hours. For our purpose, this protocol resulted disadvantageous, due to the long time required and the high reagent consumption. Therefore, we set-up an alternative sample preparation, still relying on acid digestion but exploiting the rapidity and efficiency of the microwave digestion.

As regards the insect specimen, a desiccation step in a muffle furnace was carried out for 24 h at 105 °C. Then, samples were weighed using a microbalance Crystal Micro (Gibertini, Novate, Italy) and subjected to microwave digestion with 8 mL HNO_3 and 2 mL H_2O_2, following the suggestions reported for animal tissues in the microwave instrument manual (Ethos-Up Microwave Extraction System, Milestone, Germany). The microwave program was as follows: temperature increased from room temperature to 200°C in 15 min at 1200 W, then this temperature was kept for further

15 min. After the run was complete, the digestate was transferred to a polypropylene test tube and diluted with ultrapure water to 50 mL.

For the soil samples, a similar procedure was used. Indeed, about 200 mg of soils were muffled for 24 h at 105 °C and then weighed, before being digested. The chemical analysis of the soil samples was performed with the same temperature program; anyway, a different digestion mixture was used according to the instrument manual procedures for siliceous soils. Indeed, the digestion mixture was composed of 6 mL HNO_3, 3 mL HF and 1 mL H_2O_2, with the HF being added to ensure complete degradation of the siliceous material. Once converted into a liquid matrix, both beetle ad soil samples were ready for the analysis step, which as previously mentioned was carried out involving ICP-MS, for a multielemental screening, and CVAFS, for the Hg detection. In the first case, the analyses were performed on the digestates diluted to 50 mL, without any further treatment. The determination of the elements of interest was carried out utilizing an Elan DRC-e ICP-MS instrument (Perkin-Elmer SCIEX, Canada). Samples were introduced by means of a crossflow quartz nebulizer with a Scott-type spray chamber. The ICP torch was a standard torch (Fassel type torch) with platinum injector. For the quantitative analysis, calibration curves were built on seven different concentrations in a calibration range of 0.2–1000 μg L^{-1} and having a composition similar to that of sample solutions. Standard solutions were prepared by diluting a multielement solution of As, Bi, Cd, Co, Cr, Cu, Ni, Pb, Sr, V and Zn (100 mg L^{-1}, Merck).

For the Hg quantification, this solution was further diluted 1/40 to reduce the acid content. The total mercury concentration was determined through the preliminary oxidation by BrCl to convert all mercury species to Hg^{2+} in solution, and later on, the addition of a reducing agent to generate volatile Hg^0, which was detected by CVAFS. Quantification was performed after calibration curves built on five different concentrations in the range 0.5 – 25 ng L^{-1} for insect specimen and in the range 0.5 – 100 ng L^{-1} for soils. Standard solutions were prepared by diluting a Hg solution at 100 mg L^{-1} (VWR).

To avoid mercury contamination, special care was taken during the sample preparation and the blank samples were strictly controlled. Indeed, a key step in the development of this analytical protocol was the control of the potential contamination sources which

could have compromised the whole investigation. One of the most significant was constituted by the PTFE vessels used for the microwave digestion. Although PTFE is known to be an inert material, a heavy Hg contamination was detected during the analysis of the blank samples, which was not due to the reagents involved in the sample preparation but to the microwave vessels. Therefore, we developed a new protocol for the cleaning of these sample containers. A first attempt was made modifying the traditional cleaning procedure suggested by the instrument manufacturers, which proposed to run a digestion cycle reaching 180 °C in 15 min and keeping at this temperature for 10 min after addition in each vessel of 5 mL HNO_3 and 5 mL ultrapure water. In particular, 1 mL HCl was used in addition to 4 mL of ultrapure water, instead of 5 mL, since it is well known that this acid revealed suitable to remove Hg contamination [65]. The temperature program was kept as suggested by manufacturers. Anyway, after this cleaning procedure, the analysis of the blank samples still produced a very high signal, indicating the persistence of Hg into the vessels.

At this point, considering the chemistry typical of mercury, we decided to clean the PTFE vessels using a solution of BrCl as strong oxidant, which revealed useful for the Hg removal from different contaminated utensils. In particular, different percentage ratios of BrCl in water were tested between 1-10 % v/v. Finally, a 5 % BrCl solution was sufficient to completely remove the Hg contamination from the sample containers. Fortunately, the contamination issues involved only the Hg analysis considering the higher sensitivity of the instrument used.

3.4.4 Statistical analysis

PCA is a multivariate statistical tool used to reduce the dimensionality of the data, i.e. to reduce the number of variables, eliminating the unnecessary information, which then results in the individuation of the principal components (PCs). In this case, PCA was carried out on both the dataset for soils and insects, after normalization of element concentrations, for understanding the key factors influencing the samples and explaining the relationships between the different variables.

As regards the soils, the whole dataset contained 24 samples, whereas that used for the evaluation of the metal concentrations in beetles contained 46 samples.

3.4.5 Results and discussion

3.4.5.1 Heavy metal concentration in soil samples

In Fig. 3.24 the concentration profiles of all the metals in the fertilized and control soils are reported. Clearly, the concentration value of the various elements showed a quite large variability, but, in each case, concentrations found in TB and TA soils was higher than the O soils used as control.

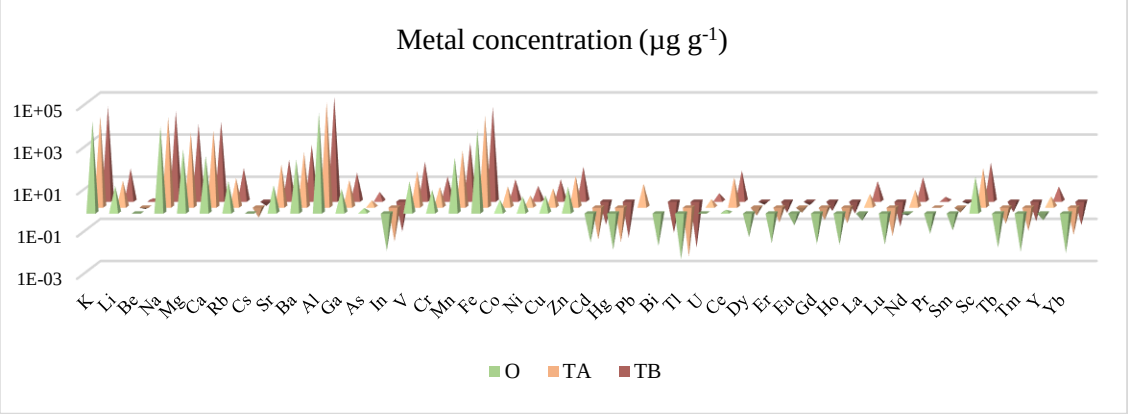

Fig. 3.24 Concentration profiles of all the metals in the fertilized (Ta and TB) and control (O) soils

In particular, a significant level of Al, Fe, Na, Zn, Co, As, U, and Pb in fertilized soils compared with control ones was detected (Fig. 3.25). In addition, a very high level of Rare Earth's Elements (REEs) in both the fertilized soils, TA and TB, was found. According to literature studies, the presence of heavy metals in crop fields could relate to the use of the fertilizers itself, which are typically used to increase the yield of agricultural products [94]. Indeed, Otero et al. characterized different fertilizers, surveying the major, trace and rare earth elements. These can be divided into primary nutrients, as K, secondary nutrients, as Mg, Ca, and Na, and micronutrients, as Co, Cu, Fe, Zn, and Mn [95]. These micronutrients are so-called because they are essential for the vital metabolic activities in organisms but in small quantities compared to those of primary and secondary nutrients.

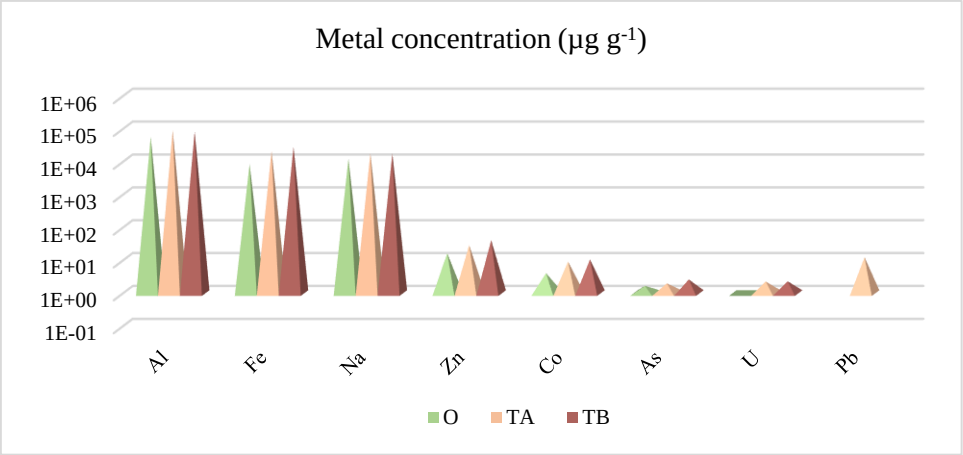

Figure 3.25 Concentration values of the most abundant metals in the fertilized (TA and TB) and control (O) soils

They become toxic only at high concentrations whereas elements as Cd, Pb, Hg, Ag and As do not have any known biological function so that they are non-essential compounds and are toxic to plants and animals, being capable to react with the bio-molecules forming extremely stable toxic compounds, difficult to dissociate [96].

In this framework, REEs, as Ce, Eu, La, Lu, and Nd were the metals with the highest concentration, with Ce being the most present in both TA and TB. The average contents of all elements were extremely variable, ranging from 0.05 µg g^{-1} (Yb) to 27.24 µg g^{-1} (Ce) in TA, and from 0.40 µg g^{-1} (Lu) to 24.99 µg g^{-1} (Ce) in TB, with total concentrations of 49.09 and 51.33 µg g^{-1} respectively. As previously mentioned, the use of REE mixtures in fertilizers is known in numerous studies, due to the success in improving crop yield [94]. However, the question of whether the use of REEs in agriculture yields an enrichment of these elements in the environment remains open. Indeed, studies of short- to medium-term REE exposure have provided multiple evidences for adverse effects in terms of oxidative stress (OS), and tissue damage (liver, lungs and kidneys) [97–99].

3.4.5.2 Heavy metal concentration in beetles and BAF calculation

The chemical analysis of the insects from the three different sampling sites revealed the presence of 36 elements: K, Na, Mg, Ca, Al, Fe, Zn, Cu, Mn, Hg, Rb, Sr, Ba, Ni, Cr, Pb, V, Cd, Ce, La, Nd, Co, Ga, Y, Li, Pr, U, Sm, Dy, Eu, Gd, Be, Tb, Er, As, Sc (Fig. 3.26).

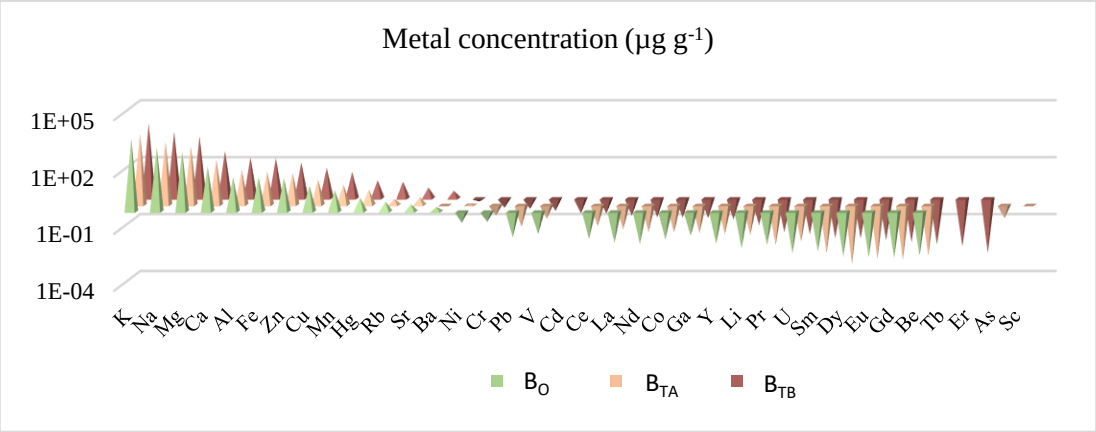

Fig. 3.26 Concentration values of all the metals present in beetles from O (B_O), TA (B_{TA}), and TB (B_{TB})

The most abundant elements were K, Na, Mg, Ca, Al, Fe, Zn, Cu, and Mn in all samples from the three field sites. Even in this case, the insect specimen collected in the treated fields showed higher concentration than the control one, with beetles from TB having the maximum concentration in most cases.

Metal accumulation in beetles was estimated through the calculation of the bioaccumulation factor under field conditions (BAF), i.e. the ratio between the metal concentration in the beetle (in µg g^{-1} dry weight) and that in the soil (µg g^{-1} dry weight). The BAF was used to classify *H. rufipes* as a macroconcentrator (BAF > 2), microconcentrator (1 < BAF < 2) or deconcentrator (BAF < 1) as proposed by Dallinger [100].

Results from this calculation showed that the accumulation of metal in beetles followed the rank order: Zn > Cu > Mg > Hg > Ca. In particular, they resulted in a macroconcentrators of Zn and Cu, and a microconcentrators of Mg. As regards the remaining elements, *H. rufipes* resulted as a deconcentrator. Therefore, even when exposed to high pollution levels from the soils, they are poor accumulators of heavy metals. This is mainly due to an efficient detoxification mechanism typical of carabid beetles, as supported by literature studies [101], which makes them able to neutralize the lethal effect of metal pollution in order to preserve the species.

A comparison with literature studies showed that high BAF values of Cu and Zn were also detected for the carabid *C. violaceus*, indicating that these specimens could accumulate these elements from soil indirect or direct way.

3.4.5.3 Results of the statistical analysis

As previously mentioned, PCA was carried out on both the dataset for soils and insects with the aim to seek for the meaningful variables As regards the soils, the scores of samples and loadings of the variables on the two first principal components explained 78.44 % of the total variance. According to the score plot in Fig. 3.27, the first two components highlighted three distinguishable clusters corresponding to the three field sites, O, TA, and TB. Furthermore, samples from TA and TB showed a quite larger variability compared to O samples.

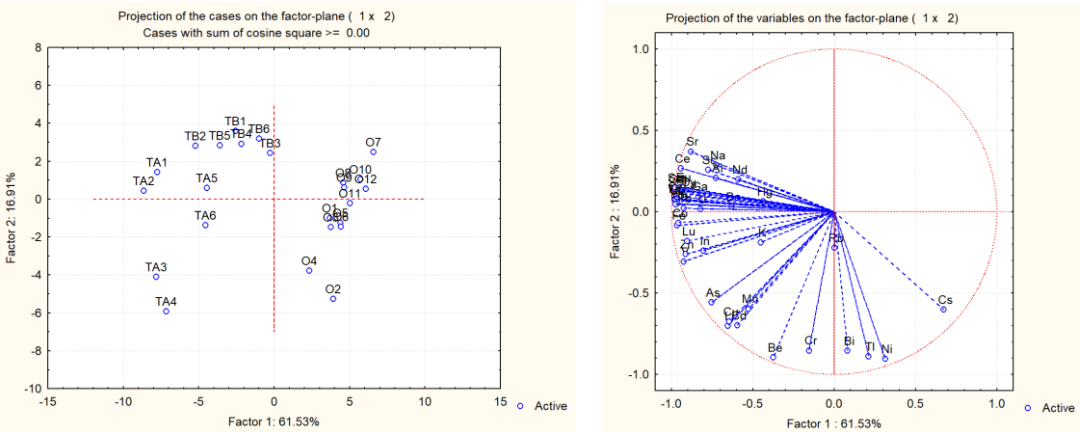

Fig. 3.27 Principal Component scores and loading plots for the multielemental composition of fertilized and control soils

Correspondingly the loadings of the variables (Fig. 3.27) confirmed the distinction among the treated and control crop fields, with the greatest numbers of the variables being characteristic of the treated fields, TA and TB. Indeed, except for Bi, Tl, Ni, and Cs, which characterized the organic samples, all the other metals, including Hg, were found to be representative of the treated samples.

As regards the beetles, the bidimensional scores plot (Fig. 3.28) on the two first principal components explained 73.57 % of the total variance. However, the scores plot obtained from PCA for the beetle samples did not show any significant discrimination among the different fields from which the beetles were captured.

Except for $B_{TB}13$ and $B_{TB}4$, which differentiated from the other samples, the remaining ones overlapped each other, so any separation could not be noticed. This supports the evidence previously discussed for the bioaccumulation factor. Indeed, the high detoxification capability of this species makes them bioaccumulating always the same amount of metals regardless of the contamination of the surrounding environment.

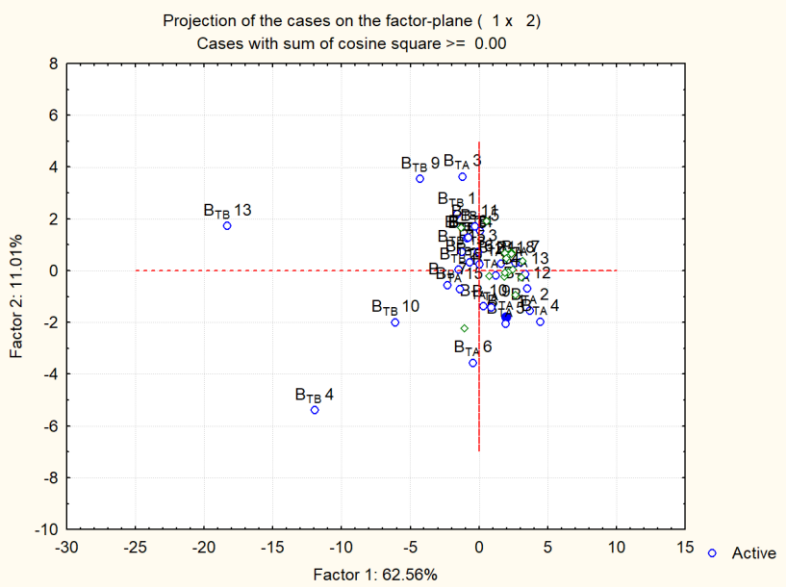

Fig. 3.28 Two-dimensional scores plot for the multielemental composition of beetles from fertilized and control soils

3.4.6 Conclusion

This study investigates the concentration levels of metals in *Harpalus (Pseudoophonus) rufipes* collected in fertilized crop fields from San Giovanni in Fiore (CS). The investigation consists of a multielemental analysis by Inductively Coupled Plasma-Mass Spectrometry (ICP-MS) in which mercury is analyzed through a more sensitive analytical technique, that is the Cold Vapor Atomic Fluorescence Spectroscopy (CVAFS).

This twofold analysis is carried out setting up a microwave acid digestion, which provides for a sample preparation strategy alternative to that suggested by EPA method 1631. Our preliminary results indicate that the use of fertilizers in crop fields leads to an accumulation of heavy metals, especially Al, Fe, Na, Zn, Co, As, U, and Pb. Further, the use of REE-based fertilizers is also responsible for the high concentration of these

toxic elements, whose effects are not completely understood. However, the high concentration of the elements observed in soils does not reflect in a bioaccumulation process in the body of *Harpalus (Pseudoophonus) rufipes*, which shows no significant differences in the metal concentrations compared to the soils where they live. In particular, relatively low values of each element are observed, resulting in turn in low bioaccumulation factor (BAF) values. Indeed, these beetles are poor accumulators of most elements, suggesting an efficient detoxification system, which makes them capable of removing metals affecting their survival, growth and reproduction. Conversely, they appear to be macroconcentrators of Zn and Cu, indicating that they can be bioindicators of the assessment of Zn and Cu pollution.

Section II

Chapter 4

Particulate matter as environmental matrix

4.1 Introduction

Nowadays, an increasing range of chemicals occurs in the atmosphere. These chemicals arise from both natural and anthropogenic sources and can be emitted directly into the atmosphere (primary sources) or be formed by several chemical reactions from gaseous sources (secondary sources). The great variety of chemical compounds present in the atmosphere makes the characterization of air pollution a difficult task. Indeed, ambient air pollution is defined as the contamination of indoor and outdoor environments by a highly variable mixture of substances, which may occur as gases, vapor-phase molecules or particulate matter (PM) [102]. According to European air quality report, particulate matter (PM), ozone (O_3) and nitrogen dioxide (NO_2) are the most problematic pollutants in Europe because many EU member countries exceed the European standard limits [103].

Airborne "Particulate Matter" or PM is defined as the mixture of solid and liquid particles suspended into a gas [104]. Some of them, such as dust, dirt, soot, or smoke, are large or dark enough to be seen with the naked eye, whereas others are so small that they are invisible and can only be detected by microscopy. Typically, a wide variety of compounds is included in PM, being in the form of inorganic salts such as nitrates, sulfates and ammonium as well as in the form of carbonaceous species (elemental carbon and organic carbon). It is commonly used to categorize PM according to the equivalent aerodynamic diameter (D_{ae}) of the particles, which is the size of a unit-density sphere (1 g cm^{-3}) with the same aerodynamic characteristics (same settling velocity in the air) as the considered particle [105]. The reason is that the size of the particles is directly linked to their potential for causing health problems. In particular, the term Total Suspended Particulate (TSP) refers to all the particles with aerodynamic diameter from 0.1 up to 50 μm. On the other hand, particles with aerodynamic diameter below 10 μm are defined as PM_{10}, whereas

particles below 2.5 μm diameter are defined as $PM_{2.5}$ and those below 0.1 μm are defined as $PM_{0.1}$. Another classification refers to "coarse" particles to define the particles between 2.5 μm and 10 μm, "fine" particles those between 1.0 μm and 2.5 μm in diameter, and "ultrafine" particles (UFPs) those with a diameter lower than 0.1 μm [102]. Among them, PM_{10} and $PM_{2.5}$ are the most commonly monitored fractions of particulate matter. The largest particles, the so-called coarse fraction (or *mode*), are mechanically produced by the break-up of larger solid particles. Because of their relatively large size, coarse particles settle out of the atmosphere in a reasonably short time by sedimentation. Smaller particles or fine particles ($D_{ae} < 2.5$ μm) consist of particles generated by industrial and urban activity but also biogenic particles. This class of particles comprises an accumulation mode ($0.1 < D_{ae} < 2.5$ μm) and a nucleation mode ($D_{ae} < 0.1$ μm) (also referred to as Aitken mode). Accumulation mode particles result from the coagulation of smaller particles as well as from the condensation of vapors onto existing particles. They can also be introduced directly into the atmosphere, mainly through the incomplete combustion of wood, oil, coal, gasoline and other fuels. Ultrafine particles are formed from ambient-temperature gas-to-particle conversion as well as condensation of hot vapors during combustion processes. These particles act as nuclei for the condensation of low vapor pressure gaseous species, causing them to grow into the accumulation range.

The chemical composition of all these fractions clearly depends on the type of emission source. Natural particles originate mainly from sea spray, volcanic emission, mineral dust (from long-range transport or erosion processes), wildfires and biogenic sources, with sea salt being the biggest contributor, considering that approximately 75% of the Earth's surface is ocean [106]. Anthropogenic emissions of primary particles result mainly from the traffic-related combustion, industrial processes (metallurgy, foundries, refineries, and mining), heating of petroleum products (housing, industrial, commercial), incineration sites and agricultural activities.

In general, the composition of particulate matter includes variable amounts of inorganic, carbonaceous, biologic, and organic compounds. In the inorganic component, metals seem to prevail, especially lead, iron, copper, aluminum, calcium, potassium, sodium, and

magnesium. Depending on their sources, these elements can be found in either fine or coarse mode, with very different concentrations even for similar pollution levels, indicating the strong effect of local sources. In general, elements such as these have the highest concentrations and are usually called “major elements”, while elements such as heavy metals (mercury, cobalt, chromium, and cadmium to name few) are characterized by low concentrations and are called “trace elements”. Trace elements are also adsorbed or condensed on the surface of the particles and may play an important role in the toxicity of the PM [107]. Water-soluble ions could also be included in this component of the particulate matter; this comprises species like ammonium, sulfate, chloride, phosphate, and nitrate ions.

The carbonaceous component in particulate matter comprises both elemental carbon (EC) and organic carbon (OC). Major source categories of carbonaceous particles include open biomass burning (e.g., agricultural burning, wildfires, prescribed burning), traffic-related sources, electricity generating units and other power production sources, residential heating and cooking sources.

A biologic fraction consists of small organisms such as bacteria, spores, pollen, seeds, cellulose fragments of plants, algae, protozoa, fungi, as well as fragments of insects [108]. Organic compounds can also be adsorbed onto atmospheric particles, being emitted from both anthropogenic and biogenic sources [109]. This component includes a huge variety of substances, each belonging to different chemical families (aromatic hydrocarbons, ketones, alcohols, alkanes, aldehydes, etc). A different section is dedicated to the organic component, being part of the Ph.D. studies.

4.2 PM as a vehicle of organic contaminants

The adhesion of organic compounds to particulate matter can modify its chemical composition through different transformation processes [110]. Contaminants present in the PM can also enter into the human body and be absorbed directly into the bloodstream, having several health effects. The process of adsorption on PM strongly depends on the specific surface area of the particles as well as on the vapor pressures of organic

compounds. The specific surface area ($m^2 g^{-1}$) is defined as the total surface area per unit mass of a divided solid, which is the geometric surface of the grains. The larger the specific surface area, the greater is the capability to adsorb the molecules [111]. For PM, this would mean that the particles are likely to have a high number of sorption sites for different compounds in the troposphere. The strength of the bonds will determine if this sorption is chemical or physical. The vapor pressure of the sorbed compounds plays an important role in determining whether they will be found in the gas or particle phase. For example, semi-volatile substances (SVOC) are found both in the particulate and vapor phases, whereas volatile compounds (VOC) occur mostly in the gas phase and substances with very low vapor pressures are adsorbed almost exclusively. Thus, in the indoor environment, SVOCs are the most important compound classes that are adsorbed onto particles while VOCs are mostly present in the gas phase and only a tiny fraction (mainly polar substances) are found to be adsorbed.

Among the organic contaminants sorbed to PM, special care is taken for a list of priority pollutants, those considered Persistent, Bioaccumulative and Toxic (PBT). Though the classification of these chemicals has been extensively studied, a great part of substances has not been regulated and a growing lack of information exists about their impact on ambient pollution, as the development of new chemicals continues. These substances have been reported as "emerging contaminants" (ECs), also known as "contaminants of emerging concern". This term is used to broadly identify natural and synthetic chemicals, as well as their transformation products, which are not included in the existing monitoring programs since little is known about their properties, sources and fate. These chemicals do not necessarily need to be new, but their environmental fate and ecotoxicological study have not been evaluated. Therefore, they have a high potential of causing environmental damage to ecosystems and human health. They may be candidates for future regulation once more is known about their eco-toxicity and potential health effects, as well as their occurrence in different environmental compartments. Indeed, once in the environment, emerging pollutants can be transported via different pathways, which depend on the physical and chemical properties of these substances, namely water solubility, vapor

pressure, and polarity. The threat of the widespread use of emerging contaminants lies not only in the lack of information about their potential effect of human and ecosystem but also in the absence or inadequacy of the analytical techniques for monitoring them, as well as in the partial removal by the water treatment plants (wastewater or drinking water plants) [112]. In addition, when these contaminants pass through treatment systems, undesired transformation products can be generated.

The behavior of these pollutants strongly depends on the physical and chemical properties of each substance. Unlike "classical" pollutants, as chlorinated hydrocarbons (PCB, DDT, dioxins, etc.) or polycyclic aromatic hydrocarbons (PAHs) which are mostly lipophilic compounds, these emerging pollutants are often more polar and less volatile. Moreover, they include numerous compound classes, pharmaceuticals, personal care products (PCPs), illicit drugs, perfluorinated compounds (PFCs), brominated flame-retardants, organophosphorus compounds, benzotriazoles, benzothiazoles, and benzenesulfonamides [112].

Pharmaceuticals and personal care products (PPCPs) include all the different chemicals used in humans and animals, which are released to the environment through individual human activities. For instance, pharmaceuticals mainly include antibiotics, analgesic and anti-inflammatory. Nonetheless, other compounds belong to this group, such as antiseptics, anticoagulants, psychiatric drugs, hormones, and anticancer. Being these pharmaceuticals primary additives in medicines, they are meant to be bioavailable; this may result in adverse environmental effects even at low concentrations [113][114]. Personal care products include synthetic fragrances (e.g., nitro and polycyclic musk fragrances), sunscreen agents (ultraviolet filters), insect repellents (as N, N diethyl-m-tolueneamide) and parabens (p-hydroxybenzoic esters), which are active ingredients in detergents, shampoos, deodorants, lotions and toothpaste [112]. The accumulation and persistence in the environment of the various PPCPs strongly depend on the physical and chemical properties; indeed, PPCPs have octanol-water partition coefficients (K_{ow}) or water solubility values that vary up to 7–8 orders of magnitude. In addition, many of the PPCPs are ionizable chemicals [115,116].

Another category of ECs is represented by the illicit drugs, also known as drugs of abuse, which refer to all the drugs with nonmedical use that are prohibited by the national and international laws [117]. A lot of chemicals belong to this category, as hallucinogens, opioids, and stimulants, with cocaine, heroin, nicotine, amphetamine, opiates or cannabis, as common target substances. Even in this case, a great variety of compounds is responsible for the occurrence in different compartments. Whilst some classes of drugs, as cannabinoids, are highly lipophilic with log K_{ow} in the range 5 – 8, and bind to sewage sludge or particulate matters, other drugs, such as amphetamine and opioids, are moderately polar, thus occurring to a higher extent in the aqueous phase.

Perfluorinated compounds (PFCs) are a blend of fluorocarbons (containing only C-F and C-C bonds) which find many industrial applications, like stain, water and grease repellent chemicals, due to their extreme stability, ensured by the strength of the chemical bond between C and F atoms. On the other hand, this is responsible for the persistence of these substances in the environment, since they break down very slowly. PFCs show peculiar chemical properties, since they contain a hydrophilic head and a lipophilic tail, resulting from the reduced polarizability of the fluorinated molecular surface. For instance, PFOA (perfluorooctanoic acid) acts as a carboxylic acid with strong surfactant and hydrophobic characteristics. Thus, it is commonly used as a surfactant, since it is more efficient at lowering the surface tension of water than comparable hydrocarbon surfactants. Other common applications of PFCs include fast food packaging, fire-fighting foam, cosmetics, pharmaceuticals, cleaning products, insecticides, and paints. In contrary to most brominated flame-retardants (BFRs), PFCs are not efficiently removed through the wastewater treatment process, enhancing the persistence of PFCs in the environment and consequently bioaccumulating in both human and wildlife. Many studies reported the presence of PFOA in the human body [118], where it can bind to proteins, reaching blood serum, kidney, and liver.

Flame-retardants (FRs) represent another group of anthropogenic emerging contaminants, which is of great concern due to the widespread use in many applications. Indeed, they are incorporated into different materials, namely polymers, plastics, and textiles, to reduce

their flammability, to delay ignition and to meet fire safety requirements. Depending on FR properties, the combustion process can be delayed or prevented. Two of the major groups of these FRs are halogenated FRs, including brominated and chlorinated flame-retardants (BFRs and CFRs, respectively), and phosphorus-containing flame-retardants (PFRs). Among the halogenated FRs, BFRs constitute the largest market group owing to the low cost and high performance, resulting from the fact that at high temperatures, their decomposition products are less volatile than those derived from chlorinated compounds (since bromine is heavier than chlorine). As far as brominated FRs are concerned, polybrominated diphenyl ethers (PBDEs) are the most studied. Indeed, PBDEs have been widely used in consumer goods such as electrical equipment, construction materials, coatings, textiles and polyurethane foam (furniture padding) [119]. The threat about their use is related to their limited biodegradability, which makes them persistent, thus tend to accumulate into the environment. In addition, they are lipophilic; therefore can bioaccumulate in animals and humans. The increasing evidence of the presence of different BFRs in the environment at various locations, far from where they are produced and used, has aroused great concern, inducing many countries to ban some of them [119]. On the other hand, restrictions on the use of BFRs, and especially PBDEs, have resulted in the increased use of alternative flame-retardant chemicals, as phosphorous-containing FRs, which show some advantages compared to BFRs. Indeed, during a fire, toxic by-products are formed from by BFRs and emission of gases and toxic is far higher than from PFRs [120]. In recent years, organophosphate esters (OPEs) [103] were thought to be a suitable alternative to the use of BFRs. Conversely, many substances belonging to this class, such as Cl-containing PFRs, have been proven to be toxic and carcinogenic, so as to reconsider them as emerging contaminants.

As previously mentioned, some classes of emerging contaminants, as organophosphate esters (OPEs), benzotriazoles (BTR), benzothiazoles (BTH) and benzenesulfonamides (BSA) were investigated during the Ph.D. work, thus are described in Chapter 6. In the following sub-sections, some of the compounds belonging to each group are described, focusing on their structure, chemical properties, and ecotoxicological risk.

4.3 PM adverse effects on human health and environment

Particulate matter covers a key role in the investigation of ambient air pollution due to the adverse effects on both the environment and human health. Depending on the PM chemical composition, the harmful impact on the environment is directly linked to the transport by wind over long distances with the subsequent possibility to settle on ground or water. Indeed, PM can make lakes and streams acidic, change the nutrient balance in waters, deplete the nutrients in the soil, damage sensitive forests and farm crops, affect the diversity of ecosystems, and contribute to acid rain effects. As regards the effects on human health, these are strongly related to the size of the particles in question. Indeed, smaller particles pose the greatest problems, because they can get deep into your lungs; particles larger than 10 µm are likely to land in proximal airways while fine particles reach the lungs and are deposited in the alveoli [102,121]. Fig. 4.1 shows the penetration ability of particles into the lungs, as defined by commonly used size-based particle terms. From a sanitary point of view, PM is divided as inhalable, thoracic, and respirable particles, each describing where particles are likely to deposit in the lungs. Inhalable particles pass into the upper airways (nose and mouth) in the respiratory tract, "thoracic particles" deposit within the lower respiratory tract, and "respirable particles" penetrate to the gas-exchange region of the lungs. It seems obvious that smaller particles may be more harmful than larger ones [102].

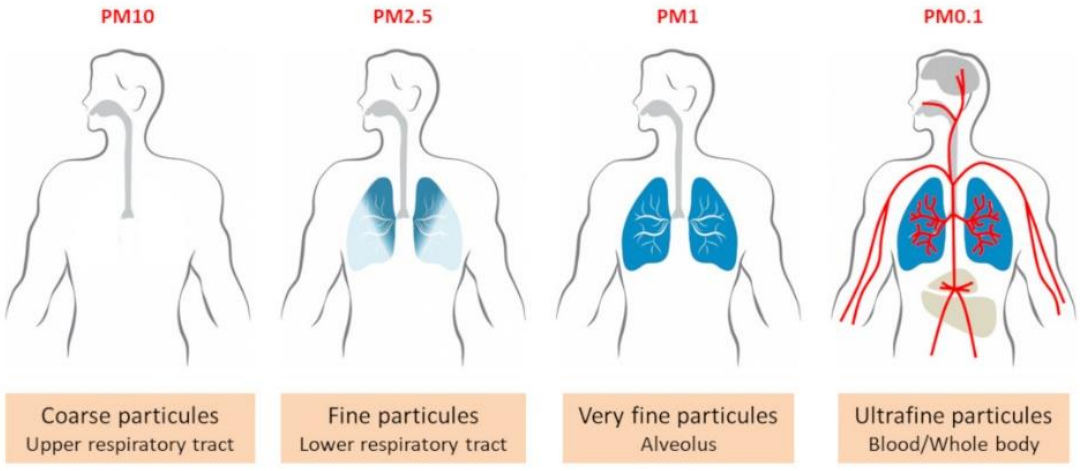

Fig. 4.1 Lung´s penetrability by different particles [122]

In addition, ultrafine particles are able to get into the bloodstream by different transfer routes and mechanisms, being then distributed into body organs, including the brain, with potential neurotoxic effects. The most severe effects in terms of the overall health burden include a significant reduction in the life expectancy of the average population, which are linked to the long-term exposure to high levels of air pollution with PM. These long-term effects, for example, involve:

- increase in lower respiratory symptoms;
- reduction in lung function in children;
- increase in chronic obstructive pulmonary disease;
- reduction in lung function in adults;
- cardiopulmonary mortality;
- lung cancer.

Indeed, WHO has designated airborne particulates as a Group 1 carcinogen [102]. Some of these effects occur at very low concentrations that were previously considered safe. In addition to the hazardous health effects previously mentioned, the risk associated with particle pollution is increased if the potential absorption on the particle surface of many harmful contaminants is considered. These harmful contaminants may be inorganic, such as heavy metals (like lead, cadmium, and mercury) or volatile and semi-volatile organic, for example, polycyclic aromatic hydrocarbons, PCBs, or dioxins. In this way, PM acts as a vehicle of pollutants worldwide, serving as sinks for a variety of species in both the outdoor and indoor environments.

Concerns about all the health effects have led to the implementation of regulations to reduce emissions of harmful air pollutants and their precursors at international, national, regional and local levels. For example, different reference guidelines for controlling the PM concentration are the World Health Organization (WHO), Air Quality Guidelines (AQG), the United States Environmental Protection Agency (US-EPA) National Ambient Air Quality Standard (NAAQS) and the European Union (EU) Limit Values for Air Quality (LVAQ). In most of these guidelines, the concentration of PM is expressed in μg

m^{-3} and averaged over a 24 h sampling period. As an example, the WHO AQG limited the annual mean of PM_{10} and $PM_{2.5}$ to 50 and 25 μg m^{-3}, respectively.

Chapter 5

Analytical techniques for the determination of organic contaminants in particulate matter

5.1 Introduction

The need to understand the processes controlling emerging contaminant sources, transport and fate in the environment and ecologic and human health effects has motivated the investigation of the environmental occurrence of these compounds down to trace levels. Therefore, sensitive analytical methods are necessary to detect and quantify accurately all types of organic contaminants. Though methods have been developed to enhance capabilities for measuring emerging contaminants and their associated degradation products in the environment, more intensive efforts are still needed in this area in order to determine these compounds at lower and lower levels within the realm of possibility. Indeed, it is well known that many organic contaminants can have severe adverse effects even if present in very small concentrations in a certain matrix.

The occurrence of organic contaminants in the airborne particulate matter has been deeply investigated in the past years by many researchers worldwide. Traditionally these studies rely on different steps, starting from the particulate matter collection, the extraction of the organic contaminants from the collection media, and the subsequent analysis. A purification of the extract, can be added according to the types of extraction and analysis techniques.

In the next sections, a brief overview of the analytical techniques involved in the determination of organic contaminants in airborne particulate matter (PM) is reported, focused on the different steps of the analytical methods. In addition, a brief summary of the multivariate approach used in the development of innovative methods for certain classes of pollutants in PM (part of the work of my Ph.D. studies) is reported.

5.2 Sampling of particulate matter

The selection of a sampling method for airborne particulate matter strongly depends on the aims of the study, as well as the sensitivity and selectivity required, the information to be obtained, the available equipment, and the sampling site. In general, two different sampling approaches exist:

- on-line methods, generally based on sampling and automated measurements of the amount of PM at the site itself, as well as some chemical composition of the particles;
- off-line methods, based on the sample collection in the selected site, the transportation and the analysis of the chemical composition of the PM in the laboratory.

Typically, the online methods are used to collect and measure the PM concentration with short resolution times (< 1 h) providing useful information on real-time characterization of the atmospheric chemistry. Therefore, they could be a useful tool for studies about the source and formation of atmospheric PM. On the other hand, off-line methodologies are usually employed to obtain more specific information for the chemical characterization of atmospheric PM. Once the sample is collected in the filter, it must be transported to a laboratory, where sampling is complemented with other analytical techniques for determining the organic contaminants present in the PM. In this case, according to the concentration of the analytes in the PM samples, longer sampling times are required, from hours to days. Off-line sampling methodologies are more suitable for studying the concentration of specific compounds. The sampling equipment involves a suction pump, an air inlet, a cut-off sampling head for preventing the undesired fraction being collected, and a filter as a retaining element of the desired PM from the air. Among the most common material used for filters, glass fiber filters (GFFs) and quartz fiber filters (QFFs) [110] show the greatest advantages due to their chemical, thermal and mechanic stability, inertness, flow resistance, loading capacity and concentration of the target compounds preexisting in the filter itself (blank). However, higher blank levels are usually found when GFFs are compared with QFFs [110].

Once the sampling is carried out and the airborne particles from the outdoor air are trapped onto the filters, the samples have to be stored until analysis, wrapping them in

aluminum foils and freezing to prevent possible compound losses. Then, the PM samples are ready for the extraction step of the target pollutants.

The mass determination of the sampled PM is usually accomplished by the gravimetric method to measure quantities of airborne particulate matter collected in a monitoring site. According to this gravimetric method, filters used to collect particles with a certain aerodynamic diameter are weighed before sampling, after being conditioned at certain values of temperature and humidity [123]. Once sampled, filters are conditioned again, to prevent artifacts due to different moisture content, and then weighed to obtain the net mass of PM by difference.

5.3 Traditional sample preparation strategies for organic pollutants in PM

In chemical analysis, sample preparation is frequently considered the bottleneck of the entire analytical method. The success of the final method strongly depends on understanding the entire process of analysis of a particular type of analyte in a sample, namely the physicochemical properties of the analytes (solubility, volatility, polarity, etc.), the environmental conditions, and the matrix components of the sample.

Even in the case of the determination of the organic pollutant bound to particulate samples, depending on all these conditions, the sample preparation step can be different. Indeed, once sampled on filter substrates, organic contaminants can be subjected to different extraction approaches, such as liquid or thermal extraction, and often a clean-up step is also necessary before the compounds are quantified. Although there is a great variety of compounds bound to the atmospheric particle samples with very different physicochemical properties, nowadays due to the improvement in some extraction techniques, the addition of novel techniques or the combination of some of them, it can be easier to extract a large number of contaminants from a single extraction. Indeed, the extraction step represents the key point since the results will depend on the efficiency of this process. The optimum would be to transfer all the target compounds retained on the filter to a liquid solution while disregarding the other compounds in the sample, which would act as interferences. Therefore, extraction with organic solvents is the preferred option. Several methods are based on this principle, starting from the simple solid-liquid extraction to more complex techniques, which

require specific equipment, such as Soxhlet extraction. This technique, combined with the use of organic solvents, as dichloromethane, acetone, n-hexane, ethyl acetate or toluene, is one of the most used for extracting organic contaminants from atmospheric PM filters. Dichloromethane has resulted as one of the most used solvents due to its low boiling points and high extraction capability. In literature studies, Wolschke et al. [124] reported the use of the Soxhlet method with DCM for 16 h coupled to GC-MS/MS detection for the determination of OPEs from glass fiber filters. The Soxhlet method proceeds by iterative percolation of the sample with re-condensed vapors of solvent. In particular, it consists of the ability of solvent vapors to extract analytes present into the solid sample, loaded into a porous cellulose sample thimble. High quantities of organic solvent are poured into a flask and heated at a certain temperature, in order to evaporate to the upward section of the Soxhlet apparatus (Fig. 5.1), which includes a reflux condenser. In this way, solvent vapors condense into the sample thimble and it is drained back into the solvent flask through a siphon device.

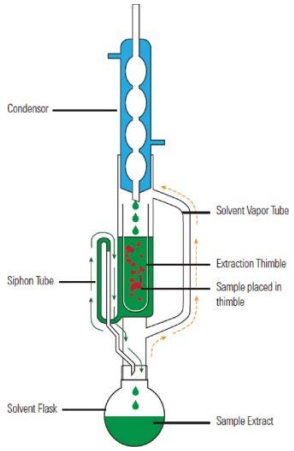

Fig. 5.1 Schematic representation of a Soxhlet apparatus [123]

A reflux cycle is started, due to the ability of the solvent to evaporate and condense back to the liquid phase, while extracting analytes from the solid sample. Since the extracted analytes have boiling points higher than the extraction solvent, they accumulate in the flask while solvent vapor is regenerated.

Unfortunately, this technique has some drawbacks due to the long extraction times and the large solvent consumption respect to other analytical methods. Indeed, since the extraction from the sample occurs at a cool temperature, extraction times can range

from 6 to 48 hours. Furthermore, large amounts of organic solvents are usually consumed, typically 300-500 mL for 10 g samples [125,126], in order that vapors are continuously generated; this also makes necessary a preconcentration step, before clean-up and analysis. These are the reasons why Soxhlet extraction has been replaced by other extraction techniques, as ultrasonic-assisted extraction (UAE) or microwave-assisted extraction (MAE). Ultrasonic-assisted extraction, also known as sonication, uses ultrasonic vibration to ensure intimate contact between the sample and the organic solvent.

It's a fast technique, indeed UAE extraction times are from 15 min to 1 h, approximately and the volume of solvent used is also lower, ranging from a few to 100 mL. This technique improves the extraction parameters (solvent volume and time) compared to Soxhlet extraction due to the help of ultrasound waves. However, a disadvantage of this technique is the need to filter the sample after extraction to separate the extract. The solvents employed to extract the analytes could be the same as mentioned for Soxhlet extraction, but including some non-volatile solvents, such as ultrapure water. Anyway, its efficiency is not as high as other techniques. Further to this, some organic compounds can undergo decomposition upon irradiation [127].

To improve efficiency, several extraction techniques with more specific equipment for favoring the extraction step, such as microwave-assisted extraction (MAE), have been used to replace the conventional ones.

5.4 Microwave-assisted extraction as an alternative technique for organic pollutants determination in PM

Microwave-assisted extraction (MAE) is an innovative approach used to minimize the solvent consumption and the extraction time, as well as to improve the extraction efficiency and facilitate the automation of the process.

In MAE, microwave energy is used to heat solvents in contact with solid samples and to promote partition of the analytes from the sample matrix into the solvent (the extractant). This way of heating is different from the classical convection heating since it is based on the interaction of the electrical component of the waves with compounds

of a material, which is converted in heat. The ability of a material to transform energy into heat is defined as the loss tangent (tangent delta):

$$\tan \delta = \frac{\varepsilon''}{\varepsilon'}$$

where ε'' is the dielectric loss coefficient and ε' is the dielectric constant, a measure of the polarizability in the electric field. Polar solvents having high $\tan \delta$ values can be heated rapidly. The non-polar solvent cannot be heated since they lack dipoles and do not absorb microwave energy. Thus, they can be used for MAE as "microwave transparent solvent" if the sample has high values of ε''. Thus, the mechanism through which electromagnetic energy is converted into thermal energy is the dipole rotation of the polar molecules which try to line up with the electric field. Multiple collisions from this agitation of molecules generate energy release and therefore a temperature increase.

The technical application of microwave energy to the samples may be performed using closed vessels (under controlled pressure and temperature), or open vessels (at atmospheric pressure). These two technologies are commonly named pressurized MAE (PMAE) or focused MAE (FMAE), respectively. While in open vessels the temperature is limited by the boiling point of the solvent at atmospheric pressure, in closed vessels the temperature may be elevated by simply setting the appropriate pressure.

In each case, the main parameters influencing MAE performance include the nature of the solvent and the matrix, the solvent volume, the temperature, and the exposure time. In general, the choice of the solvent/solvent mixture is a key factor to ensure proper extraction efficiency. As previously mentioned, three types of solvents can be used in MAE: solvent(s) of high ε'' values, a mixture of solvents with high and low ε'' values, transparent solvent(s) with a sample of high ε''.

As regards the solvent volume, on average, it may be about 10- fold less than those used in classical extractions, always considering that it must be sufficient to ensure that the whole sample is immersed [128].

Generally, recovery increases with the increase of temperature and then it could level off after a certain value if the analytes are thermally labile. This is also the case of long extraction time: recovery can increase up to a certain value, then analytes may undergo

decomposition. Usually, short extraction times (lower than 20 min) are necessary to achieve acceptable recoveries.

MAE is easy to implement, is rapid and provides good extraction efficiencies similar to or higher than those obtained with classical techniques (i.e., Soxhlet or liquid-liquid extraction) and other more recent techniques (i.e., supercritical fluid extraction or pressurized liquid extraction). Among the main advantages, it must be emphasized the MAE is a relatively greener method compared to the classical extraction, due to the great reductions of extraction time and solvent consumption, which also generates less waste. Moreover, it gives the opportunity to perform multiple extractions at the same time, increasing the sample throughput. The reasonable cost of the equipment should also be taken into account. A promising trend consists of implementing MAE with solvent-free methods (e.g., the combination of MAE with SPME) for the rapid determination of emerging pollutants from a wide range of environmental samples.

Indeed, after the extraction process, depending on the method's purpose, the selectivity of the extraction process, the complexity of the sample, and the type of target compounds, sometimes the clean-up of the obtained extracts is required to eliminate interferences from the analytes. Generally, column chromatography filled with different materials is commonly used. As an example of a clean-up step to purify PM extracts, Moller et al. [124] used a silica gel column topped on anhydrous granulated sodium sulfate to clean the Soxhlet extract after being roti-evaporated. In other cases, the obtained extracts are evaporated to dryness before being injected into the chromatographic system in order to decrease the method detection limits.

As previously mentioned, recent trends consist of the coupling of extraction with microextraction techniques, in order to combine the dissolution or releasing of analytes from the solid samples into a liquid medium with the simultaneous clean-up and preconcentration. Among microextraction approaches, one of the most used is solid-phase microextraction (SPME), which will be discussed in the following section.

5.5 Solid-phase microextraction as a convenient tool in environmental analysis

Solid-phase microextraction (SPME) is a sample preparation technique introduced by Pawliszyn and co-workers in 1989 [129] which has been widely used for the analysis

of pollutants in environmental samples [130]. The principle of operation of this technique is based on the fact that analytes are adsorbed on the surface of a polymeric coated fiber from which they can subsequently be desorbed by injection into the sample inlet of a chromatographic system[131]. This is accomplished with the help of a syringe-like handling device that protects analytes sorbed onto the material, as well as the fiber during storage.

In SPME, the extraction efficiency strongly depends on the affinity between analytes and the coating material. Currently, several coatings are commercially available, including polydimethylsiloxane (PDMS), polyacrylate (PA), divinylbenzene (DVB), Carboxen (CAR), and Carbowax (CW). Each fiber can be available in different thicknesses with single coatings, mixtures, or co-polymers. These fibers are suitable for the application of SPME to the analysis of non-polar organic compounds, for example, BTEX, PAH, pesticides, etc., and polar organic compounds such as phenols, alcohols, ketones, nitroaromatics, etc.[130]. Two modes of SPME can be considered: by direct immersion (DI-SPME) or via headspace (HS-SPME) (Fig. 5.2).

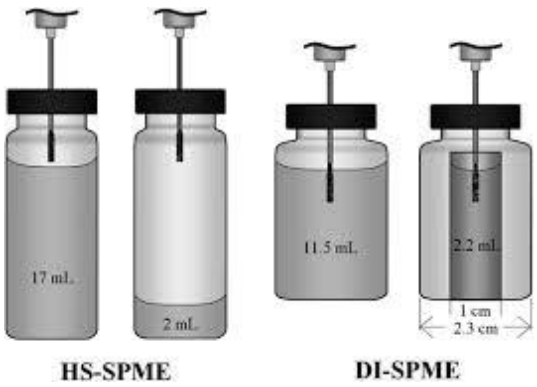

Fig. 5.2 Comparison between headspace-SPME (HS-SPME) and direct immersion- SPME (DI-SPME) [132]

In direct extraction, the coated fiber is directly immersed in the sample and the analytes undergo partitioning from the sample matrix to the fiber coating. To make aqueous extraction faster, agitation is necessary. This approach is mainly addressed to the extraction of non-volatile or low-volatile analytes. For volatile analytes, the SPME

fiber coating is exposed to the vapor phase above the sample matrix. Natural convection of air is enough to facilitate a fast equilibration.

Due to its flexibility, SPME can act both as a sampling method and as a preconcentration method. The main advantage is that SPME is a solvent-free technique, which makes SPME environmentally friendly while providing for faster separation and higher throughput. Moreover, it allows a wide range of compounds to be analyzed, ensuring high sensitivity and limit of determination, due to the complete transfer of all analytes to the quantification instrument. Indeed, after extraction, the analytes collected on the SPME coating are desorbed using thermal or solvent desorption, by GC or LC, thus minimizing any potential analyte losses due to multi-step processes.

5.6 Determination techniques

Different separation and detection techniques used to determine semi-volatile organic compounds in the PM from the air. These techniques are mainly based on chromatography as a separation technique and mass spectrometry as a detection technique, although other techniques based on nuclear magnetic resonance (NMR) or Fourier-transform infrared spectroscopy (FTIR) have been used to characterize some organic species present in the PM samples [133].

Gas chromatography (GC) is the technique most used to determine the organic compounds bound to PM present in the atmosphere due to the volatility of most of the compounds present, providing for a more exhaustive characterization of the PM sample. Gas chromatography is a technique based on the vaporization of the volatile analytes without decomposition, which interacts with the stationary phase while carried by an inert gas flow. The interaction with the stationary phase present in a capillary column is responsible for the separation of the different compounds, which then elute at different times, knowns as retention times (t_R). Usually, non-polar columns are used in order that a large group of organic compounds is determined in a single chromatographic run.

After separation, analytes are detected and quantified by means of different techniques. GC-MS is a powerful combination of techniques for determining and elucidating the

compounds present in the extracts of organic mixtures from environmental samples at low concentration levels. Indeed, mass spectrometry (MS) is able to identify the types of molecules coming from a gas chromatographic run, after ionizing them and measuring the mass-to-charge ratios. The subsequent identification is thus possible by interpretation of the fragmentation pattern characteristic for each molecule. In general, a single quadrupole provides enough selectivity and sensitivity for most of the compounds determined in the outdoor PM using the single ion monitoring (SIM) acquisition mode.

Anyway, in some cases, the sensitivity provided by a single quadrupole cannot be enough for the concentration levels to be detected. Other detection techniques, as tandem mass spectrometry (MS/MS), provide for higher sensitivity and lower detection limits. Indeed, in MS/MS, a triple quadrupole (QqQ) is used and the ions previously separated in the first mass spectrometer are further fragmented and detected in the second mass spectrometer. In conjunction with triple quadrupole mass spectrometry (GC–QqQ-MS), GC represents a reliable analytical tool since very satisfactory sensitivity and specificity can be achieved. For example, Li et al. [134] used a Soxhlet extraction followed by GC-MS/MS to determine eight organophosphates esters (OPEs) in PM samples from the North Atlantic and the Arctic and obtained MDLs from 0.0002 to 6.5 pg m^{-3}.

5.7 Experimental design for the multivariate optimization of the variables

In the development of analytical methods for the determination of some organic compounds bound to PM, which was part of the Ph.D. studies, each step of the method was critically evaluated. The values of the most important working conditions leading to the most efficient extraction of the analytes from PM resulted from the multivariate approach of the experimental design (DoE). This term refers to a statistical technique for planning the number of experiments, carrying out them, and analyzing and interpreting data. Traditionally, the optimization in analytical chemistry has been carried out by monitoring the influence of one factor at a time on an experimental response, according to the so-called OVAT (One Variable at a Time) approach. While only one parameter is changed, others are kept at a constant level [124]. Many

drawbacks can be found following this approach, the most important of them being the omission of the interactive effects among the studied variables as well as the increase in the number of experiments necessary to study the system. This all results in an overall time and costs consumption.

Nowadays, in order to overcome these problems, multivariate statistic techniques are used to obtain the optimization of analytical procedures that means to discover the best working conditions, evaluating the single variables and also the possible interactions. Among the most relevant multivariate techniques used in analytical optimization is response surface methodology (RSM) [135]. This technique, introduced by George Box and K. Wilson in 1951, explores the relationships between several and one or more response variables [136]. The main idea of RSM is to use a sequence of designed experiments to attain the best system performance, thus allowing a significant reduction in the number of experiments. Indeed, response surface methodology is a collection of mathematical and statistical techniques based on the fit of a polynomial equation to the experimental data, which must describe the behavior of a data set influenced by several variables.

Before applying the RSM methodology, it is first necessary to choose an experimental design that will define which experiments should be carried out in the experimental region under study. Obviously, a wide range of experimental design types exists. Among them, in the field of analytical method development, the common strategy first includes a screening of the variables affecting the analytical procedure, which is usually accomplished by first-order models, that is data are described by linear functions like

$$y = b_0 \sum_{i=1}^{k} b_i x_i + \varepsilon$$

where k is the number of variables, b_0 is the constant term, b_i represents the coefficients of the linear parameters, x_i represents the variables, and ε is the residual associated with the experiments. If an evaluation of the interaction effects among the variable is desired to evaluate the curvature of the model, a second-order polynomial equation should be taken into account, like

$$y = b_0 \sum_{i=1}^{k} b_i x_i + b_0 \sum_{1<i<j}^{k} b_{ij} x_i x_j + \varepsilon$$

Usually, a factorial experimental design is used to perform the screening of the variables affecting an analytical procedure. As example, in the case studies that will be discussed in the following chapter, the screening design was used to survey which variables had a significant influence on the method performances, i.e. really affected the sample preparation steps, namely the microwave-assisted extraction of the organic compounds from particulate filters and the preconcentration of the analytes by SPME. Factorial design involves testing several (k) variables (factors) at two *levels* (high and low) that represent the extreme values of the investigated domain. Once selected all the variables that potentially affect the response, the extraction efficiency in the case abovementioned, a design matrix is built, which comprises the experiments to perform in order to cover the experimental domain of each variable. The number of experiments is given from 2^k, where 2 is the number of the levels and k represents the number of variables. This means that for a system potentially affected by 3 variables, a total number of $2^3 = 8$ experiments is required. Contrary to the OVAT approach, in the factorial design variable 1, variable 2 and variable 3 are simultaneously changed. This makes the factorial design suitable for estimating the interactions between variables (i.e., the difference in changing variable 1 when variable 2 is at its higher level or at its lower level, and so on).

Nevertheless, this type of experimental design is used when the number of variables is relatively low, in order to avoid a great number of experiments. Anyway, it turns out that when k is not small, the desired information can be often obtained by performing only a fraction of the full factorial design [137]. Indeed, in some cases, a lot of calculated coefficients b_i corresponding to interactions of second (and higher) order can be supposed to be not significant. In these cases, a Fractional Factorial design is used, involving only a certain fraction of the number of runs that would be required for a Full Factorial Experiment, in order to extract the part of experiments from the full factorial design, which, for example, enables to obtain the main effects and some first-order interaction. Indeed, the total number of the experiments is calculated by the formula 2^{k-p} where p represents an integer number that would be 1, is a reduction of 1/2 is desired, or 2 if a reduction of 1/3 is desired, and so on.

The weight of contribution of each factor on the response and possible cross-effect among these factors can be estimated by the Pareto chart (Fig 5.3). Indeed, in this

chart, the bar lengths are proportional to the degree of significance for each effect and the color of the bar, orange or blue, reveals whether the variable has a positive or negative effect on the response, respectively.

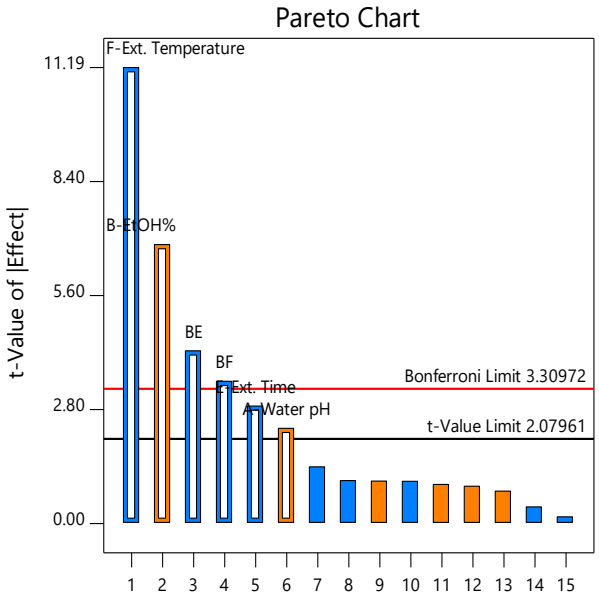

Fig. 5.3 Example of a Pareto chart resulting from the application of the experimental design

The vertical line instead represents the t value of effect, which is studied by two limit lines, namely the Bonferroni limit line and the t limit line [138]. Thus, coefficients with t value above the Bonferroni line are designated as certainly significant, those with t value between Bonferroni line and the t limit line are likely to be significant, and those with t value below the t limit line are statistically insignificant. These latter ones should be removed from the analysis or included only to support hierarchy.

As regards the optimization of the significant variables, a common DoE type is represented by the central composite design (CCD) [139], which results from the combination of two-level full or fractional factorial designs with additional axial (or star) points and at least one point at the center of the experimental domain under investigation. Indeed, the number of experiments can be calculated as $N = k^2 + 2k + cp$, where k is the factor number and cp is the replicate number of the central point. In this way, CCD allows the determination of both linear and quadratic models. With the aim to fulfill the rotatability condition, that is the experimental design will produce

information able to predict a response with the same precision at all points equidistant from the origin of the design, the value of α should be calculated by $\alpha = \sqrt{k}$; thus, for two variables, α value should be 1.41.

The mathematical model found after fitting the function to the data cannot describe the studied experimental domain satisfactorily. A more reliable way to evaluate the quality of the model fitted is by the application of analysis of variance (ANOVA). The central idea of ANOVA is to split the total variation in the data into a portion due to random error and a portion due to changes in the values of the independent variable(s) [135]. From this comparison, it is possible to evaluate the significance of the regression used to foresee responses considering the sources of experimental variance.

In the case that multiple responses need to be optimized, an appropriate response surface model for each response has to be built, including the set of operating conditions that leads to the optimal values of all the individual responses or at least keeps them in the desired range. In this sense, a useful approach is to use the Derringer's desirability function, which provides for the best compromise among the various responses.

This function searches for a combination of factor levels that jointly optimizes a set of responses by satisfying the requirements for each response in the design. The optimization is accomplished by converting the measured *i* properties related to each response into a dimensionless partial desirability (d_i) scale, with the conversion being obtained by specifying the goals, such as minimize, maximize or target the response. The scale ranges between $d_i = 0$, for a completely undesirable response, to $d_i = 1$ for a fully desired response. A weight factor, which defines the shape of the desirability function for each response, is then assigned in the range, between 0.1 and 10, with larger weights corresponding to more important responses. After the partial d_i are calculated for each response, it is possible to obtain the overall desirability (D) [140]. The overall desirability function D, commonly referred to as Derringer's desirability function, is defined as the geometric average of the individual desirability (d_i):

$$D = \sqrt[m]{d_1 \times d_2 \times \cdots \times d_m)}$$

One advantage of this function is that if any of the responses or factors fall outside its desirability range, the overall function becomes zero [141]. Thus, the simultaneous

optimization process is reduced to find the levels of factors that demonstrate the maximum overall desirability.

Chapter 6

Development of innovative methods for detecting organic contaminants in PM

6. 1 Introduction

In this chapter, two case studies concerning the development of new analytical methods for the quantification of some classes of organic contaminants adhered to airborne PM are reported. In particular, the first case aims at the determination of organophosphorus esters (OPEs) whereas the second one aims to quantify the benzotriazoles, benzothiazoles, and benzenesulfonamides in PM samples. Briefly, these methods provide for the microwave-assisted extraction (MAE) of the analytes from the PM followed by solid-phase microextraction gas chromatography-tandem mass spectrometry determination (SPME-GC-MS/MS). Each step of both the methods is optimized using the multivariate approach of the Design of Experiments (DoE) and the final working conditions are used to test the methods with real PM samples, collected in the outdoor area surrounding the Institute of Atmospheric Pollution (CNR-IIA). The key point of these methods relies on the use of an eco-compatible hydroalcoholic mixture for the extraction step in order to be compatible with the use of the direct immersion solid-phase microextraction (DI-SPME) as well as to be analyzed without any other clean-up step. Indeed, as previously described, the traditional protocols typically used for the determination of these analytes in PM rely on the use of laborious techniques, such as Soxhlet or solvent extraction, which present numerous drawbacks. For OPEs extraction, one of the most common techniques is the Soxhlet, also using chlorinated solvents, with damaging effects on the environment. As far as benzotriazoles, benzothiazoles, and benzenesulfonamides are concerned, the solvent extraction with alcoholic solvents is mainly used. In both cases, the type and the amount of solvent, the time-consuming operations, and the production of waste make the traditional techniques disadvantageous. On the contrary, the following method combines the use of an eco-friendly hydroalcoholic mixture (water/ethanol)

for the microwave-assisted extraction with the solventless SPME, sustaining the criteria of the green chemistry.

6.2 Case study 1: Organophosphate esters bound to particulate matter

Organophosphate esters (OPEs) are anthropogenic industrial compounds composed of a central molecule of phosphoric acid differently substituted with alkyl chains or aromatic groups, as well as partly halogenated alkyl chains. According to the nature of the substituents which gives them a wide range of physical-chemical properties, OPEs show several applications, for which they can be used as reactive ingredients that are covalently bound to materials or additives. Halogenated OPEs are mainly used as flame-retardants (FRs) to delay ignition of materials such as furniture, and electric and electronic instruments [142][143] whereas non-halogenated OPEs have additional uses since they are also employed as plasticizers, antifoaming agents, additives in rubber, textiles, and lacquers [142]. Analytes as tripropyl phosphate (TPP), tributyl phosphate (TBP), tris(2butoxyethyl) phosphate (TBEP), triphenyl phosphate (TPhP), (2-ethylhexyl)-diphenyl phosphate (EHDPP), tris(2-ethylhexyl) phosphate (TEHP), tricresylphosphate (TCP) (present as different isomers) belong to the first group. In particular, TPP and TBP are added in lubricants, hydraulic fluids, engine oils [144] whereas TBEP is used as an antifoaming agent and as a plasticizer in different materials, namely rubber, plastics[145], textile, and the building industry[146]. Other OPEs, as TPhP, TEHP, TCP, whose densities are similar, are used in PVC as plasticizer [145][147] and also in polyurethane foam, cellulose, cotton, electronic equipment such as cables, resins, glues, and engineering thermoplastics[142]. Typical halogenated OPEs include tris(1-chloro-2-propyl) phosphate (TCPP), tris(2-chloroethyl) phosphate (TCEP), and tris(1,3-dichloro-2-propyl) phosphate (TDCPP). TCPP is one of the most used PFRs mainly for construction applications, representing 80% of the chlorinated PFRs in Europe, due to its peculiar properties. Indeed, in the case of fire, it is active in both solid and gas phases, owing to the performance of phosphorous and chlorine, respectively. Similarly, TCEP shows this twofold action in the foam used as roof insulation for the building industry. Another halogenated FR is TDCPP, which is commonly employed in resins and latexes [148]. It also finds application in furniture, as well as in foams employed in the car industry or in baby

products. In the recent years, in order to meet specific standards TDCPP has replaced TCPP and TCEP due to a more efficient capability to act as flame-retardant, even if its price is higher. When all these analytes are used as additives, they are incorporated into polymer matrices without chemical bond, thus they could easily leak into the environment through various mechanisms as volatilization, abrasion, and dissolution, depending on the temperature and the vapor pressure of the compound. In addition, OPEs are resistant to biodegradation, especially the chlorinated ones, such as tris(1-chloro-2-propyl) phosphate (TCPP). Due to long-range transport OPEs can reach even remote regions of the world. This behavior has resulted in their occurrence in almost every environmental compartment, including wastewater and sludge [149], groundwater [150], sediment and soils [151,152], fish and biota [153,154], air and dust [155–157], and human plasma [158]. Risk assessments have recognized the carcinogenicity, high toxicity and environmental persistence of several OPEs [159]. For instance, TPhP is reported to cause neurotoxicity and contact dermatitis; besides, it is suspected to be a sensitizer for allergies. Anyway, the World Health Organization [160] reported that since its concentration in water is generally low, TPhP has no toxic effects on aquatic organisms, and since it is removed rapidly from the tissues of fish after exposure, its bioaccumulation is not considered to be a hazard. Consequently, TPhP has a low impact also on human health. TCP is considered to pose a major hazard to human health, being toxic to the central nervous system and skin. Moreover, TCP is considered harmful to aquatic organisms. In general, the toxic effect showed by the non-halogenated OPEs include eye and skin irritation, carcinogenicity, dermatitis, and neurotoxicity [142,155], but the major concern results from the halogenated ones. Indeed, TCPP, TCEP, and TDCPP are considered carcinogenic [161]. They also were reported to induce eye and skin irritation, neurotoxicity and adverse reproductive effect, like reduced fertility. Moreover, TDCPP is particularly harmful when inhaled since it can enter the blood stream [144]. Along with TCPP, they tend to accumulate in the liver and kidneys, where they are metabolized in hydroxides of phosphorous acid. As mentioned earlier, the main route of exposure is through inhalation from the air, where OPEs can exist in gas-phase particles or bounded to particulate matter (PM) as well. Anyway, several studies reported that OPEs are mostly associated with the airborne particles [155,162,163].

In the following sections, the different steps of the proposed protocol for OPEs quantification in PM will be reported. In particular, the investigated analytes were tripropyl phosphate (TPP), tributyl phosphate (TBP), tris(2-chloroethyl) phosphate (TCEP), tris(1-chloro-2-propyl) phosphate (TCPP), tris(1,3-dichloro-2-propyl) phosphate (TDCPP), tris(2-butoxyethyl) phosphate (TBEP), triphenyl phosphate (TPhP), (2-ethylhexyl)-diphenyl phosphate (EHDPP), tris(2-ethylhexyl) phosphate (TEHP), tricresylphosphate (TCP) (mixture of isomers), whose structures are reported in Fig. 6.1.

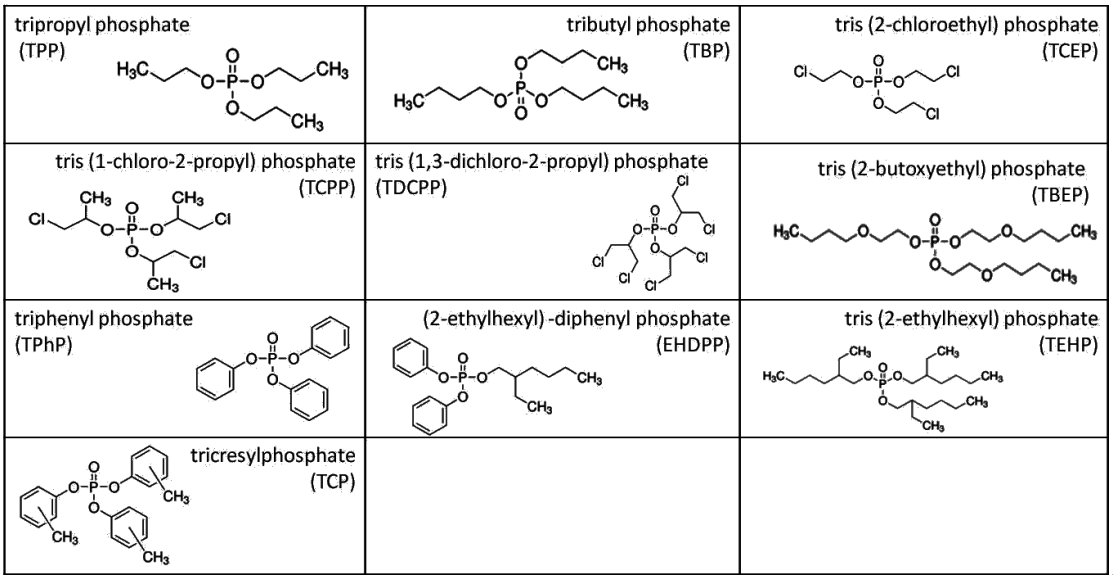

Fig. 6.1 Chemical structure of investigated OPEs

6.2.1 Microwave-assisted extraction from particulate filters

The first step of the analytical method was the microwave-assisted extraction of the analytes using an Ethos-Up Microwave Extraction System (Milestone, Leutkirch, Germany), equipped with 50 mL volume PTFE vessels. As previously mentioned, in the light of the increasing demand for eco-friendly analytical methods, a mixture of water and ethanol was chosen as extraction mixture, with the ethanol being meant as an additive in the mixture, to foster the extraction of the more hydrophobic analytes (Table 6.1). With the aim to seek the optimal working conditions leading to the best MAE performances, each parameter was carefully evaluated, and the multivariate approach of the Experimental design was used to simultaneously evaluate their optimal values while carrying out the lowest number of experiments.

Analyte	MW (g mol^{-1})	Water solubility at 25°C (mg L^{-1})	Log P [a]	Boiling Point (°C)
Tripropyl phosphate (TPP)	224.2	827	2.7	253.7±8.0
Tributyl phosphate (TBP)	266.3	280 [b]	4.3	288.3±8.0
Tris(2-chloroethyl) phosphate (TCEP)	285.5	7.0×10^{3} [c]	0.5	347.4±0.0
Tris(1-chloro-2-propyl) phosphate (TCPP)	327.6	1.60×10^{3} [d]	2.8	336.3±37.0
Tris(1,3-dichloro-2-propyl)phosphate (TDCPP)	430.9	1.50 [e]	1.8	457.4±40.0
Tris(2-butoxyethyl) phosphate (TBEP)	398.5	1.20×10^{3} [f]	4.3	413.9±0.0
Triphenyl phosphate (TPhP)	326.3	1.9 [g]	4.1	412.4±0.0
(2-ethylhexyl)-diphenyl phosphate (EHDPP)	362.4	1.9 [f]	6.6	421.2±18.0
Tris(2-ethylhexyl) phosphate (TEHP)	434.6	0.6 [f]	10.9	405.5±0.0
Tricresylphosphate (TCP)	368.4	0.36 [h]	5.5	410.4±14.0

Table 6.1 Physicochemical properties of target analytes. [a] Data reported at 760 mmHg predicted by Advanced Chemistry Development (ACD/Labs); [b] UNEP PUBLICATIONS, 2001. Tributyl Phosphate Cas No.: 126-73-8. SIDS Initial Assessment Report. For 12th SIAM, Organisation for Economic Co-operation and Development (OECD), Paris, France, pp. 1–132 (June); [c] Agency for Toxic Substances and Disease Registry (ATSDR), 2009. United States Department of Health and Human Services 2009. Draft Toxicological Profile for Phosphate Ester Flame Retardants (September). [d] WHO, 1998. EHC 209: Flame Retardants: Tris- (Chloropropyl)Phosphate and Tris-(2-Chloroethyl)phosphate, Geneva, Switzerland: [e] Chemspider, 2011. http://www.chemspider.com/Search.aspx; [f] WHO, 2000. EHC 218: Flame Retardants: Tris(2-butoxyethyl) phosphate, Tris(2- Ethylhexyl) Phosphate and Tetrakis (Hydroxymethyl) Phosphonium Salts, Geneva, Switzerland; [g] Fisk, P.R., Girling, A.E., Wildey, R.J., 2003. Prioritization of Flame Retardants for Environmental Risk Assessment. Produced for Environment Agency, United Kingdom. [h] World Health Organization (WHO), 1990. EHC 110: Tricresyl Phosphate, Geneva, Switzerland.

Extraction mixture volume, extraction time, heat-up time, extraction temperature and percentage of ethanol in the hydroalcoholic mixture were identified as the critical variables which could potentially affect the MAE and were optimized by Experimental design techniques, using Design Expert 10 (Stat-Ease, Inc, USA) software.

In particular, in the broad area of chemometrics, a fractional factorial design (FFD) was first performed to accomplish a screening of the selected factors and determine which one had a significant influence on the extraction performance. A 2^{5-1} FFD was performed, with two replications for each of the resulting 16 experiments and three replications at the center point. For each variable, a certain range of values was surveyed, selected on the basis of some preliminary tests and literature findings. In detail, the ranges were: heat-up time 1–10 min, extraction time 5–20 min, extraction temperature 70–170 °C, EtOH% in the extraction mixture 0–50 % (v/v) and volume of the extraction mixture 10–20 mL. All the experiments (Table 6.2) were carried out in a randomized order using the fortified quartz fiber filters soaked into the hydroalcoholic extraction mixture in the PTFE vessel. Before analysis, each filter was spiked with 15µg of each OPE (Sigma–Aldrich, Milan, Italy) and 100µL of a mixture of internal standards (IS), containing TBP-d_{27} and TPhP-d_{15} at 1000 ng mL^{-1}, and TCEP-d_{12} at 2000 ng mL^{-1}. The efficiency of the MAE step was assessed by injection into a gas chromatograph coupled to a mass spectrometer (GC-MS), after transferring all the analytes into an organic phase. This process was accomplished by liquid-liquid extraction (LLE) with a solvent immiscible with the extraction mixture, namely dichloromethane (DCM), in order to separate analytes from the aqueous solution. In detail, MAE extract was transferred to a 50 mL test tube and 3 mL of DCM was added; after vigorous shaking for 3 min, the organic layer was withdrawn by means of a Pasteur pipette, taking extreme care to avoid the collection of the aqueous solution. This procedure was repeated four times to ensure an accurate collection of the analytes from the aqueous phase. This fraction was subsequently dried over anhydrous Na_2SO_4 and concentrated to 0.5 mL under a gentle stream of nitrogen (0.8 bar) at 60°C (Turbovap II, Caliper Sciences, Inc.). The extract was transferred into a GC vial and the volume was adjusted to 1.5 mL with DCM, before GC-MS determination. For the analysis, an Agilent 6890 gas chromatograph coupled to a 5973 MSD quadrupole mass

spectrometer (Agilent Technologies) was used; MSD Chem (Agilent Technologies) software was used for data acquisition.

Experiment	A: Heat-up Time (min)	B: Extr. Temperature (°C)	C: Extr. Time (min)	D: EtOH Concentration (%)	E: Extr. Volume (mL)
1	10	70	5	0	10
2	5.5	120	12.5	25	15
3	10	70	5	50	20
4	1	70	5	50	10
5	1	70	5	0	20
6	1	170	5	0	10
7	10	170	5	50	10
8	10	70	20	50	10
9	5.5	120	12.5	25	15
10	10	170	20	50	20
11	10	170	5	0	20
12	5.5	120	12.5	25	15
13	1	170	20	0	20
14	10	70	20	0	20
15	1	170	5	50	20
16	1	70	20	0	10
17	1	70	20	50	20
18	10	170	20	0	10
19	1	170	20	50	10

Table 6.2 Design matrix 2^{5-1} fractional factorial design for the screening of the MAE conditions

The gas chromatograph was equipped with an HP-5MS (5 % phenyl)-methylpolysiloxane (Agilent Technologies) capillary column (30 m × 0.25 mm i.d., 0.25 µm film thickness); Helium (purity 99.999 %) was used as the carrier gas, and flow was set to 1.0 mL min^{-1}. The GC oven temperature was initially held at 80 °C for 4 min, then ramped at 20 °C min^{-1} to 140 °C and held for 2 min; then ramped again at 4 °C min^{-1} to 180 °C; finally ramped again at 20 °C min^{-1} to 280 °C held at this temperature for 6 min. The total runtime was 30 min. Analyses were performed in pulsed splitless mode by setting the injector at 270 °C and a pulse of 30 psi, for 1.5

min, was employed to improve the efficiency of the injection process. The MS operated in full scan mode, with electron ionization (EI) at 70 eV; the transfer line, MS Quad, and MS source temperatures were set at 280 °C, 150 °C, and 230 °C, respectively; the mass range was 50–450 m/z.

The impact of each variable and the possible cross-effect on the analyte response were estimated by the Pareto chart (Fig. 6.2) in which the length of the bars is proportional to the significance of the variables and the color, orange or blue, reveals the positive or negative effect of the variable on the response, respectively. As already explained, in these charts, the significance of the variables, in terms of t-value, is assumed considering the Bonferroni limit line and the t-value limit line thresholds. Effects with t-value towering above the Bonferroni line are certainly significant, effects with t-value between Bonferroni line and the t-value limit line are possibly significant, while effects with t-value below the t-value limit line are not statistically significant and should only remain in the model equation to maintain the hierarchy. The interpretation of these charts for each analyte showed that the variation of heat-up time (A) did not affect significantly the response of the analytes. On the contrary, extraction temperature (B) and ethanol concentration (D) had a positive effect on the response, whereas extraction time(C) had a negative effect. As regards the extraction volume (E), only its cross-effect with extraction temperature affected negatively the response of TCEP, TCPP, and TDCPP. It could also be noticed that extraction time was the most significant variable for TPP, TBP, TCEP, TCPP, TDCPP, and TBEP whereas ethanol percentage resulted in the most affecting variable for TPhP, EHDPP, TEHP, and TCP, i.e. the most hydrophobic analytes (log $P > 5$), indicating that the addition of ethanol to the water was fundamental to improve the extraction performance. All the obtained models were statistically significant (p-value < 0.05) and with insignificant curvature, thus showing the absence of maximum points (i.e., optimum points) within the investigated experimental domain. Therefore, in accordance with the results of FFD, the non-significant heat up time was set at 2 min, in order to reach the desired temperature without stressing the microwave equipment, whereas the remaining four variables were evaluated for further optimized in different experimental domains.

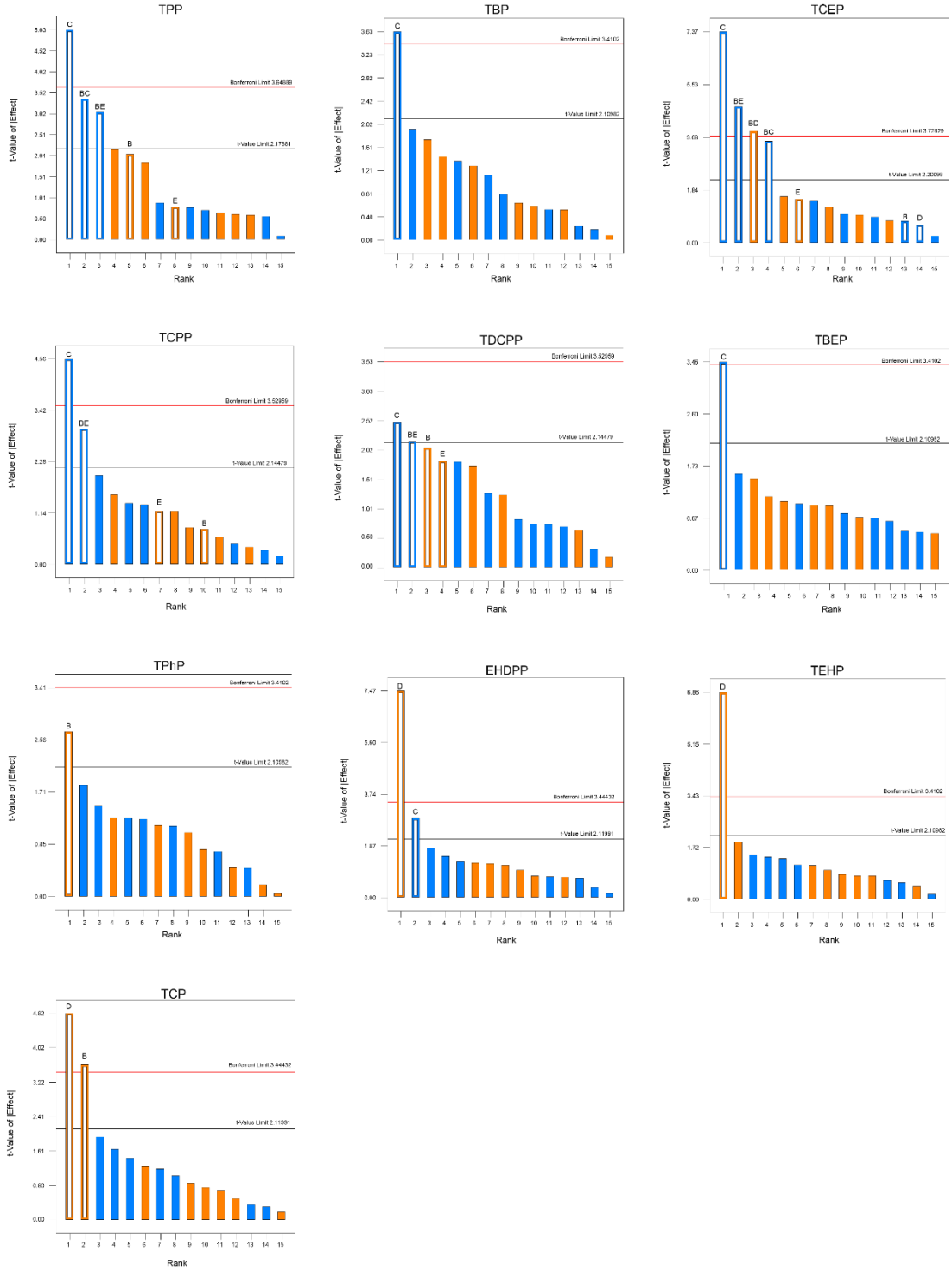

Fig. 6.2 Pareto chart from the fractional factorial design (2^{5-1}). Factors: A, heat-up time; B, extraction temperature; C, extraction time; D, ethanol concentration; E, extraction volume. The unfilled bars represent the selected statistically significant effects [164]

Indeed, the ethanol percentage in the extraction mixture was not investigated over 50% (v/v) because it was meant to be an additive able to enhance the extraction performance of water. Moreover, extraction volume was set at the lowest level in the investigated range since this was the minimum amount allowed into the microwave oven vessels. As regards the extraction time and extraction temperature, further optimization was performed shifting the experimental domain toward lower and higher values, respectively, to seek the optimum working conditions (i.e., maximum response). A central composite design (CCD) was chosen in order to estimate simultaneously the linear, quadratic and two-way interaction effects of the factors. This design consisted of a 2^2 factorial design with four star-points positioned at ± α from the center of the experimental domain and five central point replicates. The axial distance α was chosen with a value of 1.414 in order to fulfill the rotatability condition. The complete design matrix comprised 13 runs (2^2 + (2×2) +5) (Table 6.3) carried out in randomized order, in which extraction temperature (A) and extraction time (B) were allowed to vary in the range 150 - 210 °C and 1 - 6 min, respectively.

Experiment	A: Extraction Temperature (°C)	B: Extraction Time (min)
1	180	0.57
2	180	3.75
3	137.57	3.75
4	180	3.75
5	210	1.50
6	150	1.50
7	180	6.93
8	180	3.75
9	210	6
10	180	3.75
11	222.43	3.75
12	150	6
13	180	3.75

Table 6.3 Design matrix for 2^2 central composite design (CCD) used for the optimization of MAE extraction temperature (A) and extraction time (B)

The other variables were kept at their optimum values. The model coefficients were calculated by backward multiple regression to eliminate not significant factors (α=0.10). Thus, simplified models including only significant variables and those necessary to maintain hierarchy were obtained and validated by the Analysis of Variance (ANOVA) (Table 6.4). The models were considered to be statistically significant (p-value < 0.05) while, as it was desired, the lack of fit term was not significant. Finally, the best compromise for the microwave-assisted extraction was defined according to Derringer's desirability function, which showed the values of each parameter providing the maximum response of each analyte (Fig. 6.3).

Analyte	Model	Lack of fit	Recovery %
TPP	0.0103	0.4796	114
TBP	0.0024	0.6902	88
TCEP	0.0024	0.6894	105
TCPP	0.0048	0.3739	90
TDCPP	0.006	0.4075	77
TBEP	0.0092	0.12	75
TPhP	0.007	0.3294	80
EHDPP	<0.0001	0.2937	85
TEHP	0.0083	0.8843	89
TCP	<0.0001	0.9412	106

Table 6.4 Summary of the Analysis of Variance (ANOVA) for the 2^2 central composite design (CCD) used for the optimization of MAE extraction temperature (A) and extraction time (B) and recovery values under the optimum working conditions

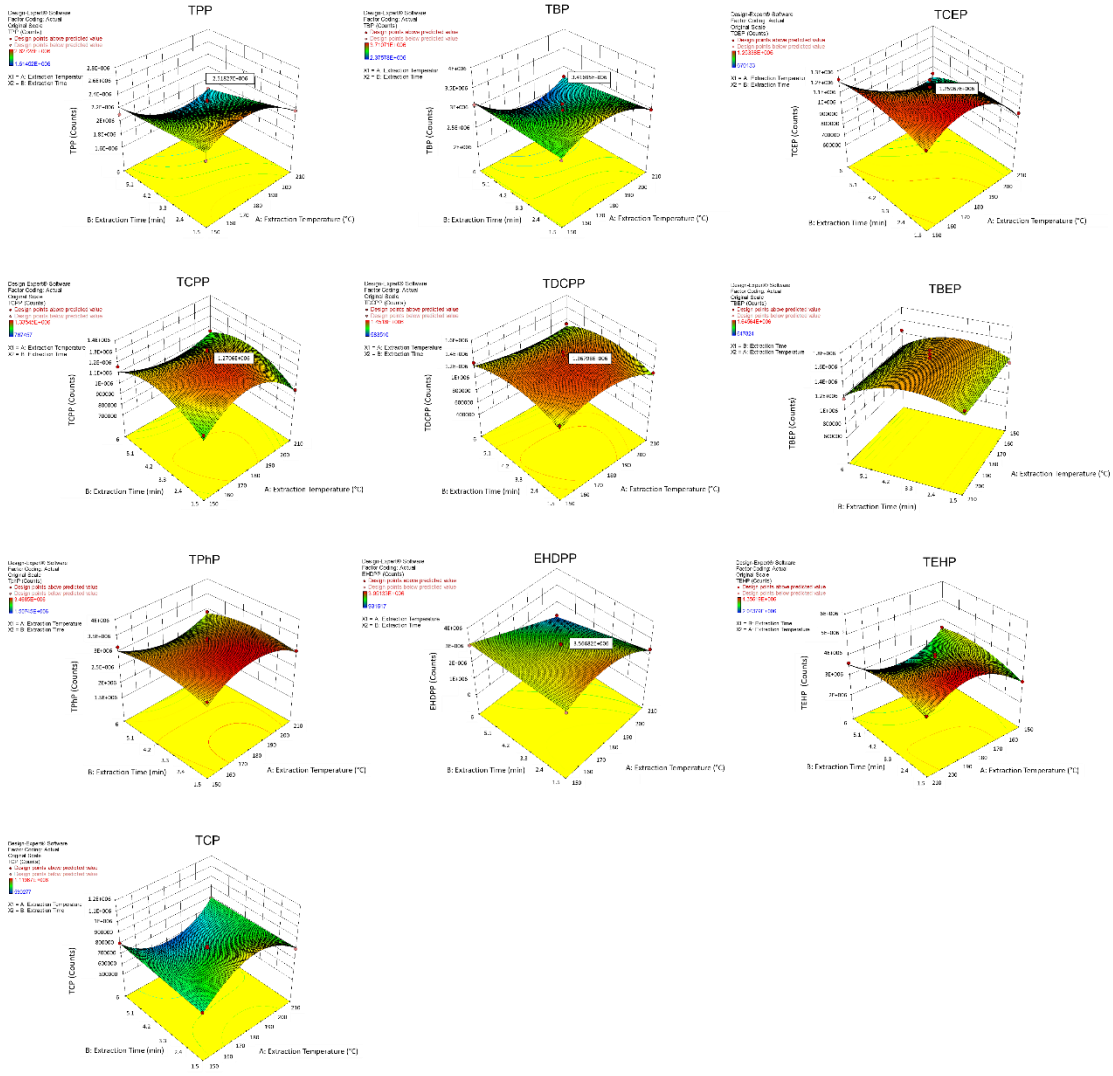

Fig. 6.3. Response surfaces of each analyte to the extraction time and temperature domain [164]

The total response surface (Fig. 6.4) showed that the maximum desirability (0.868), i.e. the best compromise among the individual desirability for each analyte, was achieved performing MAE at 180 °C for 1.5 min. Thus, according to an overall evaluation of the MAE, this step has to be performed with 10 mL of a water/ethanol 1/1 solution, for 1.5 min at 180 °C, reaching this temperature in 2 minutes, and recovery between 77 % and 114 % (Table 6.4) is obtained.

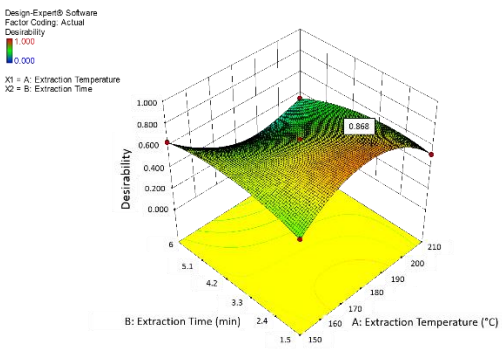

Fig. 5.4 Response surface of desirability function for MAE optimization [164]

6.2.2 Solid-phase microextraction

After MAE, the subsequent step was the OPE solid-phase microextraction (SPME) in order to simultaneously preconcentrate and extract the analytes from the aqueous phase, avoiding the use of tedious approaches as the liquid-liquid extraction previously involved for the multivariate evaluation of the MAE step. Moreover, SPME offers the possibility to inject the analytes directly into the injection system of the gas chromatograph, without the use of organic solvents [39, 40]. Each potential parameter affecting this step was also carefully evaluated and optimized through the multivariate approach of the experimental design. Conversely, the selection of the fiber suitable to collect all the analytes from the MAE hydroalcoholic extract was carried out in univariate mode. Indeed, being SPME is a microextraction technique based on the affinity between the polymeric material of the fiber coating and the analyte, the selection of the best coating usually represents a critical step of the entire SPME procedure. Five commercial SPME fibers (Supelco, Bellefonte, USA), namely polydimethylsiloxane 100 µm (PDMS), polyacrylate 85 µm (PA), polydimethylsiloxane/divinylbenzene 65 µm (PDMS/DVB), carboxen/polydimethylsiloxane 85 µm (Car/PDMS) and divinylbenzene/carboxen/polydimethylsiloxane 50/30 µm (DVB/Car/PDMS) were tested in direct immersion mode into the stirred MAE extract. However, a dilution step of the hydroalcoholic extract was necessary, in accordance with the fundamental of SPME theory. Indeed, an ethanol concentration of 50% v/v is maybe too high for SPME, which is devised for aqueous solutions to work properly. Consequently, with the aim to simulate the MAE extract, the extraction capability of each fiber was

evaluated in hydroalcoholic solutions diluted at 10 %, 5 % and 2 % as ethanol concentration (v/v), spiked with the investigated analytes. All the analyses were carried out in triplicate at 40 °C by direct immersion of the fiber into the stirred solutions for 30 min. Results showed that PA fiber, which is the most polar, was the worst coating because it was not able to extract analytes from the aqueous phase. Conversely, PDMS/DVB and DVB/Car/PDMS led to the best extraction performances. As concerns the dilution ratio, these two fibers resulted in very different responses in terms of precision of the SPME analysis (Fig. 6.5).

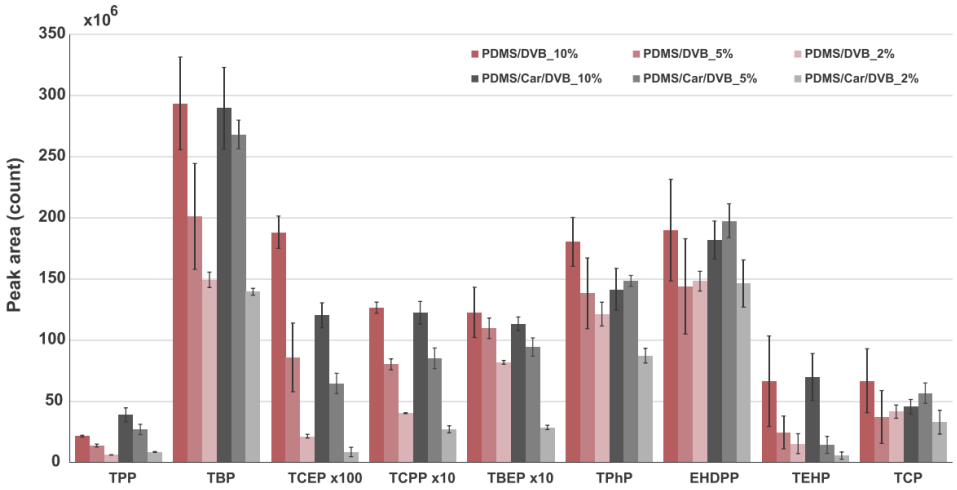

Fig. 6.5 Comparison of the extraction efficiency of PDMS/DVB and DVB/Car/PDMS fibers at different dilution of MAE extract [164]

In particular, the most hydrophobic analytes strongly suffered the competition between the hydroalcoholic solution and the fiber coating, resulting in high values of standard deviation. The best compromise between the amount of extracted analytes and reproducibility was attained with DVB/Car/PDMS coating after dilution of the MAE extract from 50 % to 5 % as ethanol concentration.

Once selected the fiber and the dilution ratio, it was possible to identify the variables potentially affecting SPME performances, taking into account the results of preliminary experiments as well as literature findings [165]. In particular, extraction time, extraction temperature, and ionic strength of the diluted sample expressed as NaCl % (w/w) were selected as the most critical factors and were optimized by using

a central composite design (CCD). The variation of the salt percentage into the hydroalcoholic solution was necessary to test the so-called "salting-out effect", that is the increase of the ionic strength in a solution aimed to enhance the partitioning of the analytes towards the fiber, due to their increased hydrophobicity of reduced solubility in the aqueous system. This variable was investigated in the range 0-10 %, expressed as w/w concentration. Extraction time, instead, was investigated between 15 and 45 min while the temperature was allowed to vary between 30 and 60°C. The CCD consisted of a full factorial 2^3 design with 6 axial points at ± α from the center of the experimental domain and 6 central points, for a total of 20 randomized runs (Table 6.5).

Run	A: NaCl (% w/w)	B: Extraction Temperature (°C)	C: Extraction Time (min)
1	5	60	30
2	5	45	45
3	5	45	30
4	5	45	30
5	8	53.9	21.1
6	5	45	30
7	0	45	30
8	8	53.9	38.9
9	2	36.1	21.1
10	2	53.9	38.9
11	10	45	30
12	8	36.1	21.1
13	5	45	30
14	8	36.1	38.9
15	2	36.1	38.9
16	5	30	30
17	5	45	30
18	5	45	30
19	2	53.9	21.1
20	5	45	15.0

Table 6.5 Design matrix for 2^3 CCD for the optimization of SPME parameters: NaCl percentage (A), extraction temperature (B) and extraction time (C)

The axial distance α was chosen with a value of 1.68 in order to fulfill the rotatability condition. In accordance with the previous tests, all the experiments were performed by direct immersion of the DVB/Car/PDMS fiber in 5 % ethanol solution obtained after dilution with ultrapure water of a spiked blank filter extract obtained through the optimized MAE protocol. As for MAE optimization, the model coefficients were calculated by backward multiple regression (α=0.10) and validated by Analysis of Variance (ANOVA) (Table 6.6).

Analyte	Model	Lack of fit	Recovery %
TPP	0.0103	0.4796	114
TBP	0.0024	0.6902	88
TCEP	0.0024	0.6894	105
TCPP	0.0048	0.3739	90
TDCPP	0.006	0.4075	77
TBEP	0.0092	0.12	75
TPhP	0.007	0.3294	80
EHDPP	<0.0001	0.2937	85
TEHP	0.0083	0.8843	89
TCP	<0.0001	0.9412	106

Table 6.6 Summary of the Analysis of Variance (ANOVA) for the 2^3 CCD used for the optimization of SPME conditions

As demonstrated by p-values, the obtained models resulted significant ($p < 0.05$), except for TEHP, and without lack of fit ($p > 0.05$) for all analytes. Indeed, NaCl percentage did not significantly affect the analysis for TEHP (the factor A did not appear in the regression equation).

The response surface of the desirability function indicated that the maximum value was achieved by setting the investigated variables to their highest values; i.e., extraction time 45 min, extraction temperature 60 °C, and NaCl percentage 10 % (Fig. 6.6). However, being the maximum response on the edge of the investigated experimental domain, further optimization was necessary, especially for the extraction temperature.

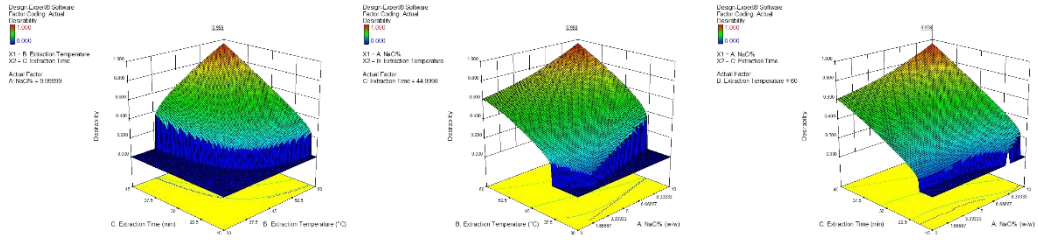

Fig. 6.6 Response surface of the desirability function for SPME optimization [164]

Indeed, as a salt percentage higher than 10 % could have led to fiber degradation and extraction time longer than 45 min would have made the protocol time consuming, these conditions were not further treated. On the other hand, extraction temperature was evaluated in univariate mode at 60, 70, and 80 °C while keeping the other variables at their optimum value. This further optimization, performed in triplicate, was carried out heating each sample at 80 °C and letting to equilibrate for 5 min. Following extraction, the fiber was first rinsed for few seconds in ultrapure water to remove the possible quartz filter debris, and thereafter the adsorbed analytes were thermally desorbed by introducing the fiber for 5 min into the GC injector set at 270 °C. For SPME evaluation, OPE detection was carried out using a TSQ Quantum GC (Thermo Fischer Scientific) system constituted by a triple quadrupole mass spectrometer (QqQ) Quantum and a TRACE GC Ultra equipped with a TriPlus autosampler for fully automated SPME analysis. TSQ Quantum GC was equipped with a Restek Rxi-5ms capillary column (30 m × 0.25 mm i.d., 0.25 µm film thickness; crossbond 95 % polydimethylsiloxane/5 % diphenyl). For SPME analyses, a Thermo PTV straight liner (0.7 mm × 2.75 mm × 105 mm) was used as GC inlet liner, and a temperature of 270°C was set for the injection. The GC oven program consisted of the same steps previously reported. The mass spectrometer operated in electron ionization (EI) in selected reaction monitoring (SRM) mode, monitoring two transitions for the confirmation of each analyte, in accordance with the European Commission Decision 2002/657/EC. In particular, the SRM transition with the best S/N ratio was used for quantification through the peak area calculation and that one resulting the most sensitive was selected for the qualitative confirmation of the target analytes. The use of tandem mass spectrometry enhanced the reliability of the proposed method due to the high

separation efficiency, selectivity and sensitivity compared to the mass spectrometry with a single quadrupole analyzer [166].

The results of this optimization revealed both an increased extraction capability and an improved precision at 80 °C. This could be due to the fact that at this temperature, ethanol from the aqueous solution evaporated, resulting in a lower competition with the SPME fiber (Fig. 6.7). In conclusion, according to these results, the optimized working conditions for the SPME analysis involved the direction immersion for 45 min at 80 °C of the DVB/Car/PDMS fiber into the MAE extract, diluted to 5 % ethanol and added of 10% (w/w) NaCl.

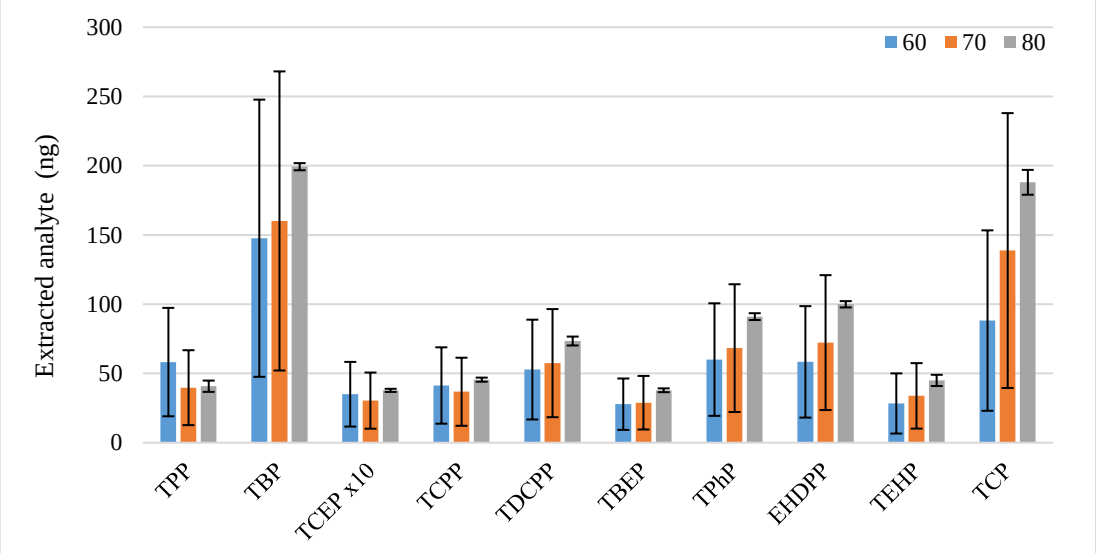

Fig.6.7 Comparison of the extraction performance of the DVB/Car/PDMS fiber at 60, 70, and 80 °C

6.2.3 Blank contamination

Due to the ubiquitarian occurrence of organophosphate esters in plastic material as flame retardants, background contamination was a major issue during the analysis of OPEs. In particular, this issue emerged during method validation, due to the increased sensitivity of tandem mass spectrometry. Therefore, proper cleaning procedures revealed necessary to seek for the lowest contamination. The contribution of each laboratory equipment, as microwave vessels, QFFs, vial septa, GC injector, as well as chemical reagents, ethanol and ultrapure water was carefully investigated. After an accurate evaluation, it was found that ultrapure water and QFFs were the main contamination sources. In order to minimize the presence of OPEs in blank samples,

the ultrapure water was further purified by passing through a C18 SPE cartridge which in turn had been previously rinsed with ACN aliquots. As concerns the QFFs, different attempts were carried out to reduce their contamination, such as soaking them in acetone, dichloromethane, acetonitrile, and ethanol, or muffling at 400 °C. Finally, it was found that their contamination was extremely reduced by soaking overnight in acetone, but despite these cleaning steps, TCPP, TDCPP, and TPhP were still detected in blank samples at concentration of 19, 66, and 33 ng L^{-1}, respectively.

6.2.4 Method validation

The validation of the proposed analytical method involved the determination of different figures of merit, namely lower limit of quantification (LLOQ), method detection limit (MDL), linearity, matrix effect, precision, and accuracy.

The lower limit of quantifications (LLOQs) for each analyte was obtained as the lowest concentration that provided a response at least five times higher than the blank signal and that could be quantified with suitable accuracy (80 - 120 %) and precision (RSD < 20 %). These values also were used as the lowest point of the calibration curve for each analyte. In order to establish the blank signal, blank PM_{10} samples were necessary. Unfortunately, since standard reference materials for organophosphate esters in airborne PM are not available, the proposed method was validated using spiked blank samples of PM_{10}. As reported in Beser et al. [167], PM_{10} was collected on quartz filters which were baked at 300 °C for 24 h in a muffle furnace in order to remove organics. LLOQ values were 0.1 ng mL^{-1} for TPP, TBP, TCEP, TCPP, TPhP, and TCP, and 0.5 ng mL^{-1} for TBEP, EHDPP, TEHP, and TDCPP. As previously mentioned, these values also represented the lowest point of the calibration curves, which were attained by the internal standard method. For the preparation of the calibration solutions, a 5 % ethanolic solution was used and treated in order to obtain a blank sample (i.e., hydroalcoholic mixture without internal standards), a zero sample (i.e., hydroalcoholic mixture with internal standards) and seven non-zero samples (i.e., hydroalcoholic mixture spiked with known amount of each analyte in the range between LLOQs and 10 ng mL^{-1}), with three replicates for each point. Three internal standards were tested, namely TCEP-d_{12}, which was used at a concentration of 2 ng mL^{-1}, and TBP-d_{27} and TPhP-d_{15}, which were both added at a concentration of 1 ng

mL^{-1}. Anyway, TCEP-d_{12} was discharged because of its unsatisfactory instrumental response. If compared to literature studies, the method herein proposed showed high sensitivity, as confirmed by the LLOQ values (0.1 – 0.5 ng mL^{-1}) which were even lower of those obtained by different approaches involving gas chromatography. For example, Quintana et al. reported LLOQ values of 10 ng mL^{-1}) [168], whereas Cristale et al. reported values of 1 ng mL^{-1} [169].

As regards the method detection limits (MDLs), these were calculated as the lowest concentration of each analyte with a peak signal-to-noise ratio of three (S/N = 3) compared to blank samples. However, for the analytes detected in the blank samples (i.e., TCPP, TDCPP, and TPhP), MDLs were calculated as concentration corresponding to the average signal in blank samples plus three times the standard deviation. It was, therefore, possible to reach MDL values between 0.020 and 0.138 ng mL^{-1}, as summarized in Table 6.7. Satisfactory results in terms of linearity were also obtained, with the coefficient of determination values higher than 0.99 for all the analytes, except for TBEP, EHDPP, and TEHP (Table 6.7).

Compound	LLOQ (ng mL^{-1})	LLOQ ** (ng m^{-3})	Internal standard	Linear range (ng mL^{-1})	R^2	MDL (ng mL^{-1})
TPP	0.1	0.15	TBP-d_{27}	0.1-10	0.9998	0.02
TBP	0.1	0.15	TBP-d_{27}	0.1-10	0.9925	0.04
TCEP	0.1	0.15	TBP-d_{27}	0.1-10	0.9926	0.07
TCPP	0.1	0.15	TBP-d_{27}	0.1-10	0.9972	0.042
TDCPP	0.5	0.73	TBP-d_{27}	0.5-10	0.9949	0.138
TPhP	0.1	0.15	TPhP-d_{15}	0.1-10	0.9919	0.051
TCP *	0.1	0.15	TPhP-d_{15}	0.1-10	0.9903	0.06

Table 6.7 Summary of calibration parameters and internal standards applied. * TCP was acquired as a sum of isomers. ** LLOQ was calculated for a sampling volume of $55m^3$

The subsequent step in the validation protocol was the determination of the matrix effect (ME), in order to investigate the potential impact of the matrix components which can induce an enhancement (ME >100 %) or a suppression (ME <100 %) of the analyte signal, affecting the reliability and accuracy of the method. Matrix effect, as well as accuracy and precision, were evaluated at three different concentration levels,

which are the quality control (QC) levels representative of the entire range of calibration curve. In detail, the low QC level was 3 times the LLOQ level for each analyte, the middle QC level was at the center of the calibration range and the high QC level was 0.8 times the upper boundary of the standard curve. Matrix effect to a given QC level was determined according to the formula:

$$ME = \frac{A_{sm} - A_{bm}}{A_{ss} - A_{bs}} \, x \, 100$$

where A_{sm} is the peak area of the matrix (blank PM_{10} sample) spiked at the QC in question, A_{bm} is the peak area of the blank PM_{10} sample, A_{ss} is the peak area of the spiked hydroalcoholic solution and A_{bs} is the peak area of the blank hydroalcoholic solution. To calculate each component of this formula, a blank PM_{10} filter sample was split in two portions: one was spiked with a known amount of internal standards (i.e., 160 ng of TBP-d_{27} and TPhP-d_{15}, and 80 ng of TCEP-d_{12}) and the other half was spiked with the same constant amount of IS plus the OPEs at the concentration of the QC levels. The same procedure was applied to the ethanolic solution. Five replicates were analyzed for each QC level. Results were assessed in terms of the ratio of analyte peak area to internal standard peak area, so as to evaluate the capability of internal standards to balance the matrix effect. An appreciable correction of the matrix effect was attained by using the internal standards, with satisfactory values for all the analytes ranging between 81 % and 117 % (Table 6.8).

Accuracy and repeatability were also assessed by analyzing five replicates for each QC level on the same day whereas reproducibility was determined by analyzing five replicates for each QC level once a day on six consecutive days. Accuracy for each analyte, calculated as the percentage ratio between the concentration estimated from the calibration curve and the spiked concentration, ranged between 83 and 115 % for TDCPP and 80-115 %for the other analytes. Precision values, expressed as the percentage relative standard deviation (RSD%) of the five replicates, were in the range 1.0-12.4 % for TDCPP and 2.3-15.2 % for the other OPEs. Satisfactory results for all the quantified analytes, summarized in Table 6.8, were obtained.

Compound	Concentration (ng/mL)	Matrix effect (%)	Intra-day accuracy (%)	Repeatability (CV%)	Inter-day accuracy (%)	Reproducibility (CV%)
TPP	0.3	88	105	2.9	97	10.2
	1	108	113	3.3	105	13.0
	8	110	98	5.6	115	14.3
TBP	0.3	84	91	1.0	83	2.3
	2	87	88	5.3	86	9.1
	8	86	98	4.4	92	7.6
TCEP	0.3	107	99	3.0	104	8.6
	2	115	92	7.8	89	7.7
	8	109	86	7.4	90	13.6
TCPP	0.3	117	85	12.4	87	11.6
	1	115	92	6.3	85	15.0
	8	97	86	8.1	84	9.1
TDCPP	1.5	85	113	3.3	108	8.2
	4	94	108	2.3	92	5.9
	8	96	98	3.7	111	4.5
TPhP	0.3	86	83	12.0	80	15.2
	2	90	100	5.2	113	10.7
	8	81	90	6.1	84	8.1
TCP	0.3	87	107	12.3	110	14.2
	2	111	115	9.6	112	11.5
	8	93	106	8.0	105	9.1

Table 6.8 Matrix effect, mean intra- and inter-day accuracy, repeatability and reproducibility attained using the proposed method (n=5, once a day on six consecutive days)

6.2.5 Application to real samples

The proposed protocol was finally applied to the determination of the selected OPEs in real PM_{10} samples collected on quartz fiber filters (QFFs, Tissuquartz™ filters 2500 QAT-UP) of 47 mm in diameter. The sampling of the PM fraction with an aerodynamic diameter lower than 10 µm was achieved using the low volume air sampler Tecora Echo PM (TCR Tecora, Italy), equipped with PM_{10} size-selective inlet head according to the European Standard UNI EN 12341:2014. A sampling flow of 2.3 m^3 h^{-1} (38.33 L min^{-1}) and a sampling time of 24 h were used providing a total volume of filtered air of approximately 55 m^3. Prior to sampling, filters were pre-cleaned by overnight soaking in acetone and, after dried, they were conditioned for 48 h according to EN 12341:2014 standard, at the temperature and the relative humidity of 20 ± 1 °C and 50 ± 5 %, respectively. Later, each filter was weighted using a microbalance Crystal Micro (Gibertini, Novate, Italy) and stored in an aluminum foil. Immediately after collection, the QFFs were wrapped in aluminum foil and stored at

−20 °C until analysis, in order to prevent changes in the sample composition and/or OPE concentration. In particular, six samples were collected and subjected to the whole optimized method. Filters averagely contained 19.1 μg m^{-3} of PM_{10}, in which values below the LLOQs for all the target analytes were detected, with the exception of TBP, TCPP, and TPhP. Indeed, due to the high sensitivity of the method, the analysis of the QFFs revealed the presence of these OPEs bound to particulate matter at sub-nanograms per cubic meter levels: TBP concentration was in the range 0.213 - 0.389 ng m^{-3}, TCPP was in the range 0.99 - 5.84 ng m^{-3}, and TPhP in the range 0.20 - 0.31 ng m^{-3}, although the use of a low volume air sampler.

As reported in different studies in literature, TCPP is one of the most persistent OPEs both indoor and outdoor. Its potential sources include vehicular traffic and industrial emission, which may be reasonable considering that the sampling area was a suburban site close to the industrial area of Cosenza and the A2 motorway, with a considerable traffic flow. Similarly, TBP and TPhP have also been detected in the outdoor environment, albeit they are less persistent, and their occurrence is mainly due to the emission from areas with intense traffic [155,159], confirming motorway as the main pollution source in the sampling area.

6.2.6 Conclusion

The proposed method for the extraction of organophosphate esters from particulate matter shows various advantages over traditional approaches generally used for the quantification of emerging pollutants. Indeed, it provides for a fast and reliable extraction due to the combined use of MAE and SPME techniques, which leads to a significant advancement also in terms of analysis time. Only 3.5 minutes allows for the simultaneous extraction of up to fifteen samples whereas SPME is able to carry out direct and automatable analysis on the obtained solutions, without any clean-up step. Furthermore, compared to the preexisting protocols reported in the literature, which involve tedious extraction techniques, the method herein proposed is not based on the consumption of damaging organic solvents, as the Soxhlet extraction with chlorinated reagents. The use of deuterated organophosphorus compounds as internal standards is essential to attain the efficient correction of matrix effect and to improve the method accuracy and precision. The performances of the analytical method are confirmed after

application of the whole protocol to real PM_{10} samples, collected in the area surrounding the CNR-IIA Institute.

6.3 Case study 2: Benzotriazoles, benzothiazoles, and benzenesulfonamides bound to particulate matter

Benzotriazoles, benzothiazoles, and benzenesulfonamides are three classes of organic compounds, which have been regarded as emerging pollutants. They include substances containing the skeleton of benzotriazole (BTR), benzothiazole (BTH) and benzenesulfonamide (BSA), respectively. Benzotriazoles (BTRs) are heterocyclic compounds containing two fused rings: a benzene ring and a triazole. Although benzotriazoles have a high affinity for an organic phase, the three lone pairs of electrons on the nitrogen atoms polarize the molecule. Due to the aromatic features of these compounds, tautomeric species can exist in their five-member ring, with the proton migrating between positions 1 and 3. This suggests that benzotriazoles have a certain acidic property (pKa > 8) even if they can act as a Bronsted base by accepting a proton in the lone pair electrons located on nitrogen atoms (pKa < 0). In addition, due to their N-H acidity, they can function as complexing agents and bind metal compounds; the resulting coordination complexes are stable and are the main responsible for the corrosion inhibitor properties that result after the coordination bond of benzotriazoles with metals, such as copper. Benzotriazoles are resistant to heat, UV radiation, and biodegradation making them persistent xenobiotics under environmental conditions. Commonly known BTRs include benzotriazole (BTR), tolyltriazole (a mixture of isomers of 4-methyl-1H-benzotriazole (4-Me-BTR) and 5-methyl-1H-benzotriazole (5-Me-BTR)), 5-chlorobenzotriazole (5-ClBTR), 5,6-dimethyl-1H-benzotriazole (5,6-MeMeBTR). As previously mentioned, benzotriazoles are extensively used as corrosion inhibitors in various fluids that come in contact with steel and metals, mainly copper and brass (an alloy of copper and zinc), on which they can form a thin complexing film surface [170][171]. An important application is their use as primary additives in aircraft de-icing/anti-icing fluids (ADAF) to reduce the flammability resulting from corrosion of metal components [172]. Other uses include the addition in automotive anti-freeze formulations, in the washing powders

commonly used as detergents, in industrial cooling systems, and brake fluids [172]. Some benzotriazoles, as 5-Cl-BTR, are used as a UV-stabilizer in different products, including plastics, building materials, vehicle components, waxes, and paints [112].

Benzothiazoles are aromatic heterocyclic compounds which contain a 1,3-thiazole ring fused to a benzene ring. The most common benzothiazoles are 2-substituted derivates, obtained by the addition of different groups to the C atom comprised between the N and S atoms. Based on the nature of these substituent groups, benzothiazoles acquire acidic or basic properties, as happens for 2-aminobenzothiazole whose pKa value is 7.8. Among the most common BTHs, benzothiazole (BTH), 2-(methylthio)benzothiazole (2-MeSBTH), 2-aminobenzothiazole (2-NH2BTH), 2-hydroxybenzothiazole (2-OHBTH), 2-mercaptobenzothiazole (2-SHBTH),2-mercaptobenzothiazole (2-SH-BTH), 2-methylthio-benzothiazole (2-Me-S-BTH), and 2-amino-benzothiazole (2-NH2-BTH) appear. Unlike benzothiazole, the 2-substituted benzothiazoles are used in several industrial applications owing to their thermal stability [112]. Indeed, they found a wide range of applications in the rubber industry, as vulcanization accelerators, with 2-mercaptobenzothiazole being extensively employed in car tires, cables, seals, shoes, rubber, gloves and toys [173]. Other common applications of BTHs include their use as biocides in the paper, leather manufacturing, and anticorrosive agents in antifreeze formulations [174]. Nevertheless, BTHs can be derived from natural sources, namely tea leaves and tobacco smoke [175].

Benzenesulfonamides are aromatic compounds with a benzene ring and a sulfonamide group substituent as a basic structure. Moreover, various derivates can be obtained by the addition of methyl in the benzene ring, obtaining toluene sulfonamides, or by the N-substitution in the sulfonamide group.

The most commonly monitored compounds of this class are benzenesulfonamide (BSA), p-toluene sulfonamide (p-TSA) and N-ethyl p-toluene sulfonamide (N-Et-p-TSA) in which the presence of the sulfonamide group with the proton donor of the amide group makes them acid substances with pKa values greater than 10. In addition, they are characterized by relatively high polarity, as depicted by the low octanol-water partition coefficient (Table 6.9).

Analiti	pKa	Log P
BTH	1.20[S]	2.01[C]
2-MeBTH	2.97[C]	2.24-2.95[C]
BTR	8.38[C]	1.44[C]
4-MeBTR	8.74[C]	1.82[C]
BSA	10.1[S]	0.326[S]
5-MeBTR	8.74[C]	1.98[C]
2-MeSBTH	2.06[C]	3.10 [C]
2-NH_2BTH	4.30[S]	1.89[C]
5-ClBTR	7.46[C]	2.13[C]
2-OHBTH	8.44[C]	1.8-2.3[S]
p-TSA	10.17[S]	0.786[S]
N-Et-p-TSA	11.67[C]	1.964[S]
5,6-MeMeBTR	8.92[C]	2.28[C]
2-SHBTH	7.03[S]	2.41[S]

Table 6.9 Chemical properties of target analytes

Benzenesulfonamides are used in several applications; for example, p-TSA is used as a plasticizer as well as an intermediate for the synthesis of pesticides and drugs. In addition, it is the primary degradation product of the chloramine-T (N-sodium-N-chloro-p-toluenesulfonamides) in water, which is an antimicrobial agent commonly used in the food industry as a disinfectant [176]. BSA is also used as an intermediate reagent for the preparation of dyes, sweeteners [177], photo chemicals and disinfectants [176].

Due to the large amounts used, the ecotoxicological risk for these compounds is expected to be high. Most benzotriazole, benzothiazole, and benzenesulfonamide derivates show low toxicity to humans but some of them have toxic or hazard effects in other organisms, such as 1-H-benzotriazole which is suspected to be carcinogenic [178,179]. Moreover, it has been shown that the could affect both nervous and endocrine systems, being their structure similar to some naturally occurring substances such as adenine, guanine, indole. Previous studies also reported that concentration

greater than 100 mg L^{-1} can be hazardous to aquatic organisms as well as to vegetation, since they can damage the root system, due to the affinities with natural plant growth regulators, like auxin and cytokinin [180]. Also, benzothiazoles can cause long-term adverse effects, due to their limited biodegradability and potential toxicity. For example, 2-Me-BTH and its derivatives are toxic to living organisms including humans and are a persistent substance in the soil. A possible source for their toxicity is the metal-chelating properties, which account for the interaction with certain groups of proteins, resulting in potential mutagenic and carcinogenic metabolites, such as aromatic hydroxylamines [181]. A lack of information exists as regards the ecotoxicological effects of benzenesulfonamides. It is known that they have moderate toxicity, but further investigations have to be carried out.

Among the numerous compounds present in these classes, the selected analytes (Fig. 6.8) for the investigation were: benzotriazole (BTR), tolyltriazole (a mixture of isomers of 4-methyl-1H-benzotriazole (4-Me-BTR) and 5-methyl-1H-benzotriazole (5-Me-BTR)), 5-chlorobenzotriazole (5-ClBTR), 5,6-dimethyl-1H-benzotriazole (5,6-MeMeBTR), benzothiazole (BTH), 2-methylbenzothiazole (2-MeBTH), 2-aminobenzothiazole (2-NH_2BTH), 2-hydroxybenzothiazole (2-OHBTH), 2-mercaptobenzothiazole (2-SHBTH), 2-methylthio-benzothiazole (2-Me-S-BTH), 2-amino-benzothiazole (2-NH_2-BTH), benzenesulfonamide (BSA), p-toluenesulfonamide (p-TSA), and N-ethyl p-toluenesulfonamide (N-Et-p-TSA).

Benzothiazole (BTH) 	2-Methylbenzothiazole (2-MeBTH) 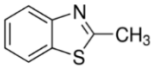	2-(Methylthio)benzothiazole (2-MeSBTH) 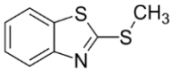	2-Aminobenzothiazole (2-NH_2BTH) 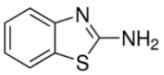	2-Hydroxybenzothiazole (2-OHBTH) 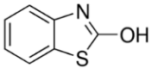
2-Mercaptobenzothiazole (2-SHBTH) 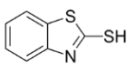	Benzotriazole (BTR) 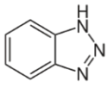	4-Methylbenzotriazole (4-MeBTR) 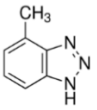	5-Methylbenzotriazole (5-MeBTR) 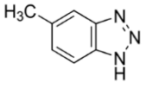	5-Chlorobenzotriazole (5-ClBTR) 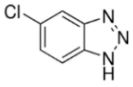
Benzosulfonamide (BSA) 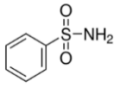	p-Toluenesulfonamide (p-TSA) 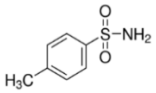	N-Ethyl-p-toluenesulfonamide (N-Et-p-TSA)		5,6-Dimethylbenzotriazole (5,6-MeMe BTR) 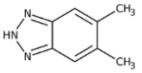

Fig. 6.8 Chemical structure of investigated BTRs, BTHs, BSAs

6.3.1 Microwave-assisted extraction from particulate filters

The first step of the proposed analytical method was the microwave-assisted extraction (MAE) of the 14 analytes (BTR, 4-Me-BTR, 5-Me-BTR, 5-ClBTR, 5,6-MeMeBTR, BTH, 2-MeBTH, 2-NH_2BTH, 2-OHBTH, 2-SHBTH, 2-Me-S-BTH, BSA, p-TSA, and N-Et-p-TSA) using an Ethos-Up Microwave Extraction System (Milestone, Leutkirch, Germany). Before extraction, quartz fiber filters (Tissuquartz™ filters 2500 QAT-UP, 47 mm dia) were spiked with 75 µL of a standard solution containing 10 mg L^{-1} of all analytes.

In order to select the significant variables affecting MAE extraction, a fractional factorial design 2^{6-2} was used, involving 6 variables regarding both the analyte properties and the instrumental parameters:

- Water pH, which was investigated in the range 2-10;
- Ethanol percentage, investigated in the range 0-50 %;
- Extraction Volume, investigated from 10 to 20 mL;
- Heat-up Time, investigated between 5 and 10 min;
- Extraction Time, investigated from 1 to 20 min;
- Extraction Temperature, investigated between 70 and 140 °C.

Considering the acid-base properties of the analytes, it was necessary to account for the role of the pH in the extraction mixture consisting of ultrapure water with a certain pH value (in the range 2-10) and ethanol. Ethanol was chosen as extracting solvent for its eco-compatibility properties, since it is non-toxic, easily available, and simplifies waste disposal. Thus, it has a low environmental impact, in agreement with the demands of green chemistry. In addition, its maximum concentration was 50 % (v/v), since it was meant to be an additive useful to enhance the extraction of the analytes from the particulate filter. The ranges of the other variables were selected according to preliminary tests.

The design matrix involved 16 experiments, which were carried out in replicate, with the addition of 3 experiments in the central point, for a total of 35 runs (Table 6.10).

Run	Water pH	EtOH%	Extr. Volume	Heat-up	Extr. Time	Extr. Temp
1	2	50	10	10	20	70
2	10	50	20	10	20	210
3	10	50	10	5	1	210
4	2	0	20	10	20	70
5	6	25	15	7.5	10.5	140
6	10	50	20	10	20	210
7	10	0	20	5	1	210
8	6	25	15	7.5	10.5	140
9	2	0	10	5	1	70
10	2	0	20	10	20	70
11	2	0	20	5	20	210
12	10	0	10	10	20	210
13	2	50	10	5	20	210
14	10	50	20	5	20	70
15	2	50	20	10	1	210
16	10	50	20	5	20	70
17	6	25	15	7.5	10.5	140
18	10	0	10	5	20	70
19	2	50	20	5	1	70
20	10	0	20	5	1	210
21	10	50	10	10	1	70
22	10	0	10	5	20	70
23	10	50	10	5	1	210
24	10	0	20	10	1	70
25	2	50	20	10	1	210
26	2	0	10	10	1	210
27	2	0	10	10	1	210
28	10	0	10	10	20	210
29	10	50	10	10	1	70
30	2	0	10	5	1	70
31	2	50	20	5	1	70
32	2	50	10	10	20	70
33	2	0	20	5	20	210
34	2	50	10	5	20	210
35	10	0	20	10	1	70

Table 6.10 Design matrix 2^{6-2} fractional factorial design for the screening of the MAE

The extraction efficiency was assessed by GC–MS/MS, after a liquid-liquid extraction step (LLE) with dichloromethane (DCM) necessary to transfer all analytes into an

organic phase. For each run, half of the spiked QFF was soaked into the hydroalcoholic extraction mixture in the PTFE vessel. At the end of the extraction, liquid-liquid extraction was performed in order to separate analytes from the aqueous solution. In detail, MAE extract was transferred to a 50 mL test tube, and pH was adjusted to 7 using $H_2PO_4^-$ /HPO_4^{2-} buffer solution (pKa = 7.21), to avoid the influence of the LLE procedure on the analytes' recovery. Then, 4 mL of DCM as extracting solvent was added; after vigorous shaking for 3 min, the organic layer was withdrawn by means of a Pasteur pipette, taking extreme care to avoid the collection of the aqueous solution. This procedure was repeated 5 times to ensure an accurate collection of the organic phase. This fraction was subsequently dried over anhydrous Na_2SO_4 and concentrated to 0.5 mL under a gentle stream of nitrogen (0.8 bar) at 60 °C (Turbovap II, Caliper Sciences, Inc.). The extract was transferred into a GC vial and the volume was adjusted to 1.5 mL with DCM, before GC–MS/MS determination. GC–MS/MS analyses were carried out using a TSQ Quantum GC (Thermo Fischer Scientific) system constituted by a triple quadrupole mass spectrometer (QqQ) Quantum and a TRACE GC Ultra equipped with a TriPlus autosampler. The gas chromatograph was equipped with a Thermo TR-5MS (95 % polydimethylsiloxane, 5 % polydiphenylsiloxane) capillary column (30 m × 0.25 mm i.d., 0.25 µm film thickness). The GC oven temperature was initially held at 40 °C for 0.3 min, then ramped at 6 °C min^{-1} to 200 °C and held at this temperature for 1 min. Analyses were performed in splitless mode and by setting the injector temperature at 250 °C. The QqQ mass spectrometer was operated in electron ionization (EI) in multiple reaction monitoring (MRM) mode. The transfer line and ionization source temperatures were set at 280 and 250 °C, respectively. Analyte peak areas were used as a response.

In order to evaluate the recovery of the analytes obtained through MAE, the working conditions of each experiment in the design matrix were reproduced through liquid-liquid extraction of the newly-prepared hydroalcoholic mixture spiked with the analytes, without processing a filter in the microwave oven. Therefore, for each combination of factors A, B and C (Water pH, EtOH%, Extraction volume) a liquid-liquid extraction with DCM was performed; the resulting extract underwent the steps of concentration and determination by GC-MS as for the previous experiments. The

response of these LLE, in terms of peak area, served as 100 % of the recovery of the analytes.

The contribution of each variable to response and the possible cross-effect among them were evaluated through the Pareto charts (Fig. 6.9), estimating the degree of significance with the support of the Bonferroni limit line and t-value of effects, as previously seen for the OPEs. From the analysis of the Pareto graphs, it resulted that all the investigated variables were significant and had a negative effect on the response, except for the pH of water (A) and EtOH% (B) which have a positive effect. The factor A (Water pH) was significant for most of the analytes, especially for benzothiazoles, for which the effect is positive (except for 2OH-BTH), in accordance to the pKa value (pKa = 8.44). For benzenesulfonamides, the water pH was not important: they exist in neutral form throughout the monitored pH range. Indeed, the species distribution diagrams suggest that all analytes, except for 2-SHBTH, are in the neutral form at pH 7. This could justify why 2-SHBTH was never detected in the chromatograms. Therefore, it seemed reasonable to set the value of this variable to 7, considered that a variation of such factor could not have improved the extraction efficiency. Under these conditions, the analyte 2-SHBTH was excluded from the subsequent studies. The ethanol percentage was significant for all analytes, except for 2-OH BTH, BTR, and N-Et-p-TSA. Thus, it was further optimized in the range of 0-50 %. As regards extraction volume, it resulted certainly significant for all the benzotriazoles; the interaction plot (Fig. 6.10- up) showed a significant curvature with the maximum corresponding to the central point of the investigated range (10-20 mL).

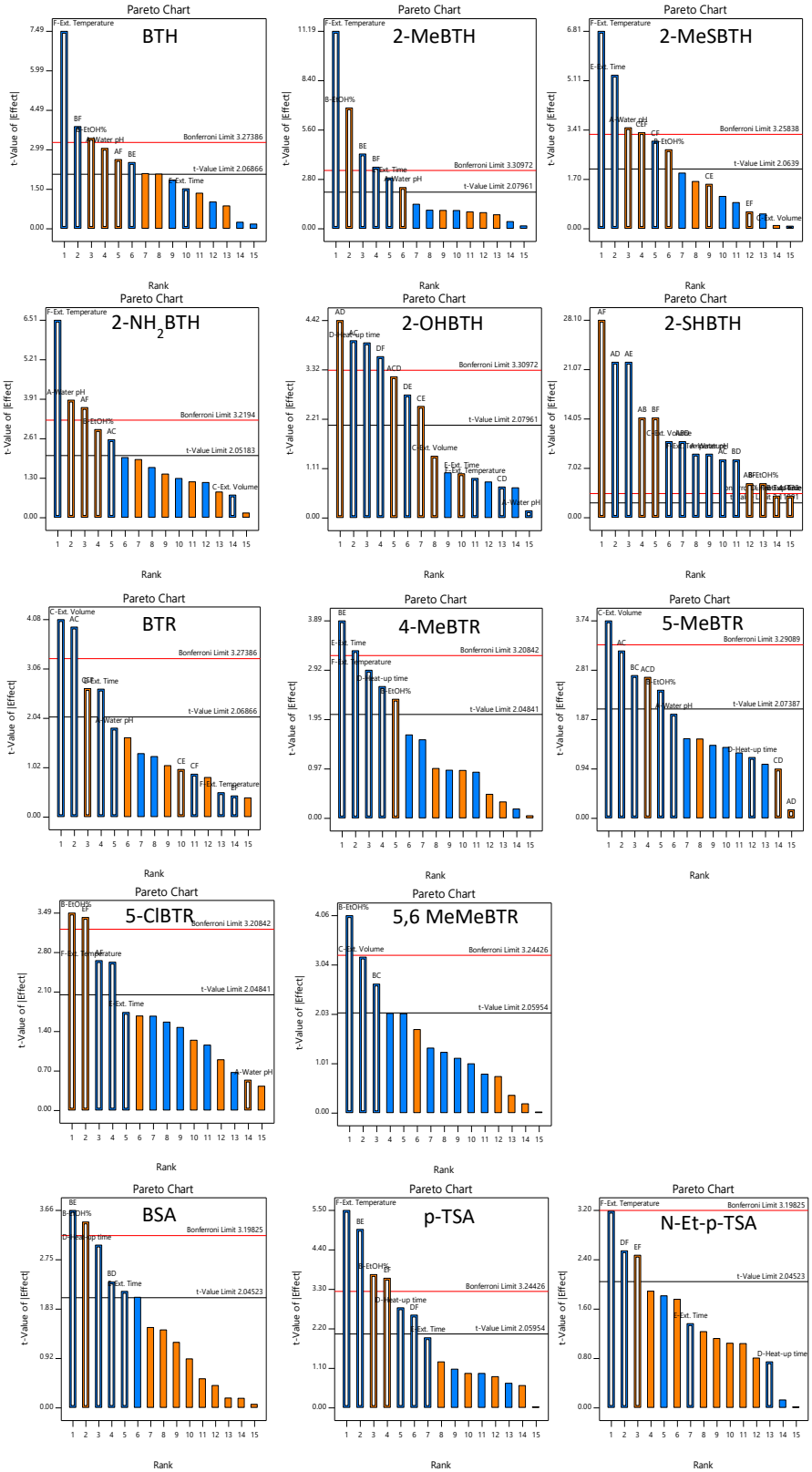

Fig. 6.9 Pareto chart from the fractional factorial design. Factors: A, water pH; B, ethanol %; C, extraction volume; D, heat up time; E, extraction time; F, extraction temperature. The unfilled bars represent the selected statistically significant effects

Thus, this factor was not considered for the optimization design. Its value was set to 15 mL for two reasons: this value resulted in the maximum response and it also ensured

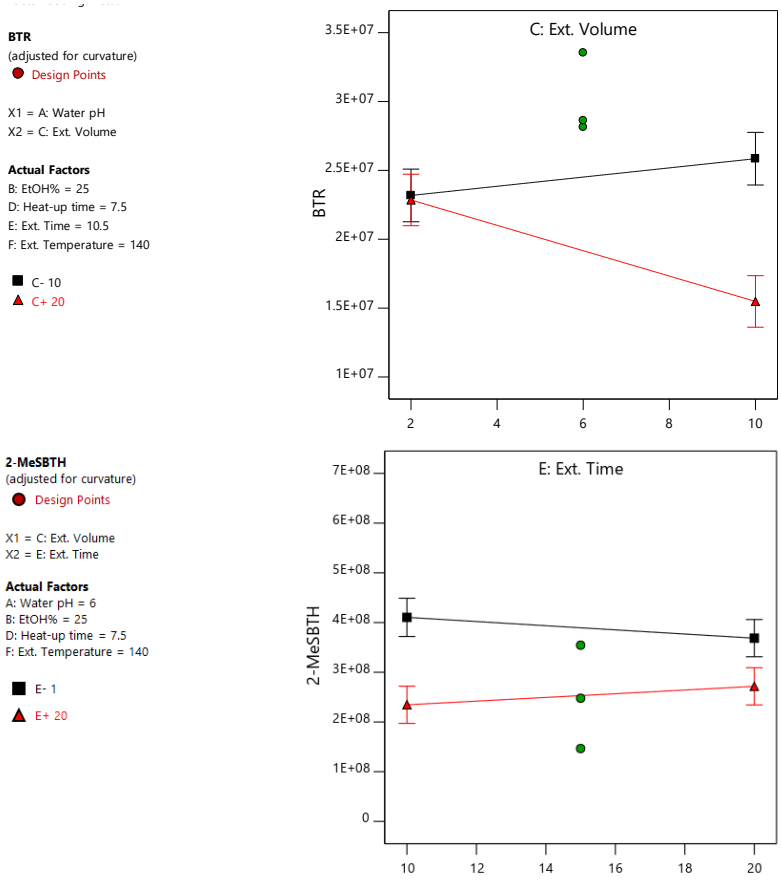

Fig. 6.10 Interaction plots for BTR (up) and 2MeSBTH (down)

a complete immersion of the spiked QFF in the solvent mixture, simplifying the LLE procedure in the test tube. Also, the D factor (Heat up Time) resulted significant for the target analytes and had a negative effect on the responses. Thus, it was optimized in the range 4-10 min, shifting the experimental domain toward lower values to seek the optimum working conditions (i.e., maximum response).

Extraction time (E) was significant for almost all analytes and had a negative effect on the responses. The interaction plot showed a minimum in the central point of the experimental domain, such as for 2-MeSBTH, (Fig. 6.10- down). Therefore, the range of values for the optimization design was shifted from 0 to 18 min. As regards the extraction temperature (F), it resulted in one of the most significant variables. Indeed, this factor was optimized in a new range of values, from 50 °C to 200 °C, being the lowest value constrained by the instrumental conditions.

The experimental design used for the optimization of the variables was a CCD, which consisted of a full factorial 2^4 design with 8 axial points at $\alpha = 2$ so as to fulfill the rotatability condition. As previously mentioned, the involved factors were investigated within the following ranges: EtOH% 0-50 %, heat up time 4-10 min, extraction time 0-18 min, and extraction temperature 50–200 °C. Performing each run in duplicate and considering 5 replications at the central point, a total of 53 runs were designed and randomly performed (Table 6.11).

Run	A: EtOH%	B: Heat-up time (min)	C: Ext. Time (min)	D: Ext. Temp (°C)
1	0	7	9	125
2	37.5	8.5	4.5	87.5
3	25	4	9	125
4	37.5	5.5	13.5	87.5
5	37.5	8.5	4.5	87.5
6	0	7	9	125
7	25	7	9	125
8	25	7	9	200
9	12.5	8.5	4.5	162.5
10	25	7	9	50
11	25	7	9	50
12	12.5	5.5	13.5	87.5
13	25	7	0	125
14	12.5	8.5	13.5	87.5
15	12.5	8.5	13.5	162.5
16	37.5	8.5	4.5	162.5
17	37.5	8.5	4.5	162.5
18	12.5	5.5	13.5	162.5
19	12.5	8.5	13.5	162.5
20	12.5	8.5	4.5	87.5
21	25	7	9	125
22	12.5	5.5	4.5	162.5
23	12.5	8.5	13.5	87.5
24	37.5	8.5	13.5	162.5
25	37.5	8.5	13.5	162.5

26	12.5	5.5	4.5	87.5
27	25	7	9	125
28	37.5	5.5	4.5	162.5
29	12.5	5.5	13.5	162.5
30	50	7	9	125
31	50	7	9	125
32	25	7	0	125
33	25	10	9	125
34	25	7	9	200
35	37.5	5.5	4.5	162.5
36	12.5	5.5	13.5	87.5
37	12.5	5.5	4.5	162.5
38	37.5	8.5	13.5	87.5
39	25	7	9	125
40	37.5	8.5	13.5	87.5
41	37.5	5.5	13.5	162.5
42	37.5	5.5	4.5	87.5
43	37.5	5.5	13.5	162.5
44	37.5	5.5	13.5	87.5
45	12.5	8.5	4.5	87.5
46	37.5	5.5	4.5	87.5
47	25	7	18	125
48	25	4	9	125
49	12.5	5.5	4.5	87.5
50	25	10	9	125
51	12.5	8.5	4.5	162.5
52	25	7	18	125
53	25	7	9	125

Table 6.11 Design matrix for 2^4 design for the optimization of the MAE conditions

With the aim to avoid bias due to the chromatographic system, 50 µL of p-TSA-d_4 as an internal standard at 15 mg L^{-1} were added to the sample vial, after MAE.

The model coefficients were calculated by backward multiple regression to eliminate not significant factors ($\alpha = 0.10$). Thus, simplified models that included only significant variables and those necessary to maintain hierarchy were obtained and validated by

the Analysis of Variance (ANOVA) (Table 6.12). The corresponding p-value for each model was lower than 0.05 thereby indicating that the models were regarded as statistically significant whereas the lack of fit term was not significant, as expected. Finally, the desirability function was successfully used to define the values that lead to the best extraction performance for the studied analytes. The desirability response surface reported in Fig. 6.11 showed that the optimal working conditions were achieved performing the extraction with 30 % EtOH, heating up to 100°C in 8 min, then keeping the temperature constant for 14 min. These conditions provided composite desirability of 0.718 and led to an analyte recovery between 79 % and 128 % (Table 6.12).

Analyte	Model	Lack of fit	Recovery (%)
BTH	<0.0001	0.4077	90
2-MeBTH	<0.0001	0.4671	79
BTR	<0.0001	0.5894	116
4-MeBTR	<0.0001	0.9786	125
BSA	0.0004	0.7537	111
5-MeBTR	<0.0001	0.9992	128
2-MeSBTH	<0.0001	0.3292	120
2-NH2BTH	<0.0001	0.3992	119
5-ClBTR	<0.0001	0.901	108
2-OHBTH	<0.0001	0.8459	122
p-TSA	<0.0001	0.9794	113
N-Et-p-TSA	<0.0001	0.5265	107
5,6-MeMeBTR	0.0016	0.8853	96

Table 6.12 Summary of the Analysis of Variance (ANOVA) for the 2^4 CCD used for the optimization of MAE conditions

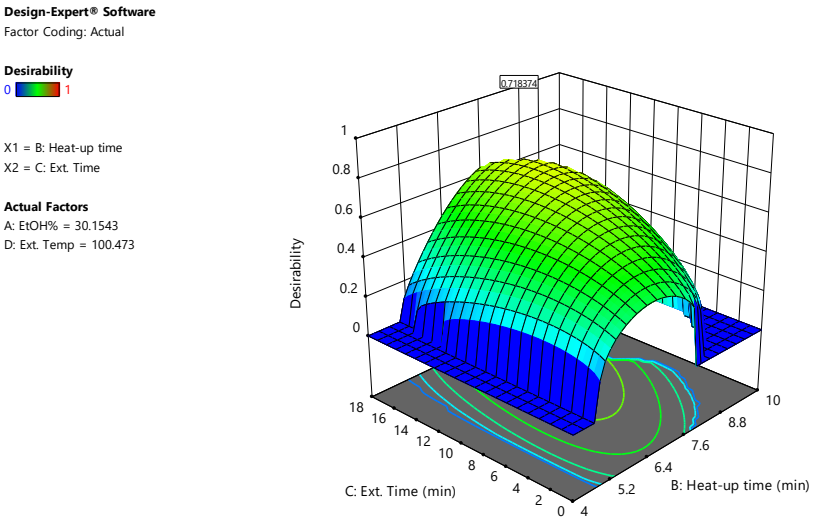

Fig. 6.11 Response surface of desirability function for MAE optimization

6.3.2 Solid-phase microextraction

The analytical step after MAE involved the use of the solid-phase microextraction technique, which presents a lot of advantages over the traditional analytical approaches for the concurrent sample preparation and concentration. Indeed, it simultaneously offers eco-compatibility and time saving, since it avoids the use of organic solvents, and does not require any further clean up step. In addition, the online coupling of SPME with gas chromatography allows an easier desorption step, which can be performed without organic solvents, thus making the whole process automated. The extraction capability of the analytes from the MAE extract primarily depends on the affinity between the analytes and the specific polymeric material coating of the SPME fiber. This step was achieved taking into account the results of a previous study [182], which used a univariate approach to seek for the best SPME coating of 5 commercial fibers: polydimethylsiloxane 100 µm (PDMS), polydimethylsiloxane/divinylbenzene 65 µm (PDMS/DVB), carboxen/polydimethylsiloxane 85 µm (CAR/PDMS), polyacrylate 85 µm (PA) and divinylbenzene/carboxen/polydimethylsiloxane 50/30 µm (DVB/CAR/PDMS). Sampling was performed deploying for 30 min each fiber in an aqueous solution spiked at 1 mg L^{-1}, at room temperature. The evaluation of the obtained peak areas showed that PA fiber was the only fiber capable of extracting all analytes, as supported by the hydrophilic character of the analytes. This fiber was therefore used for the optimization of the variables affecting SPME, which was carried

out by the multivariate approach of a central composite design (CCD). In particular, the CCD consisted of a 2^4 factorial design with 8 star points positioned at an axial distance α of $\pm$ 2 in order to fulfill the rotatability condition. The design was completed with 6 experiments in the central point so that the number of degrees of freedom for the lack-of-fit equals that for replication. The four factors selected as the most important were: extraction temperature, extraction time, percentage of sodium chloride and percentage of ethanol after dilution of the MAE extract. Each variable was investigated within the following ranges:

- Extraction Temperature 40-80 °C;
- Extraction Time 15-45 min;
- NaCl percentage 0-10 %;
- EtOH percentage 2-10 %.

Each range was determined through preliminary tests, except for the lower value of extraction temperature which was determined by technical limitations of the heater/agitator module of the TriPlus autosampler. Moreover, the salting-out effect was investigated with a maximum salt percentage of 10 % to avoid fiber degradation, whereas extraction time longer than 45 min could have led to a time-consuming protocol. As regards the percentage of ethanol in the SPME vial, a dilution step of the MAE extract was necessary to avoid competition for the extraction of the analytes between ethanol and the SPME fiber. Thus, the higher limit was set to 10 %, being the MAE extract concentration of 30 %. Unlike the protocol used for OPEs, in this case, the dilution ratio of the MAE extract was optimized in order to take into account the ethanol percentage variation during SPME heating, which could have affected the extraction efficiency. Indeed, in the previous case, the extraction efficiency as well as precision rapidly increased at 80 °C, due to the depletion of the ethanol from the aqueous solution.

All the experiments of the design matrix (Table 6.13) were carried out in SRM acquisition mode using a blank filter extract (obtained through the optimized MAE protocol) spiked at 1 mg L^{-1}. In particular, samples were prepared by spiking the hydroalcoholic extracts (diluted to 2-10 % as EtOH concentration) with analytes at 1 mg L^{-1} in vials containing the proper amount of NaCl and then diluting to 8 mL with

ultrapure water. SPME was performed using TriPlus autosampler for fully automated SPME analysis, setting the appropriate conditions for temperature and time required by the design experiment. After sampling, the fiber was allowed to desorb at 300 °C in CT Splitless mode. As previously reported, the GC oven program consisted of the same steps for MAE optimization.

Run	**A:EtOH%**	**B:Extr. Time**	**C:Extr. Temp.**	**D:NaCl%**
	v/v %	min	°C	w/w %
1	6	15	55	5
2	4	37.5	42.5	2.5
3	4	22.5	42.5	7.5
4	8	37.5	42.5	7.5
5	4	22.5	67.5	7.5
6	6	30	55	10
7	6	30	55	0
8	2	30	55	5
9	8	22.5	67.5	2.5
10	4	37.5	42.5	2.5
11	8	37.5	67.5	2.5
12	4	22.5	67.5	2.5
13	8	22.5	67.5	7.5
14	6	30	55	5
15	8	37.5	67.5	2.5
16	8	37.5	67.5	7.5
17	8	22.5	42.5	2.5
18	6	45	55	5
19	4	22.5	67.5	7.5
20	8	22.5	42.5	2.5
21	4	37.5	67.5	7.5
22	8	22.5	67.5	2.5
23	6	30	30	5
24	6	30	55	5
25	6	30	55	10
26	4	22.5	42.5	7.5
27	8	37.5	67.5	7.5
28	10	30	55	5

29	10	30	55	5
30	6	30	55	0
31	4	22.5	42.5	2.5
32	8	37.5	42.5	2.5
33	4	22.5	42.5	2.5
34	6	15	55	5
35	6	30	55	5
36	8	37.5	42.5	7.5
37	8	22.5	42.5	7.5
38	4	37.5	42.5	7.5
39	2	30	55	5
40	6	30	80	5
41	6	45	55	5
42	6	30	55	5
43	6	30	55	5
44	4	22.5	67.5	2.5
45	6	30	55	5
46	8	37.5	42.5	2.5
47	6	30	80	5
48	6	30	30	5
49	4	37.5	67.5	2.5
50	8	22.5	42.5	7.5
51	4	37.5	42.5	7.5
52	8	22.5	67.5	7.5
53	4	37.5	67.5	2.5
54	4	37.5	67.5	7.5

Table 6.13 Design matrix for 2^4 CCD for the optimization of SPME parameters

Analyte peak area was chosen as response and the model coefficients were calculated by backward multiple regression ($\alpha = 0.10$) and validated by Analysis of Variance (ANOVA) (Table 6.12). The obtained models resulted significant ($p < 0.05$) and without a lack of fit ($p > 0.05$) for all analytes. The response surface of the desirability function showed that the maximum response was achieved by setting the investigated

variables to the following values: ethanol percentage 4 %, extraction time 38 min, extraction temperature 46 °C, and NaCl percentage 10 % (Fig. 6.14). These conditions

Analyte	Model	Lack of fit
BTH	<0.0001	0.0325
2-MeBTH	<0.0001	0.0417
BTR	<0.0001	0.9276
4-MeBTR	<0.0001	0.9335
BSA	<0.0001	0.0762
5-MeBTR	<0.0001	0.905
2-MeSBTH	<0.0001	0.6537
2-NH2BTH	<0.0001	0.899
5-ClBTR	<0.0001	0.019
2-OHBTH	<0.0001	0.0562
p-TSA	<0.0001	0.5749
N-Et-p-TSA	<0.0001	0.0126
5,6-MeMeBTR	<0.0001	0.6563

Table 6.14 Summary of the Analysis of Variance (ANOVA) for the 2^4 central composite design (CCD) used for the optimization of SPME

provided composite desirability of 0.994 (Fig. 6.12). The optimal value found for the ethanol percentage reflects how low concentration values of the organic solvent corresponded to a minor competition with the fiber for the extraction of the analytes, resulting therefore in a greater extraction capability of the fiber.

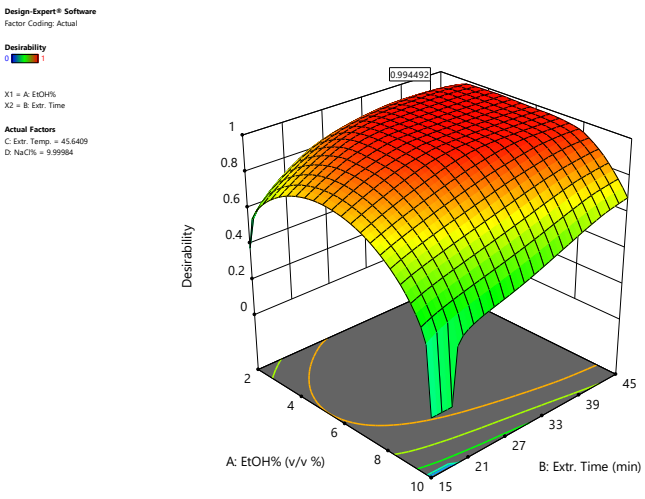

Fig. 6.12 Response surface of desirability function for SPME optimization

At the same time, the presence of an organic solvent, which retains the analytes in solution, requires the highest salt concentration to maximize the salting-out effect. This represents an important difference compared to the results obtained in previous studies [182], wherein the absence of ethanol a concentration of 6 % represented the best compromise between the salting-out effect and the decrease of the $K_{coating}/K_{solution}$ distribution constant. In conclusion, according to these results, the optimized working conditions for the SPME analysis were the following: Pa fiber, 4 % ethanol, extraction time 38 min, extraction temperature 46 °C, 10 % (w/w) NaCl.

6.3.3 Method validation

This method was validated by calculating the lower limit of quantification (LLOQ), method detection limit (MDL), linearity, matrix effect, precision, and accuracy.

As previously seen, the lower limit of quantifications (LLOQs) for each analyte was obtained as the lowest concentration providing a response at least five times higher than the blank signal and that could be quantified with suitable accuracy (80 - 120 %) and precision (RSD < 20 %). In order to establish the blank signal, blank PM_{10} samples were necessary. Even in this case, the proposed method was validated using spiked blank samples of PM_{10}, obtained as previously reported for OPEs, muffling at 300 °C for 24 h PM_{10} collected on quartz filters from the area surrounding CNR-IIA, in Rende (39°21'27.2"N 16°13'53.7"E). Results of the LLOQ values were 1 ng mL^{-1} for BTH,

2-MeBTH, 2-Me-S-BTH, 5-ClBTR, 5 ng mL^{-1} for 4-Me-BTR, 2-OHBTH, 2-NH_2BTH, p-TSA, N-Et-p-TSA and 50 ng mL^{-1} for BTR, 5-Me-BTR, 5,6-MeMeBTR, and BSA. These values were used as the concentration value of the lowest point in the calibration curves, which were attained by the internal standard method.

A comparison with literature studies revealed that the proposed method showed high sensitivity, as confirmed by the LLOQ values (1-5-50 ng mL^{-1}) which were even lower of those obtained by different approaches involving gas chromatography. For example, Maceira et al. reported LLOQ values from 2.8 to 86.4 ng mL^{-1} for the same analytes, with the exception of 5-Me-BTR, which showed an LLOQ value of 271.4 ng mL^{-1} [171]. The calibration solutions included three replicates for each of the following point: a blank sample (i.e., a 4 % ethanolic solution with BTH-d_4 and p-TSA-d_4 as internal standards at 200 ng mL^{-1}), a zero sample (i.e., a 4 % ethanolic solution) and seven non-zero samples (i.e., a 4 % ethanolic solution spiked with known amount of each analyte in the range from LLOQs to 200 ng mL^{-1} for Me-S-BTH, to 500 ng mL^{-1} for 2-OHBTH, 2-MeBTH, 5-ClBTR, N-Et-p-TSA, and to 1000 ng mL^{-1} for the remaining analytes). The method detection limits (MDLs) were determined as the lowest concentration of each analyte with a peak signal-to-noise ratio of three (S/N = 3) compared to blank samples. Values for MDL between 0.020 and 0.072 ng mL^{-1} were obtained (Table 6.15). Satisfactory results in terms of linearity were also obtained, with determination coefficients higher than 0.99 for all the analytes (Table 15). The subsequent step in the validation protocol was the determination of the matrix effect (ME), aimed to investigate the potential impact of the matrix components which can induce an enhancement (ME > 100 %) or a suppression (ME < 100 %) of the analyte signal, thus affecting the reliability and accuracy of the method. Matrix effect was evaluated at three different concentration levels, which are the quality control (QC) levels representative of the entire range of calibration curve. In detail, the low QC level was at 3 x LLOQ level for each analyte, the middle QC level was at the center of the calibration range and the high QC level was 0.8 x the upper boundary of the standard curve. Matrix effect to a given QC level was determined according to the formula:

$$ME = \frac{A_{sm}}{A_{ss}}\ x\ 100$$

where A_{sm} is the peak area of the matrix (spiked blank PM_{10} sample), and A_{ss} is the peak area of the spiked hydroalcoholic solution.

Compound	LLOQ (ng mL^{-1})	Internal standard	Linear range (ng mL^{-1})	R^2	MDL (ng mL^{-1})
BTH	1	BTH-d_4	1-500	0.9986	0.053
2-MeBTH	1	BTH-d_4	1-500	0.9956	0.052
BTR	50	BTH-d_4	50-1000	0.9926	0.072
4-MeBTR	5	BTH-d_4	5-1000	0.9974	0.027
BSA	50	p-TSA-d_4	50-1000	0.9949	0.061
5-MeBTR	50	BTH-d_4	50-1000	0.9983	0.034
2-MeSBTH	1	BTH-d_4	1-200	0.9965	0.054
2-NH_2BTH	5	BTH-d_4	5-1000	0.9947	0.02
5-ClBTR	1	BTH-d_4	1-500	0.9903	0.046
2-OHBTH	5	BTH-d_4	5-1000	0.9938	0.04
p-TSA	5	p-TSA-d_4	5-1000	0.9923	0.039
N-Et-p-TSA	5	BTH-d_4	5-500	0.9979	0.062
5,6-MeMeBTR	50	p-TSA-d_4	50-1000	0.9972	0.047

Table 6.15 Summary of calibration parameters and internal standards applied

The component A_{sm} was calculated analyzing in quintuplicate blank PM_{10} filter samples spiked with the internal standards and the analytes at the concentration of the QC levels whereas A_{ss} was calculated analyzing a 4 % ethanolic solution still spiked with the ISs and the analytes at the QC levels. Results were assessed in terms of the ratio of analyte peak area to internal standard peak area, to evaluate the capability of internal standards to balance the matrix effect. An appreciable correction of the matrix effect was attained by using the BTH-d_4 and p-TSA-d_4 internal standards, with satisfactory values for all the analytes ranging between 83 % and 115 %.

As concerns accuracy and repeatability, five replicates for each QC level were analyzed on the same day whereas reproducibility was assessed by analyzing five replicates for each QC level once a day on six consecutive days. Accuracy was calculated for each analyte as the percentage ratio between the concentration estimated from the calibration curve and the spiked concentration; the resulting values ranged between 81 and 117 % for all the analytes.

Precision values, expressed as the percentage relative standard deviation (RSD%) of the five replicates, were in the range 1.8-13.8 %.

6.3.4 Application to real samples

As for the case of organophosphate esters, the method needs to be applied to the real case scenario. However, this step is still a work in progress.

6.3.5 Conclusion

In the previous sections, an eco-friendly method for the simultaneous determination of benzotriazoles, benzothiazoles, and benzenesulfonamides bound to PM_{10} has been presented. The method relies on the use of the MAE technique for the extraction of the analytes from particulate filters with a green mixture of ultrapure water and ethanol. In this sense, the protocol differentiates from the traditional solvent extractions usually leading to the consumption of high solvent volumes, which are deuterated in most of the cases. Even the subsequent solventless SPME contributes to the attainment of a green method, also avoiding further clean-up steps and allowing the direct coupling with the injection system of the gas chromatography-tandem mass spectrometry used for the final quantification. The overall conditions of each step represents the best compromise among the possible values for the variables affecting the extraction efficiency; these are obtained using an experimental design strategy that employed a desirability function for optimization. The combination MAE-SPME-GC-MS/MS results in satisfactory limits of quantification (1- 5- 50 ng mL^{-1}), precision (RSD < 15 %), and recoveries (79 – 128 %), also achievable through the use of BTH-d_4 and p-TSA-d_4 as internal standards. The application of the method to real PM_{10} samples will confirm the performances of the analytical method.

Chapter 7

Conclusion

7.1 Summary of research findings and recommendations for future work

During the Ph.D. studies, I focused my efforts to the environmental monitoring of different contaminants through various approaches, varying from the traditionally used to some innovative ones. These investigations concerned the various environmental compartments i.e., atmosphere, water, soil, and biota. In particular, some contaminants such as the heavy metals and emerging pollutants were selected as a matter of investigation, because of their toxicity and extensive use for industrial applications. In the case of mercury, the monitoring activity was performed through direct measurements during field campaigns, using the conventional instrumentation for Hg analysis as well as new technologies, which allowed to assess passive sampling as an alternative strategy for atmospheric Hg measurements. In particular, the use of the active instruments for Hg analysis during a MED-Oceanor cruise campaign allowed the evaluation of the volcanic contribution in the Mediterranean Sea basin as potential sources affecting the Hg distribution in the atmosphere and seawater. Supported by the use of computational models such as the HYSPLIT model for the calculation of the backward trajectories of the air masses, the different GEM, GOM, and PBM peak concentrations were related to plausible sources, being due to anthropogenic, photochemical, or volcanic activity. Through this approach it was possible to identify, for example, the photochemical origin of the GOM peak detected in Marsili, also supported by ozone, reflecting the reactions that take place in the atmosphere under conditions of high synoptic pressure, clear sky and high temperatures and that are responsible for GEM to GOM oxidation. The geothermal activity due to the volcanoes, on the other hand, was detected in the first monitoring site selected around Vulcano, where both the GOM and SO_2 values significantly increased and the Hg / SO_2 ratio was compatible with the classification of passively degassing volcanoes. To date, the knowledge of the complex mechanisms characterizing the Hg cycle presents several gaps and various processes of transformation in environmental ecosystems are still

unclear. Modelers are trying to simulate the cycle of Hg, but many open questions, such as the constant rate of reactions as well as many processes of emission and/or re-emission, mainly from the water basins, are unknown and need further investigation. Only with additional analysis of Hg measurements, the knowledge of its cycle will be extended, also considering innovative low-cost methods developed to assess Hg concentrations worldwide across regional and global scale networks.

In particular, to take a step forward in this context, the active sampling system for atmospheric Hg monitoring was compared with newly-developed passive systems (PASs) constituted by Titania nanoparticles finely decorated with gold nanoparticles, resulting in a selective sorbent material which was then implemented into a common axial sampler. Through a direct comparison of the analytical performances of each sampling type, it was possible to establish PASs as a good alternative to the traditional monitoring techniques. The results obtained by the developed devices are in fact good and promising. However, additional field performance tests are necessary to confirm their robustness against meteorological parameter influence.

Further investigations are especially required to affirm if the physical parameters as well as the chemical ones, such as the presence of volatile organic compounds and gases (like halides and sulphides) could influence the PASs performance, interfering with the adsorption process of Hg. In conclusion, in this thesis, many results about possible future devices for Hg in ambient air have been presented. Moreover, their potential to substitute conventional methods still requires further investigations. In this way, the monitoring for Hg will be possible also in remote areas and in sites where actually the conventional analyzers cannot work. As final result, the employment of Passive Samplers could strengthen the Hg Network on global scale (firstly named as GMOS and to date, “GOS4M”) in support of the International Minamata Convention on Mercury, increasing the number of sites of investigation chosen and considering all the possible geographical and meteorological conditions.

As regards biota, the monitoring of Hg and other heavy metals was possible due to the development of a sample preparation protocol different from that suggested in the EPA method 1631, based on the rapid, loss-free microwave-assisted acid digestion involving the use of HNO_3 and H_2O_2. This protocol successfully applied to the monitoring of total mercury and other heavy metals in *Harpalus (Pseudoophonus)*

rufipes samples, collected from crop fields, treated with fertilizers, in San Giovanni in Fiore (CS). The simultaneous monitoring of the beetle's body concentration and the environment evaluated in terms of the bioaccumulation factor allowed the assessment of the carabid beetles as a potential bioindicator of environmental pollution of Cu and Zn.

Regarding the organic contaminants, new analytical methods for the monitoring of the target analytes bound to particulate matter (PM) were proposed. The methods developed for organophosphate esters, benzothiazoles, benzotriazoles, and benzenesulfonamides revealed a good green strategy for the quantification in PM, going countercurrent to the conventional analytical techniques, which involve tedious steps, as well as solvent consumption, with a higher impact for the environment. In each case, these advantages were conferred by the combined use of microwave-assisted extraction from the particulate filters with an eco-friendly solution of water and ethanol with the solvent-less solid-phase microextraction (SPME), compatible with the injection system of the gas chromatograph. In addition, the use of tandem mass spectrometry as a detection technique provided an added value of the proposed protocol, being fundamental for the high sensitivity of the analytical methods.

7.2 Contributions

The outcomes of this thesis have been presented as paper, oral or poster presentations in various conferences and congresses during the Ph.D. studies, which are listed below:

- Naccarato, A. Tassone, S. Moretti, R. Elliani, F. Sprovieri, N. Pirrone, A. Tagarelli, "A green approach for organophosphate ester determination in airborne particulate matter: microwave-assisted extraction using hydroalcoholic mixture coupled with solid-phase microextraction gas chromatography-tandem mass spectrometry", Talanta, https://doi.org/10.1016/j.talanta.2018.07.077

- A. Naccarato, A. Tassone, S. Moretti, M. Martino, F. Sprovieri, N. Pirrone, A. Tagarelli "Microextraction techniques and microwave-assisted extraction: a

new combined approach for the analysis of the pollutants associated to the airborne particulate matter", Conference Proceedings of the CNR-Institute of atmospheric pollution research, Montelibretti(Roma), 9-10 maggio 2018, Edizioni Ambiente, ISBN: 978-88-6627-254-0

- A. Tassone, F. Cavaliere, R. Elliani, A. Tagarelli, P. Brandmayr, N. Pirrone, F. Sprovieri, A. Giglio, A. Naccarato, "*Harpalus (Pseudoophonus) Rufipes* (De Geer, 1774) As A Bioindicator For Detecting Environmental Contamination: A Preliminary Study Of Heavy Metal Pollution In Crop Field", Poster, XXVIII Congress of the Analytical Chemistry Division, Bari 22 – 26 September 2019.

- A. Naccarato, A. Tassone, M. Martino, R. Elliani, F. Sprovieri, N. Pirrone, A. Tagarelli, "A New Green Method For The Quantification Of Benzothiazoles, Benzotriazoles And Benzosulfonamides In Airborne Particulate Matter By Microwave-Assisted Extraction Coupled With Solidphase Microextraction Gas Chromatography Tandem Mass Spectrometry", Poster, XXVIII Congress of the Analytical Chemistry Division, Bari 22 – 26 September 2019

- F. Sprovieri, A. Naccarato, A. Fino, A. Macagnano, E. Zampetti, P. Papa, A. Joshua, A. Tassone, M. Martino, S. Moretti, N. Pirrone, "Assessing mercury air levels using Passive Air Samplers as part of the GMOS network in the framework of the UNEP GEF project", 14th International Conference on Mercury as a Global Pollutant ICMGP2019", Poster, Cracovia, 08-13 settembre 2019

- J. Castagna, M. Bencardino, M. Capua, F. D'Amore, G. Esposito, V. Mannarino, S. Moretti, A. Naccarato, J. Orbe, A. Tassone, F. Sprovieri, N. Pirrone, "The atmospheric impact of volcanic activities in the Mediterranean Sea investigated during a measurements cruise campaign", Poster "III International Conference on Atmospheric Dust", Bari, 29-31 maggio 2018

- Naccarato, A. Tassone, S. Moretti, R. Elliani, F. Sprovieri, N. Pirrone, A. Tagarelli, "Organophosphate ester determination in particulate matter: a greener microwave-assisted extraction approach coupled with solid-phase microextraction gas chromatography-tandem mass spectrometry". Atti di convegni "VIII Convegno Nazionale sul Particolato Atmosferico" Matera, 23-25 maggio 2018

- Naccarato, A. Tassone, S. Moretti, R. Elliani, F. Sprovieri, N. Pirrone, A. Tagarelli, "A greener approach for organophosphate flame retardant determination in airborne particulate matter: microwave-assisted extraction using hydroalcoholic mixture coupled with solid phase microextraction gas chromatography tandem mass spectrometry". Atti di convegni "XXVI Congresso Nazionale della Società Chimica Italiana" Paestum (SA), 10-14 settembre 2017

BIBLIOGRAPHY

[1] UNEP, The Global Mercury Assessment 2013, Glob. Mercur. Assess. 2013 Sources, Emiss. Releases Environ. Transp. (2013) 44. http://www.unep.org/PDF/PressReleases/GlobalMercuryAssessment2013.pdf.

[2] N. Pirrone, R. Manson, Mercury Fate and Transport in the Global Atmosphere: Measurements, Models and Policy Implications, UNEP Glob. Mercur. Partnersh. (2008) 1–495. https://doi.org/10.1017/CBO9781107415324.004.

[3] M. Sedlar, M. Pavlin, A. Popovič, M. Horvat, Temperature stability of mercury compounds in solid substrates, Open Chem. 13 (2014) 404–419. https://doi.org/10.1515/chem-2015-0051.

[4] N. Batrakova, O. Travnikov, O. Rozovskaya, Chemical and physical transformations of mercury in the ocean: A review, Ocean Sci. 10 (2014) 1047–1063. https://doi.org/10.5194/os-10-1047-2014.

[5] K.L. Johnson, ATSDR 1999, Plant Physiol. 176 (2018) 1408–1409. https://doi.org/10.1104/pp.17.01785.

[6] D.W. Boening, Ecological effects, transport, and fate of mercury: A general review, Chemosphere. 40 (2000) 1335–1351. https://doi.org/10.1016/S0045-6535(99)00283-0.

[7] Cinnabar, Wikipedia. (n.d.). https://en.wikipedia.org/wiki/Cinnabar.

[8] T.H.E. Environmental, H. Criteria, Environmental Health Criteria 101: Methylmercury, Environ. Heal. Criteria. (1990) 1–144.

[9] U.S. Environmental Protection Agency, Exposure Factors Handbook (Final report), U.S. Environ. Prot. Agency, Washington, DC, EPA/600/P-95/002F a-C. (1997). https://doi.org/EPA/600/P-95/002F a-c,.

[10] A.P. Dastoor, Y. Larocque, Global circulation of atmospheric mercury: A modelling study, Atmos. Environ. 38 (2004) 147–161. https://doi.org/10.1016/j.atmosenv.2003.08.037.

[11] B. Nurfatini, S. Amir, Recent Advances in Mercury Detection; Towards Enabling a Sensitive and Rapid Point-of-Check Measurement, J. Toxicol. Risk Assess. (2018). https://doi.org/10.23937/2572-4061.1510010.

[12] R. Ferrara, B. Mazzolai, E. Lanzillotta, E. Nucaro, N. Pirrone, Volcanoes as

emission sources of atmospheric mercury in the Mediterranean basin, Sci. Total Environ. 259 (2000) 115–121. https://doi.org/10.1016/S0048-9697(00)00558-1.

[13] J.O. Nriagu, Mechanistic steps in the photoreduction of mercury in natural waters, Sci. Total Environ. (1994). https://doi.org/10.1016/0048-9697(94)90608-4.

[14] Li, Feng review.pdf, (n.d.).

[15] E.G. Pacyna, J.M. Pacyna, J. Fudala, E. Strzelecka-Jastrzab, S. Hlawiczka, D. Panasiuk, Mercury emissions to the atmosphere from anthropogenic sources in Europe in 2000 and their scenarios until 2020, Sci. Total Environ. 370 (2006) 147–156. https://doi.org/10.1016/j.scitotenv.2006.06.023.

[16] K.M. Rice, E.M. Walker, M. Wu, C. Gillette, E.R. Blough, Environmental mercury and its toxic effects, J. Prev. Med. Public Heal. 47 (2014) 74–83. https://doi.org/10.3961/jpmph.2014.47.2.74.

[17] H. Selin, S.E. Keane, S. Wang, N.E. Selin, K. Davis, D. Bally, Linking science and policy to support the implementation of the Minamata Convention on Mercury, Ambio. 47 (2018) 198–215. https://doi.org/10.1007/s13280-017-1003-x.

[18] Unep, Minamata Convention on Mercury - Text and Annexes, UNEP, 2013a. (2013) 69.

[19] G. Liu, Y. Cai, N. O'Driscoll, Environmental Chemistry and Toxicology of Mercury, 2011. https://doi.org/10.1002/9781118146644.

[20] M.S. Alam, C.E. West, A.G. Scarlett, S.J. Rowland, R.M. Harrison, Application of 2D-GCMS reveals many industrial chemicals in airborne particulate matter, Atmos. Environ. 65 (2013) 101–111. https://doi.org/10.1016/j.atmosenv.2012.10.014.

[21] S.E. Lindberg, S. Brooks, C.J. Lin, K.J. Scott, M.S. Landis, R.K. Stevens, M. Goodsite, A. Richter, Dynamic oxidation of gaseous mercury in the arctic troposphere at polar sunrise, Environ. Sci. Technol. (2002). https://doi.org/10.1021/es0111941.

[22] S.E. Lindberg, W.J. Stratton, Atmospheric Mercury Speciation : Concentrations and Behavior of Reactive Gaseous Mercury in Ambient Air, Environ. Sci.

Technol. 32 (1998) 49–57. https://doi.org/doi:10.1021/es970546u.

[23] C.D. Holmes, D.J. Jacob, X. Yang, Global lifetime of elemental mercury against oxidation by atomic bromine in the free troposphere, Geophys. Res. Lett. (2006). https://doi.org/10.1029/2006GL027176.

[24] C.J. Lin, S.O. Pehkonen, The chemistry of atmospheric mercury: A review, Atmos. Environ. (1999). https://doi.org/10.1016/S1352-2310(98)00387-2.

[25] W.H. Schroeder, J. Munthe, Atmospheric mercury - An overview, in: Atmos. Environ., 1998. https://doi.org/10.1016/S1352-2310(97)00293-8.

[26] Q. Wan, X. Feng, J. Lu, W. Zheng, X. Song, P. Li, S. Han, H. Xu, Atmospheric mercury in Changbai Mountain area, northeastern China II. The distribution of reactive gaseous mercury and particulate mercury and mercury deposition fluxes, Environ. Res. 109 (2009) 721–727. https://doi.org/10.1016/j.envres.2009.05.006.

[27] M. Horvat, J. Kotnik, M. Logar, V. Fajon, T. Zvonarić, N. Pirrone, Speciation of mercury in surface and deep-sea waters in the Mediterranean Sea, Atmos. Environ. 37 (2003). https://doi.org/10.1016/S1352-2310(03)00249-8.

[28] J. Munthe, I. Wangberg, N. Pirrone, A. Iverfeldt, R. Ferrara, R. Ebinghaus, X. Feng, K. Gardfeldt, G. Keeler, E. Lanzillotta, S.E. Lindberg, J. Lu, Y. Mamane, E.M. Prestbo, S. Schmolke, W.H. Schroeder, J. Sommar, F. Sprovieri, R.K. Stevens, W. Stratton, G. Tuncel, A. Urba, Intercomparison of methods for sampling and analysis of atmospheric mercury species, Atmos. Environ. 35 (2001) 3007–3017. https://doi.org/10.1016/s1352-2310(01)00104-2.

[29] N. Pirrone, R. Ferrara, I.M. Hedgecock, G. Kallos, Y. Mamane, J. Munthe, J.M. Pacyna, I. Pytharoulis, F. Sprovieri, A. Voudouri, I. Wangberg, Dynamic processes of mercury over the Mediterranean region: Results from the Mediterranean Atmospheric Mercury Cycle System (MAMCS) project, Atmos. Environ. 37 (2003). https://doi.org/10.1016/S1352-2310(03)00251-6.

[30] F. Sprovieri, N. Pirrone, K. Gärdfeldt, J. Sommar, Mercury speciation in the marine boundary layer along a 6000 km cruise path around the Mediterranean Sea, Atmos. Environ. 37 (2003) 63–71. https://doi.org/10.1016/S1352-2310(03)00237-1.

[31] I.M. Hedgecock, G.A. Trunfio, N. Pirrone, F. Sprovieri, Mercury chemistry in

the MBL: Mediterranean case and sensitivity studies using the AMCOTS (Atmospheric Mercury Chemistry over the Sea) model, Atmos. Environ. 39 (2005) 7217–7230. https://doi.org/10.1016/j.atmosenv.2005.09.002.

[32] I.M. Hedgecock, N. Pirrone, G.A. Trunfio, F. Sprovieri, Integrated mercury cycling, transport, and air-water exchange (MECAWEx) model, J. Geophys. Res. Atmos. (2006). https://doi.org/10.1029/2006JD007117.

[33] S.A. Strode, L. Jaeglé, N.E. Selin, D.J. Jacob, R.J. Park, R.M. Yantosca, R.P. Mason, F. Slemr, Air-sea exchange in the global mercury cycle, Global Biogeochem. Cycles. (2007). https://doi.org/10.1029/2006GB002766.

[34] S. Balshaw, J. Edwards, B. Daughtry, K. Ross, Mercury in seafood: Mechanisms of accumulation and consequences for consumer health, Rev. Environ. Health. 22 (2007) 91–113. https://doi.org/10.1515/reveh.2007.22.2.91.

[35] C.J. Watras, R.C. Back, S. Halvorsen, R.J.M. Hudson, K.A. Morrison, S.P. Wente, Bioaccumulation of mercury in pelagic freshwater food webs, in: Sci. Total Environ., 1998. https://doi.org/10.1016/S0048-9697(98)00228-9.

[36] N.S. Bloom, On the Chemical Form of Mercury in Edible Fish and Marine Invertebrate Tissue, Can. J. Fish. Aquat. Sci. (1992). https://doi.org/10.1139/f92-113.

[37] M.M. Storelli, R. Giacominelli-Stuffler, G.O. Marcotrigiano, Total and methylmercury residues in cartilaginous fish from Mediterranean Sea, Mar. Pollut. Bull. (2002). https://doi.org/10.1016/S0025-326X(02)00223-0.

[38] P. Bustamante, V. Lahaye, C. Durnez, C. Churlaud, F. Caurant, Total and organic Hg concentrations in cephalopods from the North Eastern Atlantic waters: Influence of geographical origin and feeding ecology, Sci. Total Environ. (2006). https://doi.org/10.1016/j.scitotenv.2006.01.038.

[39] B. Gworek, O. Bemowska-Kałabun, M. Kijeńska, J. Wrzosek-Jakubowska, Mercury in Marine and Oceanic Waters—a Review, Water. Air. Soil Pollut. 227 (2016). https://doi.org/10.1007/s11270-016-3060-3.

[40] US Food and Drug Administration, Mercury In Fish : Cause For Concern?, FDA Consum. (1995).

[41] M. Ao, X. Xu, Y. Wu, C. Zhang, B. Meng, L. Shang, L. Liang, R. Qiu, S. Wang,

X. Qian, L. Zhao, G. Qiu, Newly deposited atmospheric mercury in a simulated rice ecosystem in an active mercury mining region: High loading, accumulation, and availability, Chemosphere. (2020). https://doi.org/10.1016/j.chemosphere.2019.124630.

[42] K.R. Olson, H.L. Bergman, P.O. Fromm, Uptake of Methyl Mercuric Chloride and Mercuric Chloride by Trout: A Study of Uptake Pathways into the Whole Animal and Uptake by Erythrocytes in vitro, J. Fish. Res. Board Canada. (1973). https://doi.org/10.1139/f73-209.

[43] I. Ipolyi, P. Massanisso, S. Sposato, P. Fodor, R. Morabito, Concentration levels of total and methylmercury in mussel samples collected along the coasts of Sardinia Island (Italy), Anal. Chim. Acta. 505 (2004) 145–151. https://doi.org/10.1002/chem.201202697.

[44] W.H. Schroeder, M.C. Hamilton, S.R. Stobart, The use of noble metals as collection media for mercury and its compounds in the atmosphere: A review, Rev. Anal. Chem. (1985). https://doi.org/10.1515/REVAC.1985.8.3.I.

[45] M.S. Gustin, H.M. Amos, J. Huang, M.B. Miller, K. Heidecorn, Measuring and modeling mercury in the atmosphere: a critical review, Atmos. Chem. Phys. 15 (2015) 5697–5713. https://doi.org/10.5194/acp-15-5697-2015.

[46] F. Pankratov, Dynamics of Atmospheric Mercury in the Russian Arctic on the rights of a manuscript Dynamics of atmospheric mercury in the Russian arctic as a result of long- term monitoring extended abstract A thesis submitted for the degree of Candidate of Geographical, (2017). https://doi.org/10.13140/RG.2.1.4255.1767.

[47] S.C. Method, Low Level Mercury Analysis - Gas Phase Calibration Background Information, 5726 (1985) 3–4.

[48] F. D'Amore, M. Bencardino, S. Cinnirella, F. Sprovieri, N. Pirrone, Data quality through a web-based QA/QC system: Implementation for atmospheric mercury data from the global mercury observation system, Environ. Sci. Process. Impacts. 17 (2015) 1482–1491. https://doi.org/10.1039/c5em00205b.

[49] F. Sprovieri, N. Pirrone, M. Bencardino, F. D'Amore, F. Carbone, S. Cinnirella, V. Mannarino, M. Landis, R. Ebinghaus, A. Weigelt, E.G. Brunke, C. Labuschagne, L. Martin, J. Munthe, I. Wängberg, P. Artaxo, F. Morais, H. De

Melo Jorge Barbosa, J. Brito, W. Cairns, C. Barbante, M. Del Carmen Diéguez, P. Elizabeth Garcia, D. Aurélien, H. Angot, O. Magand, H. Skov, M. Horvat, J. Kotnik, K. Alana Read, L. Mendes Neves, B. Manfred Gawlik, F. Sena, N. Mashyanov, V. Obolkin, D. Wip, X. Bin Feng, H. Zhang, X. Fu, R. Ramachandran, D. Cossa, J. Knoery, N. Marusczak, M. Nerentorp, C. Norstrom, Atmospheric mercury concentrations observed at ground-based monitoring sites globally distributed in the framework of the GMOS network, Atmos. Chem. Phys. 16 (2016) 11915–11935. https://doi.org/10.5194/acp-16-11915-2016.

[50] U.S. EPA, Compendium of Methods for the Determination of Inorganic Compounds in Ambient Air, 2014 (2009). http://www.epa.gov/ttnamti1/files/ambient/inorganic/iocompen.pdf.

[51] GMOS Standard Operational Procedure, Methods for the determination of speciated ambient Hg, (n.d.).

[52] J.Y. Lu, W.H. Schroeder, T. Berg, J. Munthe, D. Schneeberger, F. Schaedlich, A Device for Sampling and Determination of Total Particulate Mercury in Ambient Air, Anal. Chem. (1998). https://doi.org/10.1021/ac971278l.

[53] M. Gustin, D. Jaffe, Reducing the uncertainty in measurement and understanding of mercury in the atmosphere, Environ. Sci. Technol. (2010). https://doi.org/10.1021/es902736k.

[54] D.S. McLagan, M.E.E. Mazur, C.P.J. Mitchell, F. Wania, Passive air sampling of gaseous elemental mercury: A critical review, Atmos. Chem. Phys. 16 (2016) 3061–3076. https://doi.org/10.5194/acp-16-3061-2016.

[55] J. Namieśnik, B. Zabiegała, A. Kot-Wasik, M. Partyka, A. Wasik, Passive sampling and/or extraction techniques in environmental analysis: A review, Anal. Bioanal. Chem. 381 (2005) 279–301. https://doi.org/10.1007/s00216-004-2830-8.

[56] D.S. McLagan, C.P.J. Mitchell, A. Steffen, H. Hung, C. Shin, G.W. Stupple, M.L. Olson, W.T. Luke, P. Kelley, D. Howard, G.C. Edwards, P.F. Nelson, H. Xiao, G.R. Sheu, A. Dreyer, H. Huang, B. Abdul Hussain, Y.D. Lei, I. Tavshunsky, F. Wania, Global evaluation and calibration of a passive air sampler for gaseous mercury, Atmos. Chem. Phys. 18 (2018) 5905–5919.

https://doi.org/10.5194/acp-18-5905-2018.

[57] D.S. McLagan, C.P.J. Mitchell, H. Huang, Y.D. Lei, A.S. Cole, A. Steffen, H. Hung, F. Wania, A High-Precision Passive Air Sampler for Gaseous Mercury, Environ. Sci. Technol. Lett. 3 (2016) 24–29. https://doi.org/10.1021/acs.estlett.5b00319.

[58] D.S. McLagan, C.P.J. Mitchell, H. Huang, B. Abdul Hussain, Y. Duan Lei, F. Wania, The effects of meteorological parameters and diffusive barrier reuse on the sampling rate of a passive air sampler for gaseous mercury, Atmos. Meas. Tech. 10 (2017) 3651–3660. https://doi.org/10.5194/amt-10-3651-2017.

[59] A. Macagnano, P. Papa, J. Avossa, V. Perri, M. Marelli, F. Sprovieri, E. Zampetti, F. De Cesare, A. Bearzotti, N. Pirrone, Passive Sampling of Gaseous Elemental Mercury Based on a Composite TiO2NP/AuNP Layer, Nanomaterials. 8 (2018) 798. https://doi.org/10.3390/nano8100798.

[60] G. Bertoni, R. Tappa, I. Allegrini, Assessment of a new passive device for the monitoring of benzene and other volatile aromatic compounds in the atmosphere, Ann. Chim. (2000).

[61] US-EPA, Method 1631: Mercury in water by oxidation, purge and trap, and cold vapor atomic fluorescence spectrometry, EPA 821-R-96-012. US EPA, Off. Water, Washington, DC. (2002).

[62] GMOS Standard Operational Procedure, Method for the determination of total mercury in precipitation, (n.d.) 1–22.

[63] L.O. Methods, C.R. Hammerschmidt, K.L. Bowman, M.D. Tabatchnick, C.H. Lamborg, Storage bottle material and cleaning for determination of total mercury in seawater, (2011) 426–431. https://doi.org/10.4319/lom.2011.9.426.

[64] V. Krivan, H.F. Haas, O. Eselsberg, Prevention of loss of mercury (II) during storage of dilute solutions in various containerse, Fresenius. J. Anal. Chem. 332 (1988) 1–6. https://doi.org/10.1007/BF00487020.

[65] US-EPA, Appendix to Method 1631 Total Mercury in Tissue , Sludge , Sediment , and Soil by Acid Digestion and BrCl Oxidation, (2001) 1–13.

[66] J. Sneddon, C. Hardaway, K.K. Bobbadi, A.K. Reddy, Sample preparation of solid samples for metal determination by atomic spectroscopy - An overview and selected recent applications, Appl. Spectrosc. Rev. (2006).

https://doi.org/10.1080/05704920500385445.

[67] F. Sprovieri, I.M. Hedgecock, N. Pirrone, An investigation of the origins of reactive gaseous mercury in the Mediterranean marine boundary layer, Atmos. Chem. Phys. 10 (2010) 3985–3997. https://doi.org/10.5194/acp-10-3985-2010.

[68] M.M. Bencardino, N.N. Pirrone, F.F. Sprovieri, Aerosol and ozone observations during six cruise campaigns across the Mediterranean basin: Temporal, spatial, and seasonal variability, Environ. Sci. Pollut. Res. (2014). https://doi.org/10.1007/s11356-013-2196-6.

[69] M.C. Bove, P. Brotto, G. Calzolai, F. Cassola, F. Cavalli, P. Fermo, J. Hjorth, D. Massabò, S. Nava, A. Piazzalunga, C. Schembari, P. Prati, PM10 source apportionment applying PMF and chemical tracer analysis to ship-borne measurements in the Western Mediterranean, Atmos. Environ. (2016). https://doi.org/10.1016/j.atmosenv.2015.11.009.

[70] A. Finizola, F. Sortino, J.F. Lénat, M. Aubert, M. Ripepe, M. Valenza, The summit hydrothermal system of Stromboli. New insights from self-potential, temperature, CO2 and fumarolic fluid measurements, with structural and monitoring implications, Bull. Volcanol. 65 (2003) 486–504. https://doi.org/10.1007/s00445-003-0276-z.

[71] M.S. Landis, R.K. Stevens, F. Schaedlich, E.M. Prestbo, Development and characterization of an annular denuder methodology for the measurement of divalent inorganic reactive gaseous mercury in ambient air, Environ. Sci. Technol. 36 (2002) 3000–3009. https://doi.org/10.1021/es015887t.

[72] D. Simpson, Hydrocarbon reactivity and ozone formation in Europe, J. Atmos. Chem. (1995). https://doi.org/10.1007/BF00696556.

[73] D.M. Pyle, T.A. Mather, The importance of volcanic emissions for the global atmospheric mercury cycle, Atmos. Environ. 37 (2003) 5115–5124. https://doi.org/10.1016/j.atmosenv.2003.07.011.

[74] R.R. Draxler, G.D. Rolph, HYSPLIT (HYbrid Single-Particle Lagrangian Integrated Trajectory), NOAA Air Resour. Lab. Coll. Park. MD. (2003).

[75] R. Von Glasow, Atmospheric chemistry in volcanic plumes, Proc. Natl. Acad. Sci. U. S. A. (2010). https://doi.org/10.1073/pnas.0913164107.

[76] E.G. Malcolm, G.J. Keeler, M.S. Landis, The effects of the coastal environment

on the atmospheric mercury cycle, J. Geophys. Res. Atmos. (2003). https://doi.org/10.1029/2002jd003084.

[77] I.M. Hedgecock, N. Pirrone, Mercury and photochemistry in the marine boundary layer-modelling studies suggest the in situ production of reactive gas phase mercury, Atmos. Environ. (2001). https://doi.org/10.1016/S1352-2310(01)00109-1.

[78] P. Warneck, Chemistry of the natural atmosphere, Chem. Nat. Atmos. (1988). https://doi.org/10.1029/89eo00197.

[79] R.R. Dickerson, K.P. Rhoads, T.P. Carsey, S.J. Oltmans, J.P. Burrows, P.J. Crutzen, Ozone in the remote marine boundary layer: A possible role for halogens, J. Geophys. Res. Atmos. (1999). https://doi.org/10.1029/1999JD900023.

[80] R. Vogt, P.J. Crutzen, R. Sander, A mechanism for halogen release from sea-salt aerosol in the remote marine boundary layer, Nature. (1996). https://doi.org/10.1038/383327a0.

[81] R. Von Glasow, R. Sander, A. Bott, P.J. Crutzen, Modeling halogen chemistry in the marine boundary layer 1. Cloud-free MBL, J. Geophys. Res. Atmos. (2002). https://doi.org/10.1029/2001JD000942.

[82] C.N. Gencarelli, I.M. Hedgecock, F. Sprovieri, G.J. Schürmann, N. Pirrone, Importance of ship emissions to local summertime ozone production in the mediterranean marine boundary layer: A modeling study, Atmosphere (Basel). (2014). https://doi.org/10.3390/atmos5040937.

[83] D. Cossa, J.-M. Martin, K. Takayanagi, J. Sanjuan, The distribution and cycling of mercury species in the western Mediterranean, Deep Sea Res. Part II Top. Stud. Oceanogr. 44 (1997) 721–740. https://doi.org/10.1016/S0967-0645(96)00097-5.

[84] J. Kotnik, M. Horvat, E. Tessier, N. Ogrinc, M. Monperrus, D. Amouroux, V. Fajon, D. Gibičar, S. Žižek, F. Sprovieri, N. Pirrone, Mercury speciation in surface and deep waters of the Mediterranean Sea, Mar. Chem. 107 (2007) 13–30. https://doi.org/10.1016/j.marchem.2007.02.012.

[85] S.P. Hopkin, M.H. Martin, Assimilation of zinc, cadmium, lead, copper, and iron by the spider Dysdera crocata, a predator of woodlice, Bull. Environ.

Contam. Toxicol. (1985). https://doi.org/10.1007/BF01609722.

[86] M. Lagisz, R. Laskowski, Evidence for between-generation effects in carabids exposed to heavy metals pollution, Ecotoxicology. (2008). https://doi.org/10.1007/s10646-007-0176-7.

[87] A. Grant, Pollution-tolerant species and communities: Intriguing toys or invaluable monitoring tools?, Hum. Ecol. Risk Assess. (2002). https://doi.org/10.1080/1080-700291905765.

[88] F. Talarico, A. Giglio, R. Pizzolotto, P. Brandmayr, A synthesis of feeding habits and reproduction rhythm in Italian seed-feeding ground beetles (Coleoptera: Carabidae), Eur. J. Entomol. 113 (2016) 325–336. https://doi.org/10.14411/eje.2016.042.

[89] C. Monzó, B. Sabater-Muñoz, A. Urbaneja, P. Castañera, The ground beetle Pseudophonus rufipes revealed as predator of Ceratitis capitata in citrus orchards, Biol. Control. (2011). https://doi.org/10.1016/j.biocontrol.2010.09.004.

[90] B. Kromp, Carabid beetles in sustainable agriculture: A review on pest control efficacy, cultivation impacts and enhancement, Agric. Ecosyst. Environ. (1999). https://doi.org/10.1016/S0167-8809(99)00037-7.

[91] J.M. Holland, Carabid beetles : their ecology , survival and use in agroecosystems The Game Conservancy Trust , Fordingbridge , Hampshire , SP6 1EF , UK Abbreviations : SADIE , Spatial Analysis by Distance IndiciEs ., (2014).

[92] W. Jiao, W. Chen, A.C. Chang, A.L. Page, Environmental risks of trace elements associated with long-term phosphate fertilizers applications: A review, Environ. Pollut. (2012). https://doi.org/10.1016/j.envpol.2012.03.052.

[93] S. Ghannem, S. Touaylia, M. Boumaiza, Beetles (Insecta: Coleoptera) as bioindicators of the assessment of environmental pollution, Hum. Ecol. Risk Assess. 24 (2018) 456–464. https://doi.org/10.1080/10807039.2017.1385387.

[94] R. Articles, R. Elements, Application of Rare-earth Elements in the Agriculture of China and its.pdf, 9 (2002) 143–148.

[95] N. Otero, L. Vitòria, A. Soler, A. Canals, Fertiliser characterisation: Major, trace and rare earth elements, Appl. Geochemistry. 20 (2005) 1473–1488.

https://doi.org/10.1016/j.apgeochem.2005.04.002.

[96] M.N.A.A. Emi Fazlina Hashim, Irence John, Intan Faraha, Siti Hasmah Mohtar, Determination of concentration boundaries for the toxicity of Terminalia catappa Linn. leaves extract on healthy Ca, Indian J. Fundam. Appl. Life Sci. (2016). https://doi.org/10.4103/0971-9962.214596.

[97] G. Pagano, M. Guida, F. Tommasi, R. Oral, Health effects and toxicity mechanisms of rare earth elements-Knowledge gaps and research prospects, Ecotoxicol. Environ. Saf. (2015). https://doi.org/10.1016/j.ecoenv.2015.01.030.

[98] G. Pagano, F. Tommasi, M. Guida, Comparative toxicity of cerium and of other rare earth elements (REEs) in plant and invertebrate test systems, in: Cerium Mol. Struct. Technol. Appl. Heal. Eff., 2012.

[99] G. Pagano, F. Aliberti, M. Guida, R. Oral, A. Siciliano, M. Trifuoggi, F. Tommasi, Rare earth elements in human and animal health: State of art and research priorities, Environ. Res. (2015). https://doi.org/10.1016/j.envres.2015.06.039.

[100] R. Dallinger, Invertebrate organisms as biological indicators of heavy metal pollution, Appl. Biochem. Biotechnol. 48 (1994) 27–31. https://doi.org/10.1007/BF02825356.

[101] F. Talarico, P. Brandmayr, P.G. Giulianini, F. Ietto, A. Naccarato, E. Perrotta, A. Tagarelli, A. Giglio, Effects of metal pollution on survival and physiological responses in Carabus (Chaetocarabus) lefebvrei (Coleoptera, Carabidae), Eur. J. Soil Biol. 61 (2014) 80–89. https://doi.org/10.1016/j.ejsobi.2014.02.003.

[102] WHO Regional Office for Europe, Health Aspects of Air Pollution Results from the WHO Project "Systematic Review of Health Aspects of Air Pollution in Europe," World Health. (2004) 30.

[103] Annual report 2012 and Environmental statement 2013, (2013).

[104] G. Dziubanek, I. Hajok, Impact of Air Pollution on Public Health, (n.d.).

[105] W.C. Hinds, Properties, Behavior, and Measurement ofAirborne Particles, J. Aerosol Sci. (1999). https://doi.org/10.1016/0021-8502(83)90049-6.

[106] E.R. Lewis, S.E. Schwartz, Sea salt aerosol production: Mechanisms, methods, measurements and models—A critical review, in: Geophys. Monogr. Ser.,

2004. https://doi.org/10.1029/152GM01.

[107] M. Leili, K. Naddafi, R. Nabizadeh, M. Yunesian, A. Mesdaghinia, The study of TSP and PM10 concentration and their heavy metal content in central area of Tehran, Iran, Air Qual. Atmos. Heal. 1 (2008) 159–166. https://doi.org/10.1007/s11869-008-0021-z.

[108] J.A. Huffman, A.J. Prenni, P.J. Demott, C. Pöhlker, R.H. Mason, N.H. Robinson, J. Fröhlich-Nowoisky, Y. Tobo, V.R. Després, E. Garcia, D.J. Gochis, E. Harris, I. Müller-Germann, C. Ruzene, B. Schmer, B. Sinha, D.A. Day, M.O. Andreae, J.L. Jimenez, M. Gallagher, S.M. Kreidenweis, A.K. Bertram, U. Pöschl, High concentrations of biological aerosol particles and ice nuclei during and after rain, Atmos. Chem. Phys. (2013). https://doi.org/10.5194/acp-13-6151-2013.

[109] J.I. Steinfeld, Atmospheric Chemistry and Physics: From Air Pollution to Climate Change, Environ. Sci. Policy Sustain. Dev. (1998). https://doi.org/10.1080/00139157.1999.10544295.

[110] E.S. Galvão, J.M. Santos, A.T. Lima, N.C. Reis, M.T.D.A. Orlando, R.M. Stuetz, Trends in analytical techniques applied to particulate matter characterization: A critical review of fundaments and applications, Chemosphere. (2018). https://doi.org/10.1016/j.chemosphere.2018.02.034.

[111] M. Corn, T.L. Montgomery, N.A. Esmen, Suspended Particulate Matter: Seasonal Variation in Specific Surface Areas and Densities, Environ. Sci. Technol. (1971). https://doi.org/10.1021/es60049a001.

[112] S.D. Richardson, S.Y. Kimura, Emerging environmental contaminants: Challenges facing our next generation and potential engineering solutions, Environ. Technol. Innov. 8 (2017) 40–56. https://doi.org/10.1016/j.eti.2017.04.002.

[113] L. Sanchez-Prado, C. Garcia-Jares, T. Dagnac, M. Llompart, Microwave-assisted extraction of emerging pollutants in environmental and biological samples before chromatographic determination, TrAC - Trends Anal. Chem. 71 (2015) 119–143. http://dx.doi.org/10.1016/j.trac.2015.03.014.

[114] B. Albero, C. Sánchez-Brunete, A.I. García-Valcárcel, R.A. Pérez, J.L. Tadeo, Ultrasound-assisted extraction of emerging contaminants from environmental

samples, TrAC - Trends Anal. Chem. 71 (2015) 110–118. https://doi.org/10.1016/j.trac.2015.03.015.

[115] M.J.M. Wells, Log DOW: Key to understanding and regulating wastewater-derived contaminants, Environ. Chem. (2006). https://doi.org/10.1071/EN06045.

[116] N. Ratola, A. Cincinelli, A. Alves, A. Katsoyiannis, Occurrence of organic microcontaminants in the wastewater treatment process. A mini review, J. Hazard. Mater. (2012). https://doi.org/10.1016/j.jhazmat.2012.05.040.

[117] R. Pal, M. Megharaj, K.P. Kirkbride, R. Naidu, Illicit drugs and the environment - A review, Sci. Total Environ. (2013). https://doi.org/10.1016/j.scitotenv.2012.05.086.

[118] The European Commission (EC), Commission Regulation (EU) No 757/2010 of 24 August 2010 amending Regulation (EC) No 850/2004 of the European Parliament and of the Council on persistent organic pollutants as regards Annexes I and III, Off. J. Eur. Union. L 223 (2010) 29–36.

[119] M.A. Siddiqi, R.H. Laessig, K.D. Reed, Polybrominated diphenyl ethers (PBDEs): new pollutants-old diseases., Clin. Med. Res. (2003). https://doi.org/10.3121/cmr.1.4.281.

[120] CPA (Clean Production Agency), Brominated Flame Retardants in Dust on Computers : The case for Safer Chemicals and Better Computer Design, (2004) 43. http://www.cleanproduction.org/library/bfr_report_pages1-43.pdf.

[121] D. Laxen, F. Kirk-Lloyd, C. Beattie, Health Impacts of Air Pollution in Bristol, (2017) 18. https://www.bristol.gov.uk/documents/20182/32675/Health+Impacts+of+Air+Pollution+in+Bristol+February+2017/4df2fce5-e2fc-4c22-b5c7-5e7a5ae56701.

[122] Airborne particulate matter and their health effects, (n.d.). https://www.encyclopedie-environnement.org/en/health/airborne-particulate-health-effects/.

[123] ASTM D6552: Standard Practice for Controlling and Characterizing Errors in Weighing Collected Aerosols, Am. Soc. Test. Mater. (2006).

[124] H. Wolschke, R. Suhring, W. Mi, A. M??ller, Z. Xie, R. Ebinghaus,

Atmospheric occurrence and fate of organophosphorus flame retardants and plasticizer at the German coast, Atmos. Environ. 137 (2016) 1–5.

[125] J. Cortés, C.M. González, L. Morales, M. Abalos, E. Abad, B.H. Aristizábal, PCDD/PCDF and dl-PCB in the ambient air of a tropical Andean city: Passive and active sampling measurements near industrial and vehicular pollution sources, Sci. Total Environ. (2014). https://doi.org/10.1016/j.scitotenv.2014.01.113.

[126] X. Yang, D. Ren, W. Sun, X. Li, B. Huang, R. Chen, C. Lin, X. Pan, Polycyclic aromatic hydrocarbons associated with total suspended particles and surface soils in Kunming, China: Distribution, possible sources, and cancer risks, Environ. Sci. Pollut. Res. (2015). https://doi.org/10.1007/s11356-014-3858-8.

[127] A. Kotronarou, G. Mills, M.R. Hoffmann, Decomposition of Parathion in Aqueous Solution by Ultrasonic Irradiation, Environ. Sci. Technol. (1992). https://doi.org/10.1021/es00031a026.

[128] V. Camel, Microwave-assisted solvent extraction of environmental samples, TrAC - Trends Anal. Chem. 19 (2000) 229–248. https://doi.org/10.1016/S0165-9936(99)00185-5.

[129] C.L. Arthur, J. Pawliszyn, Solid Phase Microextraction with Thermal Desorption Using Fused Silica Optical Fibers, (1990) 2145–2148. https://doi.org/10.1021/ac00218a019.

[130] G. Ouyang, J. Pawliszyn, SPME in environmental analysis, Anal. Bioanal. Chem. 386 (2006) 1059–1073. https://doi.org/10.1007/s00216-006-0460-z.

[131] R. Eisert, K. Levsen, Solid-phase microextraction coupled to gas chromatography: A new method for the analysis of organics in water, J. Chromatogr. A. 733 (1996) 143–157. https://doi.org/10.1016/0021-9673(95)00875-6.

[132] N.W. Lloyd, S.R. Dungan, S.E. Ebeler, Measuring gas-liquid partition coefficients of aroma compounds by solid phase microextraction, sampling either headspace or liquid, Analyst. (2011). https://doi.org/10.1039/c1an15270j.

[133] M. Hallquist, J.C. Wenger, U. Baltensperger, Y. Rudich, D. Simpson, M. Claeys, J. Dommen, N.M. Donahue, C. George, A.H. Goldstein, J.F. Hamilton, H. Herrmann, T. Hoffmann, Y. Iinuma, M. Jang, M.E. Jenkin, J.L. Jimenez, A.

Kiendler-Scharr, W. Maenhaut, G. McFiggans, T.F. Mentel, A. Monod, A.S.H. Prévôt, J.H. Seinfeld, J.D. Surratt, R. Szmigielski, J. Wildt, The formation, properties and impact of secondary organic aerosol: Current and emerging issues, Atmos. Chem. Phys. (2009). https://doi.org/10.5194/acp-9-5155-2009.

[134] J. Li, Z. Xie, W. Mi, S. Lai, C. Tian, K.C. Emeis, R. Ebinghaus, Organophosphate Esters in Air, Snow, and Seawater in the North Atlantic and the Arctic, Environ. Sci. Technol. (2017). https://doi.org/10.1021/acs.est.7b01289.

[135] M.A. Bezerra, R.E. Santelli, E.P. Oliveira, L.S. Villar, L.A. Escaleira, Response surface methodology (RSM) as a tool for optimization in analytical chemistry, Talanta. 76 (2008) 965–977. https://doi.org/10.1016/j.talanta.2008.05.019.

[136] G.E.P. Box, K.B. Wilson, On the Experimental Attainment of Optimum Conditions, J. R. Stat. Soc. Ser. B. (1951). https://doi.org/10.1111/j.2517-6161.1951.tb00067.x.

[137] T. Lundstedt, E. Seifert, L. Abramo, B. Thelin, Å. Nyström, J. Pettersen, R. Bergman, Experimental design and optimization, Chemom. Intell. Lab. Syst. 42 (1998) 3–40. https://doi.org/10.1016/S0169-7439(98)00065-3.

[138] W. Schedule, Bonferroni Draws the Line on Over-Selection of Effects, (2007) 1–4.

[139] S.L.C. Ferreira, R.E. Bruns, E.G.P. da Silva, W.N.L. dos Santos, C.M. Quintella, J.M. David, J.B. de Andrade, M.C. Breitkreitz, I.C.S.F. Jardim, B.B. Neto, Statistical designs and response surface techniques for the optimization of chromatographic systems, J. Chromatogr. A. 1158 (2007) 2–14. https://doi.org/10.1016/j.chroma.2007.03.051.

[140] A. Gonzalez, K.L. Foster, G. Hanrahan, Method development and validation for optimized separation of benzo[a]pyrene-quinone isomers using liquid chromatography-mass spectrometry and chemometric response surface methodology, J. Chromatogr. A. (2007). https://doi.org/10.1016/j.chroma.2007.08.035.

[141] D.C. Montgomery, Design and Analysis of Experiments Eighth Edition, 2012. https://doi.org/10.1198/tech.2006.s372.

[142] I. van der Veen, J. de Boer, Phosphorus flame retardants: Properties, production,

environmental occurrence, toxicity and analysis, Chemosphere. 88 (2012) 1119–1153. http://dx.doi.org/10.1016/j.chemosphere.2012.03.067.

[143] A. Marklund, B. Andersson, P. Haglund, Screening of organophosphorus compounds and their distribution in various indoor environments, Chemosphere. 53 (2003) 1137–1146. https://doi.org/10.1016/S0045-6535(03)00666-0.

[144] A. for T.S. and D. Registry, Draft Toxicological Profile for Phosphate Ester Flame Retardants, 153 (2008) 451–459.

[145] WHO, Environmental Health Criteria 218: Tbep-Tris(2-Butoxyethyl)Phosphate , Tris(2-Ethylhexyl)Phosphate and Tetrakis (Hydroxymethyl) Phosphonium Salts, (2000) 1–154.

[146] Flame retardants found in groundwater, (2011) 2011.

[147] J. Bjorklund, S. Isetun, U. Nilsson, J. Bjorklund, S. Isetun, U. Nilsson, Selective determination of organophosphate flame retardants and plasticizers in indoor air by gas chromatography, positive-ion chemical ionization and collision-induced dissociation mass spectrometry, Rapid Commun. Mass Spectrom. 18 (2004) 3079–3083.

[148] Screening of selected metals and new organic contaminants 2007. Phosphorus flame retardents, polyfluorinated organic compounds, nitro-PAHs, silver, platinum and sucralose in air, wastewater treatment falcilities, and freshwater and marine recipients, 2008.

[149] L. Pang, P. Yang, L. Ge, J. Du, H. Zhang, Accelerated solvent extraction combined with solid phase extraction for the determination of organophosphate esters from sewage sludge compost by UHPLC–MS/MS, Anal. Bioanal. Chem. 409 (2017) 1435–1440. http://link.springer.com/10.1007/s00216-016-0078-8.

[150] E. Fries, W. Puttmann, Occurrence of organophosphate esters in surface water and ground water in Germany, J. Environ. Monit. 3 (2001) 621–626. http://www.ncbi.nlm.nih.gov/entrez/query.fcgi?cmd=Retrieve&db=PubMed&dopt=Citation&list_uids=11785636.

[151] M. García-López, I. Rodríguez, R. Cela, K.K. Kroening, J.A. Caruso, Determination of organophosphate flame retardants and plasticizers in sediment samples using microwave-assisted extraction and gas chromatography with

inductively coupled plasma mass spectrometry, Talanta. 79 (2009) 824–829.

[152] H.W. Chung, W.H. Ding, Determination of organophosphate flame retardants in sediments by microwave-assisted extraction and gas chromatography-mass spectrometry with electron impact and chemical ionization, Anal. Bioanal. Chem. 395 (2009) 2325–2334.

[153] A.K. Greaves, R.J. Letcher, A Review of Organophosphate Esters in the Environment from Biological Effects to Distribution and Fate, Bull. Environ. Contam. Toxicol. (2016) 1–6.

[154] Y. Ma, K. Cui, F. Zeng, J. Wen, H. Liu, F. Zhu, G. Ouyang, T. Luan, Z. Zeng, Microwave-assisted extraction combined with gel permeation chromatography and silica gel cleanup followed by gas chromatography-mass spectrometry for the determination of organophosphorus flame retardants and plasticizers in biological samples, Anal. Chim. Acta. 786 (2013) 47–53. http://dx.doi.org/10.1016/j.aca.2013.04.062.

[155] G. Ren, Z. Chen, J. Feng, W. Ji, J. Zhang, K. Zheng, Z. Yu, X. Zeng, Organophosphate esters in total suspended particulates of an urban city in East China, Chemosphere. 164 (2016) 75–83. http://dx.doi.org/10.1016/j.chemosphere.2016.08.090.

[156] T. Staaf, C. Ostman, Indoor air sampling of organophosphate triesters using solid phase extraction (SPE) adsorbents, J Env. Monit. 7 (2005) 344–348. http://www.ncbi.nlm.nih.gov/pubmed/15798801.

[157] H. Fromme, T. Lahrz, M. Kraft, L. Fembacher, C. Mach, S. Dietrich, R. Burkardt, W. Völkel, T. Göen, Organophosphate flame retardants and plasticizers in the air and dust in German daycare centers and human biomonitoring in visiting children (LUPE 3), Environ. Int. 71 (2014) 158–163. http://dx.doi.org/10.1016/j.envint.2014.06.016.

[158] M. Shah, J. Meija, B. Cabovska, J.A. Caruso, Determination of phosphoric acid triesters in human plasma using solid-phase microextraction and gas chromatography coupled to inductively coupled plasma mass spectrometry, J. Chromatogr. A. 1103 (2006) 329–336.

[159] T. Reemtsma, M. García-López, I. Rodríguez, J.B. Quintana, R. Rodil, Organophosphorus flame retardants and plasticizers in water and air I.

Occurrence and fate, TrAC - Trends Anal. Chem. 27 (2008) 727–737.

[160] WHO, Environmental Health Criteria 111: Triphenyl phosphate, (1991) 79.

[161] M. Baril, G.J. Van Esch, R. Benson, R. Cary, S. Dobson, D. Renshaw, E. Soderlund, J. Wagstaff, Environmental Health Criteria 209: Flame retardants: Tris(chloropropyl) phosphate and tris(2-chloroethyl) phosphate, Environ. Heal. Criteria. (1998).

[162] R. Suhring, M.L. Diamond, M. Scheringer, F. Wong, M. Pucko, G. Stern, A. Burt, H. Hung, P. Fellin, H. Li, L.M. Jantunen, M. Pu??ko, G. Stern, A. Burt, H. Hung, P. Fellin, H. Li, L.M. Jantunen, M. Pucko, G. Stern, A. Burt, H. Hung, P. Fellin, H. Li, L.M. Jantunen, Organophosphate esters in Canadian Arctic air: Occurrence, levels and trends, Environ. Sci. Technol. 50 (2016) 7409–7415.

[163] J. Castro-Jiménez, N. Berrojalbiz, M. Pizarro, J. Dachs, Organophosphate ester (OPE) flame retardants and plasticizers in the open mediterranean and black seas atmosphere, Environ. Sci. Technol. 48 (2014) 3203–3209.

[164] A. Naccarato, A. Tassone, S. Moretti, R. Elliani, F. Sprovieri, N. Pirrone, A. Tagarelli, A green approach for organophosphate ester determination in airborne particulate matter: Microwave-assisted extraction using hydroalcoholic mixture coupled with solid-phase microextraction gas chromatography-tandem mass spectrometry, Talanta. 189 (2018) 657–665. https://doi.org/10.1016/j.talanta.2018.07.077.

[165] A. Naccarato, E. Gionfriddo, R. Elliani, G. Sindona, A. Tagarelli, A fast and simple solid phase microextraction coupled with gas chromatography-triple quadrupole mass spectrometry method for the assay of urinary markers of glutaric acidemias, J. Chromatogr. A. (2014). https://doi.org/10.1016/j.chroma.2014.10.069.

[166] A. Naccarato, S. Moretti, G. Sindona, A. Tagarelli, Identification and assay of underivatized urinary acylcarnitines by paper spray tandem mass spectrometry, Anal. Bioanal. Chem. (2013). https://doi.org/10.1007/s00216-013-7232-3.

[167] M.I. Beser, J. Beltrán, V. Yusà, Design of experiment approach for the optimization of polybrominated diphenyl ethers determination in fine airborne particulate matter by microwave-assisted extraction and gas chromatography coupled to tandem mass spectrometry, J. Chromatogr. A. 1323 (2014) 1–10.

http://dx.doi.org/10.1016/j.chroma.2013.10.081.

[168] J.B. Quintana, R. Rodil, P. López-Mahía, S. Muniategui-Lorenzo, D. Prada-Rodríguez, Optimisation of a selective method for the determination of organophosphorous triesters in outdoor particulate samples by pressurised liquid extraction and large-volume injection gas chromatography-positive chemical ionisation-tandem mass spectrometry, Anal. Bioanal. Chem. 388 (2007) 1283–1293.

[169] J. Cristale, S. Lacorte, Development and validation of a multiresidue method for the analysis of polybrominated diphenyl ethers, new brominated and organophosphorus flame retardants in sediment, sludge and dust, J. Chromatogr. A. 1305 (2013) 267–275. http://dx.doi.org/10.1016/j.chroma.2013.07.028.

[170] D. Salas, F. Borrull, R.M. Marcé, N. Fontanals, Study of the retention of benzotriazoles, benzothiazoles and benzenesulfonamides in mixed-mode solid-phase extraction in environmental samples, J. Chromatogr. A. 1444 (2016) 21–31. https://doi.org/10.1016/j.chroma.2016.03.053.

[171] A. Maceira, R.M. Marcé, F. Borrull, Occurrence of benzothiazole, benzotriazole and benzenesulfonamide derivates in outdoor air particulate matter samples and human exposure assessment, Chemosphere. 193 (2018) 557–566. https://doi.org/10.1016/j.chemosphere.2017.11.073.

[172] A. Kiss, E. Fries, Occurrence of benzotriazoles in the rivers Main, Hengstbach, and Hegbach (Germany), Environ. Sci. Pollut. Res. 16 (2009) 702–710. https://doi.org/10.1007/s11356-009-0179-4.

[173] G. Leng, W. Gries, New specific and sensitive biomonitoring methods for chemicals of emerging health relevance, Int. J. Hyg. Environ. Health. (2017). https://doi.org/10.1016/j.ijheh.2016.09.014.

[174] H. Jafari, K. Akbarzade, I. Danaee, Corrosion inhibition of carbon steel immersed in a 1 M HCl solution using benzothiazole derivatives, Arab. J. Chem. (2019). https://doi.org/10.1016/j.arabjc.2014.11.018.

[175] A. Speltini, M. Sturini, F. Maraschi, A. Porta, A. Profumo, Fast low-pressurized microwave-assisted extraction of benzotriazole, benzothiazole and benezenesulfonamide compounds from soil samples, Talanta. (2016).

https://doi.org/10.1016/j.talanta.2015.09.074.

[176] D. Richter, G. Massmann, T. Taute, U. Duennbier, Investigation of the fate of sulfonamides downgradient of a decommissioned sewage farm near Berlin, Germany, J. Contam. Hydrol. (2009). https://doi.org/10.1016/j.jconhyd.2009.03.001.

[177] D. Richter, U. Dünnbier, G. Massmann, A. Pekdeger, Quantitative determination of three sulfonamides in environmental water samples using liquid chromatography coupled to electrospray tandem mass spectrometry, J. Chromatogr. A. (2007). https://doi.org/10.1016/j.chroma.2007.04.042.

[178] A.G. Asimakopoulos, L. Wang, N.S. Thomaidis, K. Kannan, Benzotriazoles and benzothiazoles in human urine from several countries: A perspective on occurrence, biotransformation, and human exposure, Environ. Int. 59 (2013) 274–281. https://doi.org/10.1016/j.envint.2013.06.007.

[179] L. Wang, A.G. Asimakopoulos, H.B. Moon, H. Nakata, K. Kannan, Benzotriazole, benzothiazole, and benzophenone compounds in indoor dust from the United States and East Asian countries, Environ. Sci. Technol. 47 (2013) 4752–4759. https://doi.org/10.1021/es305000d.

[180] D.A. Pillard, D.L. DuFresne, Toxicity of formulated glycol deicers and ethylene and propylene glycol to Lactuca sativa, Lolium perenne, Selenastrum capricornutum, and Lemna minor, Arch. Environ. Contam. Toxicol. (1999). https://doi.org/10.1007/s002449900486.

[181] G. Ginsberg, B. Toal, T. Kurland, Benzothiazole toxicity assessment in support of synthetic turf field human health risk assessment, J. Toxicol. Environ. Heal. - Part A Curr. Issues. (2011). https://doi.org/10.1080/15287394.2011.586943.

[182] A. Naccarato, E. Gionfriddo, G. Sindona, A. Tagarelli, Simultaneous determination of benzothiazoles, benzotriazoles and benzosulfonamides by solid phase microextraction-gas chromatography-triple quadrupole mass spectrometry in environmental aqueous matrices and human urine, J. Chromatogr. A. 1338 (2014) 164–173. https://doi.org/10.1016/j.chroma.2014.02.089.